NTNU – Trondheim
Norwegian University of
Science and Technology

Testing and Optimization of PVAm/PVA Blend Membranes for Biogas Upgrading

Eivind Berstad

Chemical Engineering and Biotechnology
Submission date: June 2012
Supervisor: May-Britt Hägg, IKP
Co-supervisor: Xuezhong He, IKP

Norwegian University of Science and Technology
Department of Chemical Engineering

Preface and acknowledgements

This master's thesis was carried out at the Department of Chemical Engineering, at the Norwegian University of Science and Technology in the period January 23th to June 7th, 2012. The main supervisor has been Professor May-Britt Hägg and co-supervisor has been Dr. Xuezhong He. I would like to reward the Memfo group for continuous work with environment friendly technology, and good collaboration and discussions at the lab. A special gratitude is given to Dr. He for his guidance and patience.

May the Force be with you

I declare that this is an independent work according to the exam regulations of the Norwegian University of Science and Technology.

Trondheim, June 7th 2012

Eivind Berstad

Abstract

Membrane technology is an energy saving, environment friendly and low cost separation technology. This master's thesis has focused on testing and optimization of polyvinylamine/polyvinylalcohol (PVAm/PVA) blend fixed-site-carrier (FSC) membranes on polysulfone supports for separation of carbon dioxide (CO_2) and methane (CH_4). Permeation tests, process simulation and cost estimation were applied to evaluate CO_2/CH_4 separation performance and process feasibility for biogas upgrading. Utilization of biogas as a natural gas substitute or as vehicle fuel can contribute to reduced greenhouse gas emissions.

Orthogonal experimental design (OED) was employed to study the influences of membrane preparation conditions on the gas transport properties of flat sheet PVAm/PVA blend FSC membranes. The conjoint analysis method was applied for the statistical analysis of OED results using SPSS software, and the importance of the investigated membrane preparation condition parameters on the CO_2/CH_4 separation performance was found to be: polymer concentration in casting solution > heat treatment temperature > heat treatment duration > content of carbon nanotubes (CNTs) in polymer. The optimized membrane preparation conditions in the interval investigated were: 1 wt% polymer in the casting solution, containing 3 wt% of CNTs, heat-treated at 105 °C for 0.5 h. It was found that a membrane with a very thin selective layer (375 nm) was able to achieve both high CO_2/CH_4 selectivity and CO_2 permeance.

Reinforcing the PVAm/PVA membrane with CNTs was investigated, but no significant effect was found within the range of investigation. SEM analysis has shown that CNTs gathers in large aggregates, and that an even distribution of well-dispersed CNTs is needed to secure a defect free selective layer.

Permeation tests were performed in an advanced mixed gas permeation rig and operating conditions were optimized on the basis of OED and conjoint analysis by SPSS software. The relative importance of the operating condition parameters investigated in this work was in the following order: relative humidity > sweep gas flow rate > feed gas pressure > feed gas flow rate. The optimized operating conditions were found at a feed gas pressure of 2 bar with a relative humidity of 80 % and a feed gas flow rate and sweep gas flow rate at 12.3 cm^3/s and 0.18 cm^3/s, respectively. CO_2/CH_4 selectivity of 31 with a CO_2 permeance of 0.16 $m^3(STP)/(m^2.h.bar)$ was obtained at optimized conditions.

A conceptual design of a biogas upgrading process with a feed gas flow rate at 300 Nm^3/h (60 vol% CH_4 and 40 vol% CO_2) was conducted. Two different process designs with a feed gas pressure of 2 and 5 bar were simulated in UniSim. In a two-stage membrane module separation system with recycle it was possible to purify biogas up to 99.3 vol% CH_4 (vehicle fuel quality), and obtain a CH_4 recovery of 98 %. The total membrane area was reduced a lot by increasing the feed gas pressure from 2 to 5 bar. The capital cost of the most promising process design was estimated to be US\$4.622 million, and the running costs were estimated to be US\$0.603/Nm^3 upgraded biogas. The total membrane area was 7900 m^2. The most important economic parameter for upgrading biogas is the price of upgraded biogas as vehicle fuel, and a price of US\$1.22/Nm^3 is necessary to secure a positive net present value of the project after 10 years.

Sammendrag

Membranteknologi er en energieffektiv, miljøvennlig og rimelig separasjonsteknologi. I denne masteroppgaven er det fokusert på testing og optimalisering av en membran av to blandede polymere, polyvinylamin og polyvinylalkohol (PVAm/PVA), på en støttestruktur av polysulfon for oppgradering av biogass. PVAm/PVA-membranen har bæregrupper bundet til hovedkjeden som fasiliterer transport av karbondioksid (CO_2). Permeansmålinger, prosessimulering og kostnadsestimering ble benyttet for å evaluere membranens separasjonseffektivitet av CO_2 og metan (CH_4) og gjennomførbarhet for oppgradering av biogass. Benyttelse av biogass som et naturgass-substitutt eller som drivstoff kan bidra til reduksjon av drivhusgassutslipp.

Ortogonalt eksperimentelt design (OED) ble benyttet for å studere hvordan betingelsene i prosedyren for tillagning av membran påvirket separasjons-effektiviteten til flatark PVAm/PVA-membraner. Conjoint-analyse ble benyttet for den statistiske analysen av OED–resultatene vha. SPSS-programvare, og den relative signifikansen av betingelsene i tillagningsprosedyren ble sortert i rekkefølgen: polymerkonsentrasjon i tillagningsløsning > varmebehandlingstemperatur > varmebandlingsvarighet > innhold av karbon-nanorør i polymer. I den undersøkte variasjonsbredden var de optimale betingelsene i tillagningsprosedyren: 1 vekt% polymer i tillagningsløsning med 3 vekt% karbon-nanorør, varmebehandlet ved 105 °C i 0,5 timer. Det ble funnet at en membran med et meget tynt selektivt lag (375 nm) kunne oppnå både høy CO_2/CH_4-selektivitet og CO_2-permeans. Forsterkning av PVAm/PVA-membranen med karbon-nanorør ble undersøkt, men ingen signifikant effekt ble funnet i den undersøkte variasjonsbredden. SEM-analyser viste at karbon-nanorør samler seg i store aggregater, og at en jevn distribusjon av godt dispergerte karbon-nanorør er nødvendig for å sikre et defektfritt selektivt lag.

Permeansmålinger ble utført i en avansert permeasjonsrigg for gassblandinger og driftsbetingelsene ble optimalisert ved OED og conjoint-analyse med SPSS-programvare. Den relative signifikansen av driftsbetingelsene ble sortert i rekkefølgen: relativ fuktighet > strømningshastighet av bæregass > fødegasstrykk > strømningshastighet av fødegass. De optimaliserte driftsbetingelsene ble funnet til å være: fødegasstrykk ved 2 bar og en relativ fuktighet på 80 % med en strømningshastighet av fødegass på og bæregass på henholdsvis 12,3 cm^3/s og 0,18 cm^3/s. Ved optimale driftsbetingelser ble det registrert en CO_2/CH_4-selektivitet på 31 og en CO_2-permeans på 0.16 $m^3(STP)/(m^2.time.bar)$.

Et konseptuelt prosessdesign for oppgradering av biogass med en strømningshastighet av fødegass på 300 Nm^3/time (60 vol% CH_4, 40 vol% CO_2) ble konstruert ved å simulere to ulike prosessdesign med fødegasstrykk på 2 og 5 bar i UniSim. I et separasjonssystem med en to-trinns membranmodul med resirkulasjon var det mulig å oppgradere biogass til 99.3 vol% CH_4 (drivstoffkvalitet) og oppnå en gjenvinningsgrad av CH_4 på 98 %. Det totale membranarealet som var nødvendig for å utføre separasjonen ble vesentlig redusert ved å øke fødegasstrykket fra 2 til 5 bar. Anleggsomkostningene av det mest lovende prosessdesignet ble estimert til 4,622 millioner US$, og driftskostnadene ble estimert til 0,603 US$ per Nm^3 oppgradert biogass. Det totale membranarealet var 7900 m^2. Den viktigste økonomiske parameteren i oppgradering av biogass er prisen på oppgradert biogass til drivstoffkvalitet. En pris på 1,22 US$ per Nm^3 er nødvendig for å sikre en positiv nåverdi av prosjektet etter 10 års drift.

Table of contents

Preface and acknowledgements i
Abstract iii
Sammendrag v
Table of contents vii
List of Figure captions x
List of Table captions xii
List of Symbols xiii
1 Introduction 1
  1.1 Energy consumption and climate change 1
  1.2 Biogas upgrading 2
  1.3 Aim of the project 3
  1.4 Outline of thesis 3
2 Background and theory 5
  2.1 Membrane definition 5
  2.2 Benefits and challenges of membranes 5
  2.3 Classification of membranes 5
    2.3.1 Microporous membranes 6
    2.3.2 Ceramic, zeolite and metallic membranes 7
    2.3.3 Mixed matrix membranes 8
    2.3.4 Liquid membranes 8
    2.3.5 Nonporous, dense membranes 9
    2.3.6 Composite membranes 9
    2.3.7 Facilitated transport membranes 10
  2.4 Important physical properties for polymer membranes 10
    2.4.1 Crystallinity and glass transition temperature 10
    2.4.2 Free volume 12
    2.4.3 Swelling 14
    2.4.4 Plasticization 14
    2.4.5 Crosslinking 15
  2.5 Gas transport mechanisms through polymer membranes 15
    2.5.1 Solution-Diffusion mechanism 16
    2.5.2 Facilitated transport mechanism 20
    2.5.3 Gas transport through composite membranes 25
  2.6 Preparation of polymer membranes 25
  2.7 Membrane separation principles 26
    2.7.1 Membrane modules 26
    2.7.2 Complete mixing model 27
  2.8 Important applications for gas separation membranes 28
3 Facilitated transport membranes 29
  3.1 Preparation of FSC membranes 29
    3.1.1 Material selection 29
    3.1.2 Material functionalization 30
    3.1.3 Casting 30
    3.1.4 Post treatment 31
  3.2 Characterization of FSC membranes 31

3.2.1 Scanning electron microscopy 31
3.2.2 Gas permeation tests 32
3.3 Potential applications of FSC membranes 33
3.3.1 Biogas upgrading 33
3.3.2 CO_2 removal from natural gas 35
3.3.3 Pre-combustion H_2/CO_2 separation 36
3.3.4 CO_2 capture from flue gas 36

4 Experimental 37
4.1 Materials 37
4.1.1 Polyvinylalcohol 37
4.1.2 Polyvinylamine 37
4.1.3 Carbon nanotubes 38
4.1.4 Polysulfone 38
4.1.5 Gases 38
4.2 Membrane preparation 38
4.2.1 Preparation of aqueous solutions of PVAm, PVA and CNTs 38
4.2.2 Mixing of the aqueous solutions to prepare casting solutions 39
4.2.3 Membrane casting and post-treatment 39
4.3 Membrane characterization 40
4.3.1 Gas permeation test 40
4.3.2 Scanning electron microscopy 41
4.4 Orthogonal experimental design and conjoint analysis 42

5 Results and discussion 43
5.1 Optimization of membrane preparation conditions 43
5.1.1 Orthogonal experimental design and results 43
5.1.2 Analysis of OED 44
5.1.3 Effect of selective layer thickness 48
5.1.4 Effect of heat treatment conditions 48
5.1.5 Effect of CNTs 49
5.2 Optimization of operating conditions 51
5.2.1 Orthogonal experimental design and results 51
5.2.2 Analysis of the OED 52
5.2.3 Effect of relative humidity 56
5.2.4 Effect of sweep gas flow rate 57
5.2.5 Effect of pressure and feed gas flow rate 57
5.3 Scanning electron microscopy analysis 58
5.3.1 Effect of dissolving carbon nanotubes with ultrasound 59
5.3.2 SEM analysis of membranes 60

6 Process simulation 63
6.1.1 Process description 63
6.1.2 Process design and simulation basis 64
6.2 Simulation results and economic cost estimation 66
6.2.1 Simulation results 66
6.2.2 Economic cost estimation 68

7 Uncertainty 71
7.1 Experimental 71
7.2 Simulation and economics 72

8 Conclusion 73

9 Suggestions for future work 75

References 77

Appendix A: Gas composition at Ecopro I
Appendix B: Mass and energy balance of simulation case D I
Appendix C: Economic calculations V
  C.1 Cost estimation V
  C.2 Project fixed capital cost VII
  C.3 Running costs VIII
  C.4 Running income IX
Appendix D: Original project description........ XI
Appendix E: Risk assessment XIII

List of Figure captions

Figure 2.1 Schematic drawing of porous membrane (left), dense membrane (centre) and carrier-mediated membrane (right) [12] 6

Figure 2.2 Selective permeation of molecules by molecular sieving [13] 6

Figure 2.3 Permeation of condensable and noncondensable gas molecules though a membrane by selective surface flow [13] 7

Figure 2.4 Two-layer composite membrane made by a thin selective layer coated on a porous support layer that provides mechanical strength [13] 9

Figure 2.5 Correlation between diffusion coefficients on permeant kinetic diameter in a) glassy polymers: poly(1-trimethylsilyl-1-propyne) (PTMSP), polyvinyltrimethylsilane (PVTMS), polycarbonate (PC), per-fluorocarbon copolymers of 2,2-bis(trifluoromethyl)-4,5-difluoro-1,3-dioxole (BDD) and tetrafluoroethylene (TFE) containing 65 mol% BDD (AF1600) and 87 mol% BDD (AF2400), and b) rubbery polymers including crosslinked poly(ethylene glycol diacrylate) (XLPEGDA), semicrystalline poly(ethylene oxide) (SC PEO), natural rubber (NR) and polydimethylsiloxane (PDMS) [22] 11

Figure 2.6 The change in volume as a function of temperature for a typical polymer [13] 13

Figure 2.7 Correlation between CO_2 permeability and fractional free volume in glassy aromatic polysulfone, polyimides and polycarbonates. FFV denotes fractional free volume, υ_f [22] 14

Figure 2.8 The driving force gradients for permeation through a membrane according to the solution-diffusion mechanism [22] 17

Figure 2.9 Schematic drawing of mobile carrier membrane (left) and fixed carrier membrane (right) [12] 21

Figure 2.10 Schematic drawing of diffusion of component A via Fick's first law (curve b) and facilitated diffusion (curve a) [12] 22

Figure 2.11 Facilitated transport mechanism proposed by Matsuyama et al. [33] 23

Figure 2.12 Facilitated transport mechanism in a fixed-site-carrier membrane [29] 23

Figure 2.13 A proposed mechanism of facilitated transport in a fixed-site–carrier membrane [11] 24

Figure 2.14 Schematic drawing of a membrane separation process [12] 26

Figure 2.15 Membrane gas separation with perfect mixing at feed and permeate side 27

Figure 3.1 The Robeson´s upper bound for CO_2/CH_4 separation [42] 29

Figure 3.2 SEM image of PVAm/PVA blend membrane cross-section [39] 32

Figure 3.3 Process overview of a biogas production and upgrading system providing gas to a natural gas network. 1: Bioreactor; 2: thickener; 3: filter; 4: 1st stage membrane module; 5: 2nd stage membrane module [58] 34

Figure 3.4 Interior of a membrane upgrading plant [7] 34

Figure 3.5 Two-stage low-pressure feed cascade with recycle [7] 35

Figure 3.6 Process configuration for CO_2 removal from natural gas [61] 36

Figure 4.1 Schematic structure of the repeating unit in polyvinylalcohol (PVA) [10] 37

Figure 4.2 Schematic structure of the repeating unit of polyvinylamine (PVAm) [66] 37

Figure 4.3 Chemical structure of Polysulfone [50] 38

Figure 4.4 Illustration of the assembly of the membrane cell 40
Figure 4.5 Experimental set-up for gas permeation tests 41
Figure 5.1 Normalized mixed gas permeation test results for the OED experiments for optimization of membrane preparation conditions 44
Figure 5.2 Effects of membrane preparation conditions, a) Polymer concentration b) CNT content in polymer c) Heat treatment temperature d) Heat treatment duration, on the membrane separation performance (averaged and normalized CO_2/CH_4 selectivity and CO_2 permeance) 45
Figure 5.3 Separation performance of four membranes prepared at optimal preparation conditions (16A, 16B, 16C, 16D) compared with the best membrane tested (12) 47
Figure 5.4 The effect of CNT in the PVAm/PVA blend membrane on CO_2/CH_4-selectivity and CO_2 permeance at 2 bar, 25 °C, feed gas (35% CO_2) flow rate at 8.2 ml/s, sweep gas flow rate at 0.07 ml/s and various levels of relative humidity 50
Figure 5.5 The effect of CNT in the PVAm/PVA blend membrane on CO_2/CH_4-selectivity and CO_2 permeance at 10 bar, 25 °C, feed gas flow rate at 8.2 ml/s, sweep gas flow rate at 0.07 ml/s and various levels of relative humidity 51
Figure 5.6 Normalized mixed gas permeation test results for the OED experiments for optimization of process operating conditions 52
Figure 5.7 Effects of operating conditions, a) Relative humidity b) Feed gas pressure c) Sweep gas flow rate d) Feed gas flow rate, on the membrane separation performance (average normalized CO_2/CH_4 selectivity and CO_2 permeance).... 53
Figure 5.8 SEM image of CNT aggregates in a) CNTs dissolved in water and PVA and b) CNTs dissolved by ultrasound in water and PVA 59
Figure 5.9 SEM image of CNT aggregates in a) CNTs dissolved in water and PVA and b) CNTs dissolved by ultrasound in water and PVA 60
Figure 5.10 SEM pictures of PSf support membrane with asymmetric structure at 2700 and 3200 x magnification 60
Figure 5.11 SEM image a) cross section and b) surface of membrane no. 12: 1 wt% polymer, 1 wt% CNT in polymer, high CO_2/CH_4 separation performance 61
Figure 5.12 SEM image of a) cross section and b) surface of membrane no. 5: 5 wt% polymer in coating solution, 3 wt% CNTs in polymer. Low CO_2/CH_4 separation performance 61
Figure 5.13 Comparison between measured selective layer thickness by SEM analysis with the corresponding concentrations of polymers in the casting solution........ 62
Figure 6.1 Flow chart of a typical biogas upgrading process [75] 64
Figure 6.2 Process design 1 and 2 used for simulation 65
Figure 6.3 Flow sheet of the simulated process of case D in UniSim 67
Figure 6.4 Net cash flow diagram of case D 68
Figure 6.5 Sensitivity analysis of case D that show how net present value changes with a +/- 10% change in price of upgraded biogas and cost of feed biogas, electricity, cooling water and membrane module 69

List of Table captions

Table 2.1 Comparison of membrane separation performance of some inorganic membranes 8
Table 5.1 The factors and levels of the orthogonal experimental design for optimization of membrane preparation conditions 43
Table 5.2 Experimental design and permeation test results for optimization of membrane preparation conditions 44
Table 5.3 Utilities and averaged importance scores for different factors in optimization of membrane preparation conditions 46
Table 5.4 An example of different membrane preparation conditions 47
Table 5.5 Simulation results by conjoint analysis for optimization of membrane preparation conditions 48
Table 5.6 The factors and levels of the orthogonal experimental design for optimization of operating conditions 51
Table 5.7 Experimental design and permeation test results for optimization of operating conditions 52
Table 5.8 Utilities and averaged importance scores for different factors for optimization of operating conditions 54
Table 5.9 An example of different operating conditions 54
Table 5.10 Comparison of membrane separation performance in current work and other polymer membranes and fixed-site-carrier membranes 55
Table 5.11 Simulation results from conjoint analysis of optimization of operating conditions 56
Table 6.1 Biogas composition at Ecopro 63
Table 6.2 Basis for simulation case A, B, C and D 65
Table 6.3 Results of simulation case A, B, C and D 66
Table B.1 Mass balance of simulation case D III
Table B.2 Energy balance of simulation case D III
Table C.1 Compressor capacities and investments costs for case A V
Table C.2 Compressor capacities and investments costs for case B V
Table C.3 Compressor capacities and investments costs for case C VI
Table C.4 Compressor capacities and investments costs for case D VI
Table C.5 Cost estimation of membranes for simulation case A, B, C and D VII
Table C.6 Total fixed capital cost for simulation case A, B, C and D VII
Table C.7 The cost of electricity for simulation case A, B, C and D VIII
Table C.8 The cost of cooling water for simulation case A, B, C and D VIII
Table C.9 Total running cost for simulation case A, B, C and D IX

List of Symbols

Symbol	Explanation	Unit/Value
Latin letters		
A	area	m^2
C	cost; concentration	US\$; m^3(STP)/m^3
Cp	heat capacity	J/(kg.K)
D	diffusion coefficient	m^2/h or cm^2/s
d_k	kinetic diameter	Å
E	activation energy	J/mol
I	Chemical engineering plant cost index	-
J	flux	m^3(STP)/(m^2.s) or m^3(STP)/(m^2.h)
L_A	proportionality coefficient	(m^3(STP).mol)/(J.m.h)
ℓ	membrane thickness	m
m	molecular weight	g/mol
n	exponential factor; mole fraction	- ; -
p	pressure	Pa or bar
P	permeability	Barrer or m^3(STP) m/(m^2.h.bar)
Q	permeance; heat transfer	m^3(STP)/(m^2.h.bar); kW
q	flow rate	m^3(STP)/h
R	universal gas constant	8.314 J/(mol.K)
S	solubility coefficient; capacity	m^3(STP)/(m^3.bar); kW,m^2
T	temperature	°C or K
T_g	glass transition temperature	°C
U	heat transfer coefficient	W/(m^2.K)
υ	specific volume of the polymer	cm^3/g
υ_0	volume occupied by polymer molecules	cm^3/g
υ_f	free volume fraction	-
ν_A	partial molar volume	m^3/mol
x	mole fraction in feed	-
y	mole fraction in permeate	-
Greek letters		
α	selectivity	
$\Delta\alpha$	thermal expansion coefficient	cm^3/(cm^3.K)
ΔH_S	heat of solution	J/mol
ΔT_{lm}	logarithmic mean temperature	K
μ	chemical potential	J/mol
γ_A	activity coefficient	mol/mol

Symbol	Explanation	Unit/Value

Subscripts

A	component A	
AC	carrier-solute complex	
B	component B	
d	diffusion	
p	permeability	
STP	standard temperature and pressure	0°C and 100 kPa

Abbreviations

CNG	compressed natural gas
CNT	carbon nanotube
CMS	carbon molecular sieve
FSC	fixed-site-carrier
MMM	Mixed matrix membrane
MWCO	molecular weight cut-off
OED	orthogonal experimental design
PIM	polymer of intrinsic microporosity
PVA	polyvinylalcohol
PVAm	polyvinylamine
PSA	pressure swing absorption
PSf	polysulfone
SEM	scanning electron microscopy
TR	thermally rearranged

1 Introduction

The use of polymer membranes to selectively remove carbon dioxide (CO_2) from gas mixtures attracts great interest for many applications, such as natural gas sweetening, biogas upgrading, separation of CO_2 in enhanced oil recovery applications and separation of CO_2 from air in a spacecraft or enclosed space [1, 2]. Separation of CO_2 from flue gases has become increasingly important with the concerns about climate change. As membrane technology is energy efficient, environment friendly and at a low cost it has a potential to become an attractive technology for CO_2 separation [3].

1.1 Energy consumption and climate change

The U.S. Energy Information Administration (EIA) 2011 predicts a 53 percent growth in the world marketed energy consumption from 2008 to 2035 [4]. Most of the growth is due to the demand by strong economic growth in the non-OECD nations. The International Energy Outlook 2011 (IEO 2011) reference case predicts that fossil fuels will continue to supply much of the worldwide energy demand, but renewable energy will be the fastest growing energy source [4].

The transport sector is predicted to account for 82 percent of the 26.5 million barrels per day increase in worldwide oil consumption from 2008 to 2035 [4]. Unconventional resources (mostly Canadian oil sands, Brazilian biofuels and Venezuelan extra-heavy oil) will by then have grown to 12 percent of the total world liquids supply [4]. The worldwide consumption of natural gas is likely to increase from 3.14 to 4.79 trillion cubic meters (52 percent) from 2008 to 2035 [4]. Unconventional gas production (mostly shale gas) is estimated to cover 47 percent of the U.S. natural gas production in 2035 [4].

Energy-related CO_2 emission is likely to increase from 30.2 billion metric tons in 2008 to 43.2 billion metric tons in 2035. Coal continues to account for the largest share of CO_2 emissions, and much of the projected increase in CO_2 emissions occurs among the developing non-OECD nation. [4]. CO_2 is the most important greenhouse gas emission in the atmosphere caused by humans [5]. The atmospheric concentration of CO_2 in 2005 exceeds by far the natural range over the last 650,000 years (180 to 300 ppm) as determined from ice cores. Burning of fossil fuel is the primary source of increased atmospheric concentration of CO_2 since the pre-industrial period. The concentrations of methane and nitrous oxides in the atmosphere have also increased drastically since the industrial revolution. IPCC claims it is very likely that the observed increase in global temperature is due to the increase in greenhouse gas emissions caused by human activity. IPCC projects that the global surface temperature is likely to increase by 1.1 to 6.4 °C between 1990 and 2100 [5]. Warmer climate leads to sea level rise, melting of glaciers, more intense and longer droughts, more extreme winds and loss of biodiversity [5].

IPCC reported three possible options to reduce the greenhouse gas emissions: More efficient usage of energy, switch to renewable and nuclear energy and carbon capture and storage (CCS) [6]. This master's thesis will focus mainly on biogas upgrading since biogas will not contribute to an increased concentration of CO_2 in the atmosphere, and upgrading biogas to high purity of CH_4 is considered more energy efficient than to use biogas for electrical energy generation [7].

1.2 Biogas upgrading

Production of biogas is associated with high energy content per area and a flexible feedstock e.g. sludge from sewage treatment plants, organic waste at landfill sites and pure energy crops for on-farm biogas production [7]. Biogas is usually produced by anaerobic fermentation of the feedstock material and contains a mixture of 40-60 % methane (CH_4), the rest being mostly carbon dioxide (CO_2) with traces of water (H_2O), hydrogen (H_2), nitrogen (N_2), oxygen (O_2), and hydrogen sulphide (H_2S) [8]. The total biogas production in Europe was around fourteen billion cubic meters in 2006 and is expected to grow with a 10-20 percent rate each year. Combined Heat and Power (CHP) is often the preferred technology for utilizing biogas as an energy source, and is economically favourable if there are heat consumers nearby the plant. It is also possible to use biogas as a natural gas substitute by removing most of the CO_2, and this is considered as more energy efficient than CHP [7]. Upgraded biogas as a natural gas substitute can be injected to a natural gas grid or be used as fuel for vehicles run on compressed natural gas. The combustion will then not contribute to a higher concentration of carbon in the atmosphere [7].

Separating CO_2 from CH_4 can be achieved by several existing technologies: Absorption using physical or chemical wet scrubbing, pressure swing or temperature swing adsorption, cryogenic distillation or by different types of membranes [9]. Gas separations by membranes is preferred if there is a relatively low volumetric flow and a fairly high CO_2 concentration in the feed gas [7], which is usually the case at biogas plants. One of the major advantages for membrane separation is that upgraded biogas can be delivered at high pressure [8].

The majority of membranes currently used for gas separation are polymer membranes, due to their good separation performance and ease of inexpensive fabrication of hollow fiber or spiralled-wound membrane modules. But the separation performance of polymer membranes is usually less than a CO_2/CH_4 selectivity of 40 combined with a CO_2 permeance above 0.27 $m^3(STP)/(m^2.h.bar)$, which is required to be competitive with amine absorption [2]. Several breakthroughs in recent years have lead to the development of new membranes with high separation performance for CO_2/CH_4 mixtures, e.g. carbon molecular sieve membranes, zeolite membranes, mixed matrix membranes and polymers of intrinsic microporosity. Expensive and complicated fabrication processes, difficulties with up-scaling and durability problems are issues that must be solved before the full potential of these membranes is known [10].

Fixed-site-carrier (FSC) membranes have gained a lot of interest because they show high separation performance due to the facilitated transport mechanism. FSC membranes may selectively permeate CO_2 by a reversible reaction between CO_2 and a carrier in the membrane. Other gases such as H_2, N_2 and CH_4 will only permeate by the solution-diffusion mechanism [11]. Polyvinylamine (PVAm) has been reported as an excellent FSC membrane material as it contains over 30 % amino groups that serves as carriers for CO_2, the highest among all amine containing polymers [10]. The PVAm FSC membrane is at the development stage, but with the combination of good CO_2/CH_4 separation performance and the advantages of polymer membranes it is a promising process alternative for biogas upgrading.

1.3 Aim of the project

The principal objective of this work has been to further develop a high performance PVAm/PVA FSC membrane for biogas upgrading. To achieve high CO_2/CH_4 separation performance the following sub-objectives were stated:

- Optimization of membrane preparation conditions, including membrane thickness, reinforcement with carbon nanotubes, heat treatment temperature and duration. Identification of the relative importance of the variables and characterization of membranes by scanning electron microscopy.
- Investigation of operating parameters, including feed gas pressure, feed gas flow rate, sweep gas flow rate and relative humidity, to optimize the operating conditions to gain high CO_2/CH_4 separation performance and identify the relative importance of the parameters.
- Based on the prepared PVAm/PVA membranes at optimal conditions, process simulation was also to be conducted to evaluate membrane separation performance and process feasibility using Unisim and economic cost estimation.

The motivation for this project was to contribute to increased membrane CO_2 separation efficiency and optimum process design for making an environment friendly alternative to other separation processes.

1.4 Outline of thesis

This master's thesis includes 9 chapters. Chapter 1 gives a brief introduction to the project background, the advantages of FSC membranes for biogas upgrading and the aim of the project. Chapter 2 presents the fundamental theory of membranes and transport mechanisms. Chapter 3 describes the PVAm/PVA FSC membrane in detail from preparation to industrial application. Chapter 4 gives a detailed description of the experimental equipment, methods and procedures for preparation and characterization of PVAm/PVA FSC membranes. Chapter 5 presents the results and discussions of optimization of membrane preparation conditions and operating conditions and SEM analysis. Chapter 6 gives the simulation basis and the results and discussion of the process simulation. Chapter 7 presents the uncertainties in these experiments, chapter 8 gives the conclusions and chapter 9 gives suggestions for future work. Some supporting information and calculations are attached in the appendices.

Appendix A: Gas composition at Ecopro
Appendix B: Mass and energy balance of simulation case D
Appendix C: Economic calculations
Appendix D: Original project description
Appendix E: Risk assessment

2 Background and theory

2.1 Membrane definition

Membranes are semi permeable barriers that separate two liquid phases, two gas phases or a liquid and a gas phase by differences in transport rate through the membrane.

2.2 Benefits and challenges of membranes

Membranes can be used for a large number of separation processes, and the benefits of membranes can be summed up as the following [12]:

- Continuous separation.
- Low energy consumption.
- Membranes can easily be used in combination with other separation processes.
- Easy to scale up.
- No moving parts.
- Relatively easy to operate and control.

There are also some general challenges to be mentioned:

- Low membrane lifetime.
- Trade off between selectivity and flux.

2.3 Classification of membranes

A membrane can be made from many different materials, and synthetic membranes are tailor made for a specific separation process. Synthetic membranes can be divided into organic and inorganic membranes. Organic membranes are made of polymers and this group can be used for a large area of applications. Inorganic membranes can be made from glasses and ceramics. Different types of membranes can be made by different preparation techniques. Membranes are usually divided into three basic types: Porous membranes used for microfiltration and ultrafiltration, dense membranes used for gas separation, pervaporation and dialyses, and carrier-mediated membranes used for gas separation and liquid separation [12]. A schematic drawing of the basic types of membranes is given in Figure 2.1, but not all membranes and membrane structures are covered by this classification.

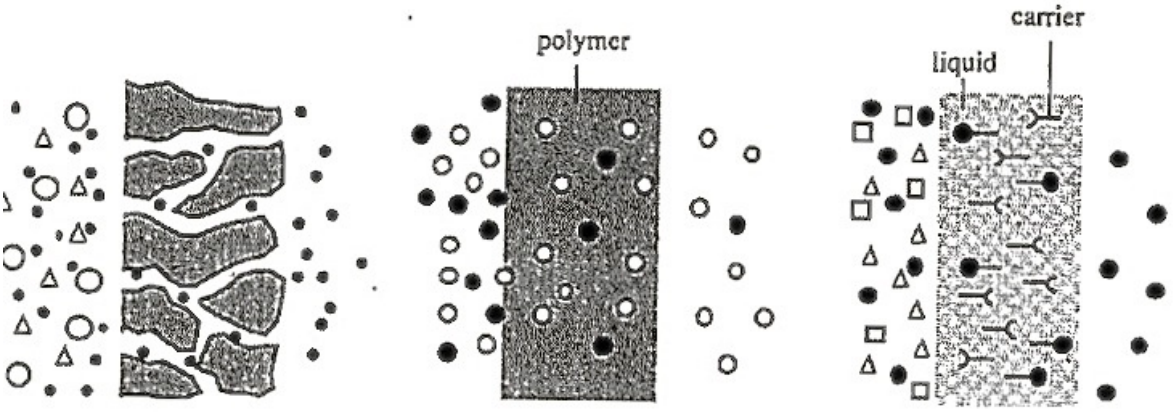

Figure 2.1 Schematic drawing of porous membrane (left), dense membrane (centre) and carrier-mediated membrane (right) [12]

Polymer membranes can be divided into two broad categories – rubbery and glassy. Rubbery polymers are soft and elastic, and segments of the polymer backbone can rotate freely around their axis. Glassy polymers have a more rigid, though structure, and steric hindrance give no space for segmental rotation of the polymer backbone [13].

2.3.1 Microporous membranes

A microporous membrane has much in common with a conventional filter when it comes to structure and function. It has a rigid, highly voided structure with interconnected pores [13]. Porous membranes have fixed pores in the range of 0.1-10 µm for microfiltration and 2-100 nm for ultrafiltration. Porous membranes separate two species by discriminating between particle sizes. The pore size determines which particles or molecules are retained and which are able to pass through the membrane, as illustrated in Figure 2.2. High selectivities can be obtained when particle size is large relative to the pore size [12].

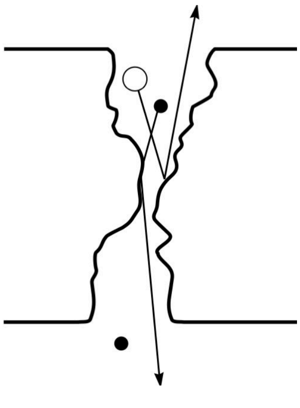

Figure 2.2 Selective permeation of molecules by molecular sieving [13]

Carbon molecular sieve (CMS) membranes are new high performance materials for gas separation. Selectivities obtained are usually higher than those of polymeric materials, and CO_2 transport though the membrane is kept high. CMS membranes are able to separate molecules with quite similar kinetic diameter e.g. oxygen (0.346 nm) and nitrogen (0.364 nm), and withstand harsh environments, like high temperature and acidic solutions [14]. CMS membranes are often brittle and module construction is a challenge. CMS membranes are also much more expensive than polymer membranes, so very high performance is needed for CMS membranes to be preferred over polymer membranes [15].

Polymers of intrinsic microporosity (PIMs) have recently been synthesized. PIMs are prepared with a backbone that has no conformational freedom, but also prevents packing and contains a large free volume fraction. PIMs represents a new class of microporous material that have interconnected pores less than 2 nm in size [15], and have received attention as potential membrane material for CO_2 separation.

Thermally rearranged (TR) polymers are prepared with tuned microvoids that can result in performance enhancement by selective transport trough polymer membranes. It is possible to control the average interchain spacing and free volume elements to increase the molecular sieving effect [16]. TR polymer membranes can separate CO_2 and CH_4 by letting CO_2 pass though hourglass-shaped pores connected by size selective throats that hinders the passage of larger molecules, e.g. CH_4 [15].

2.3.2 Ceramic, zeolite and metallic membranes

Ceramics have been developed for microfiltration and ultrafiltration purposes, but can also be prepared as dense membranes. They are usually made of aluminium, titanium or silica oxides. Ceramics have the ability to withstand high temperature and show high chemical stability. Ceramics are attractive materials for gas separation at high temperature, in the food industry and for pharmaceutical applications [13]. Zeolites are inorganic membranes that separate a mixture on the basis of molecular size and shape and/or adsorption properties. Selectivity based on adsorption/diffusion of permeants on the pore walls is illustrated in Figure 2.3. Molecules that adsorb and diffuse at the highest rate will cross the membrane faster than the weakly adsorbed and slow permeants. The molecules that have the largest diameter are usually the most soluble. As a result, the larger molecules will pass through the membrane, while the small molecules will be retained [12].

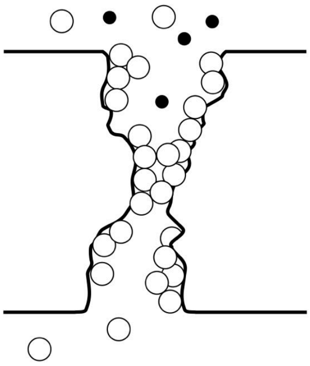

Figure 2.3 Permeation of condensable and noncondensable gas molecules though a membrane by selective surface flow [13]

Zeolites show high thermal and chemical resistance compared to polymer membranes, and can be prepared to obtain high selectivity. Zeolites have been reported with separation factors for H_2/N_2 up to 140. It is expected that mass-produced zeolite membrane modules will cost less than US\$1000/m^2 and is then competitive in both economics and performance with other membrane modules. Zeolites might also separate CO_2 and CH_4. A drawback is the possible formation of defects that gives larger pathways than the zeolite pores [15]. Recent zeolite membranes show drastic improvement in gas separation properties compared to current commercial polymer membranes, but they are still very expensive, difficult to process and difficult to handle [17]. Table 2.1 show a comparison of CO_2/CH_4 separation performance of inorganic membranes.

Metallic membranes are usually prepared by sintering of metal powders, but the commercial applications are limited [12]. Dense palladium-based membranes have been considered for hydrogen separation even though they cost 50 times more than polymer membranes [13].

Table 2.1 Comparison of membrane separation performance of some inorganic membranes

Membrane	CO_2/CH_4 Selectivity (-)	CO_2 permeance m^3(STP)/ (m^2.h.bar)	System	Δp (bar)	Ref.
Highly hydrophobic DDR- type zeolite membrane on a-alumina support	200	2.35	50/50 vol% CO_2/CH_4	2	[18]
Dual-layer hollow carbon fiber membrane with closely packed beta zeolite nanoparticles	128	0.03	50/50 vol% CO_2/CH_4	10	[19]
Dual-layer microporous silica membrane prepared by a novel sol–gel dip-coating process	200	0.82	50/50 vol% CO_2/CH_4	5.5	[20]

2.3.3 Mixed matrix membranes

Mixed matrix membranes (MMMs) consist of zeolite particles dispersed in a polymer matrix. MMMs are expected to combine the selectivity and chemical resistance of zeolite membranes with the low cost and easy processability of polymer membranes. Permeation occurs by a combination of diffusion through the polymer phase and the zeolite particles [13]. Inorganic and polymer membranes, together with MMMs and palladium membranes have been reported as promising membrane materials for CO_2/CH_4 separation [9]. The drawbacks of MMMs are high cost, difficulties of commercial scale manufacture as well as brittleness and interfacial defects between the two phases [15].

2.3.4 Liquid membranes

Liquid membranes consist of a liquid film immobilized and stabilized in a porous membrane. The porous membrane serves only as a support for the liquid film. Selectivity is obtained based on the distribution coefficients of the components to be separated in the liquid. Liquid membranes show rather low selectivities [12], but liquid membranes containing carriers to facilitate selective transport of gases or ions have been of interest for a long time [13]. Supported ionic liquid membranes have recently been considered for industrial gas separation applications, specially, low pressure systems such as upgrading of biogas and CO_2 capture from flue gases [21].

2.3.5 Nonporous, dense membranes

In nonporous, dense membranes permeants diffuse through a dense film by driving forces of pressure, concentration or electrical potential gradient. The separation of components in a mixture is based on the different rate of transport of the components through the membrane. The transport rate is determined by the solubility and diffusivity of the components in the membrane [13], as will be further discussed in chapter 2.5. This type of membranes can separate molecules that are in the same size range. Nonporous membranes are used in pervaporation, gas separation, reverse osmosis and dialysis [12]. Polymer membranes dominates the gas separation market because of low cost and good processability, even though they possess poor gas permeance and moderate selectivity [17]. For separation of CO_2 and CH_4, cellulose acetate membranes has slowly been replaced by polyimide and polyaramide membranes [2]. Polyimides were highlighted as an especially good membrane material for gas separation due to high selectivity and permeance, high thermal stability, chemical resistance and mechanical strength [9]. Important physical properties for polymer membranes are given in chapter 2.4.

2.3.6 Composite membranes

The transport rate of a species through a membrane is inversely proportional to the membrane thickness. A thin membrane has a high transport rate, which is desired. Anisotropic membranes consist of a thin surface layer supported by a more porous substructure, where most of the resistance is found in the top layer [12]. The surface layer determines the separation performance of the membrane, while the substructure provides mechanical support [13]. Composite membranes consist of a top dense layer, usually in the range 0.5-2.0 μm, on a porous support made from different materials, as indicated in Figure 2.4. An additional top layer can be coated on top of the selective layer to seal any defects. The advantage of composite membranes is that each layer can be adjusted to obtain high selectivity and permeation rate as well as chemical and thermal stability [12]. Lately, composite membranes have taken over more of the membrane market, because custom made polymers can be tailored to a specific gas separation problem [2].

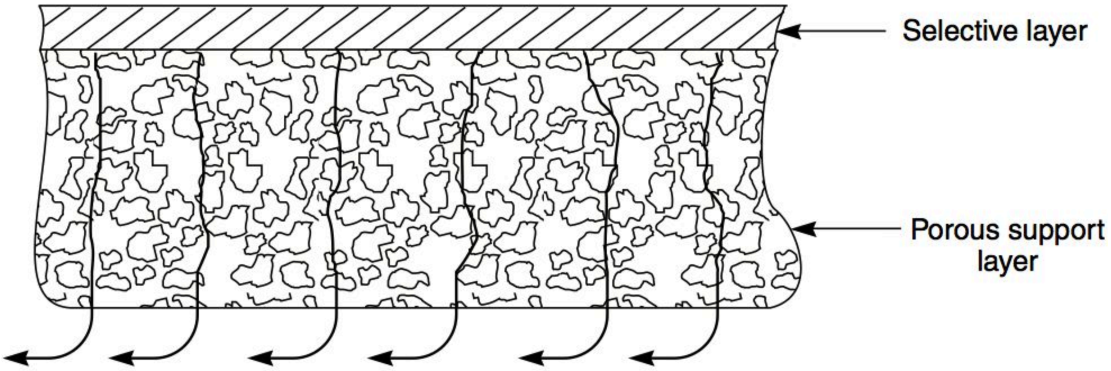

Figure 2.4 Two-layer composite membrane made by a thin selective layer coated on a porous support layer that provides mechanical strength [13]

2.3.7 Facilitated transport membranes

The transport through facilitated transport membranes is based on a specific carrier molecule that selectively favours the transport of one of the species present in the feed. Specially tailored carriers can obtain extremely high selectivity in gas and liquid separation [12]. A lot of research has been devoted to facilitated transport membranes, but it is suggested by some that only a limited attention should be given to these membranes in the future. Facilitated transport membranes was looked upon as a "long shot", and a breakthrough was needed to change the pessimistic view [1, 9]. Some authors find facilitated transport membranes to have proved promising results [2, 15]. A poly(amidoamide) dendrimer as an immobilized liquid membrane and a FSC membrane of crosslinked PVA/PVAm by Hägg et al. [11] have been highlighted as the most promising ones. Facilitated transport membranes will de described in detail in chapter 2.5.2 and chapter 3.

2.4 Important physical properties for polymer membranes

Gas transport through polymeric materials is affected by numerous polymer properties, such as morphology, fractional free volume, crosslinking, polymer polarity, defects, thermal treatment, glass transition temperature, average molecular weight, molecular weight distribution, degree of crystallization, etc. [9].

2.4.1 Crystallinity and glass transition temperature

Crystallinity affect mechanical properties and permeability of polymers. Crystallinity depends on regularity of the structure, which implicates that isotactic polymers may be very crystalline while atactic polymers are non-crystalline [12]. Thermal motion in rubbery polymers leads to high permeant diffusion coefficients. Thermal motion in glassy polymers is limited, and low permeant diffusion coefficient is expected. If the temperature of a glassy polymer is raised, at one point the thermal energy is sufficient to overcome the steric hindrance that prohibits segmental movement of the polymer backbone. This temperature, where a non-crystalline polymer changes from a glassy to a rubbery state, is defined as the glass transition temperature (T_g) [13]. T_g is determined by chain flexibility and chain interaction. Chain flexibility is mainly determined by the flexibility of the main chain. Vinyl polymers are very flexible since the main chain consists entirely of –C–C–bonds. High flexibility gives a low T_g. When aromatic groups are present in the main chain, as in polysulfone, T_g is high (190 °C). Polymers with low T_g are generally more permeable than polymers with high T_g, but there is roughly a trend. Other effects may also influence the permeability [12]. Diffusivity and permeance have been reported to have good correlations with T_g, while solubility is essentially independent of T_g. Side chain mobility might also affect T_g, and thereby also the transport parameters [22]. In general, rubbery polymers have moderate permeabilities and low selectivities while glassy polymers show low permeability and moderate selectivity. By combining a rubbery and a glassy polymer, a membrane can be adjusted to meet a specific separation problem [23].

The relative mobility of gases is characterized by their diffusion coefficient, and it differs significantly in rubbers and glasses. Diffusion coefficients in glassy polymers decrease more rapidly with increasing permeant size than in rubbers [13]. Figure 2.5 shows how diffusion coefficient, D (cm^2/s), and the size of the permeant are correlated for glassy and rubbery polymers. An almost linear relationship is observed between diffusion coefficient and the square of the kinetic diameter, d_k^2 (Å^2), of the permeant. It comes from an accepted model that suggests that activation energy of diffusion is proportional to the effective cross-sectional area of inert gas molecules. This relationship might not exist when CO_2 is transported through an amine-containing polymer membrane [22].

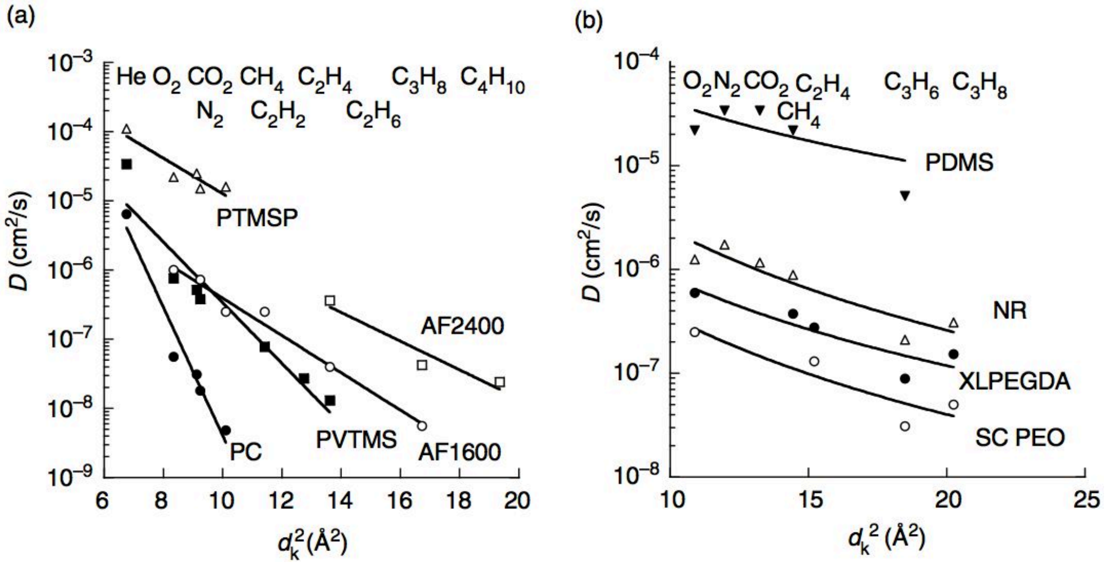

Figure 2.5 Correlation between diffusion coefficients on permeant kinetic diameter in a) glassy polymers: poly(1-trimethylsilyl-1-propyne) (PTMSP), polyvinyltrimethylsilane (PVTMS), polycarbonate (PC), per-fluorocarbon copolymers of 2,2-bis(trifluoromethyl)-4,5-difluoro-1,3-dioxole (BDD) and tetrafluoroethylene (TFE) containing 65 mol% BDD (AF1600) and 87 mol% BDD (AF2400), and b) rubbery polymers including crosslinked poly(ethylene glycol diacrylate) (XLPEGDA), semicrystalline poly(ethylene oxide) (SC PEO), natural rubber (NR) and polydimethylsiloxane (PDMS) [22]

The change in diffusion coefficient when the state of the polymer changes can be illustrated with the plasticization phenomenon. If a glassy polymer is exposed to a permeant that causes plasticization the polymer changes from a glassy state to rubbery state, to a solvent-swollen gel, and finally to a dilute polymer solution. The diffusion coefficient of the permeant increases with higher degree of plasticization and the respective matrix material changes observed. T_g is decreased by plasticization of the polymer, and the thermal energy overcomes the steric hindrance so that polymer chains have the freedom to rotate and the polymer becomes a rubber [13].

Rubbery membranes operate above T_g. Examples of rubbery polymers are polydimethylsiloxane, polyethylene glycol and silicone rubber. They often achieve their selectivity by difference in solubility, and larger molecules often permeate faster than smaller molecules. Rubbery membranes is then often used when the retentate stream with small molecules at high pressure is the desired product, as in syngas separation where it is desired to keep H_2 at elevated pressure, and let larger gases, like CO_2, transport through the membrane [24].

Glassy membranes operate below T_g. The polymer chain rearrangement operates at a very long time scale, and never reaches thermodynamic equilibrium. The polymer chains are packed imperfectly, leading to form microscopic voids in the polymer matrix. Within these voids Langmuir adsorption of gases occurs that increases the solubility. Examples of glassy membranes are polysulfone and Matrimid© polyimide.

Glassy polymer membranes often selectively permeate one species faster than another based on differences in diffusivity, and have been suggested for post-combustion CO_2 capture and natural gas sweetening [24].

A lot of work has been done to quantify the relation between polymer structure and permeation properties, but a complete understanding of the structure-property relationship does not exist today. A set of semi empirical rules allow permeation properties of related families of polymers to be correlated based on small changes in their chemical structures. The most common correlating tool is the polymer's fractional free volume [13].

2.4.2 Free volume

Free volume in polymers is defined as the volume not directly occupied by atoms constituting the polymer chains. It is a characteristic of all solid materials, but in the case of glassy polymers and their application as membrane material it is of particular interest. Polymers below T_g are in a non-equilibrium state and may give rise to a time-dependent relaxation phenomena or physical aging, leading to a gradual decrease of the free volume. The free volume cannot be measured directly, but calculated by investigation of the surroundings [24]. The polymer's fractional free volume, υ_f (cm^3/cm^3), is usually defines as [13]:

$$\upsilon_f = \frac{\upsilon - \upsilon_0}{\upsilon} \qquad (2.1)$$

where υ is the specific volume of the polymer (cm^3/g), and υ_0 is the volume occupied by the polymer molecules themselves (cm^3/g). The free volume of a polymer is then the sum of the spaces between the polymer chains, the volume not occupied by macromolecules [13]. In the glassy state ($T < T_g$) the free volume fraction is almost constant, while it increases above T_g with the following correlation [12]:

$$\upsilon_f = \upsilon_{f,T_g} + \Delta\alpha(T - T_g) \qquad (2.2)$$

where $\upsilon_{f,Tg}$ is the free volume fraction at T_g, $\Delta\alpha$ ($cm^3/(cm^3.K)$) is the thermal expansion coefficient, T (K) is the temperature and T_g (K) is the glass transition temperature. Figure 2.6 shows polymer volume as a function of temperature, and illustrates the concept of free volume. At high temperature the polymer is in a rubbery state, and some unoccupied spaces – free volume – exist between the polymer chains because the polymer does not pack perfectly. The free volume is higher in the rubbery state than in the glassy state, since the packing density is higher in a crystal lattice than in an amorphous, rubbery structure. The free volume is a small fraction of the total volume, but it allows some rotation of the polymer backbone at high temperatures. The free volume decreases with decreased temperature. At the glass transition temperature, the free volume is decreased to a point where the polymer chains no longer can rotate freely. When the motion of the polymer chains stop, the free volume freezes into the polymer matrix. When continuingly decreasing the temperature, a decrease in occupied volume is observed as the vibrational energy of the groups forming the polymer decreases, but the free volume elements remain essentially constant. Therefore, in a glassy polymer, the free volume consists of the free volume elements caused by incomplete packing of polymer chains and the excess free volume frozen into the polymer matrix because polymer chains cannot rotate [13].

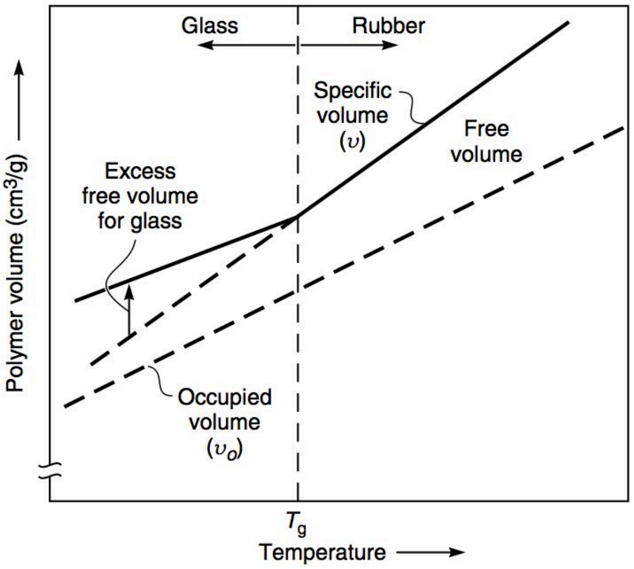
Glass
Rubber
Specific volume (υ)
Free volume
Excess free volume for glass
Occupied volume (υ_o)
Polymer volume (cm^3/g)
T_g
Temperature

Figure 2.6 The change in volume as a function of temperature for a typical polymer [13]

There has not been reported a clear relationship between a polymers free volume and its permeation properties, but there is a correlation between the free volume and the gas diffusion constant within a single class of materials [13]. Diffusion coefficients are very sensitive to the free volume in a polymer. Other factors that influence T_g can be both intermolecular interactions and intramolecular interactions. Intermolecular interactions may be influenced by the free volume, while intramolecular interactions are more likely to be influenced by energy barriers to rotation than on the free volume. Correlations of diffusivity and permeance with T_g do not, to a great enough extent, include the effect of free volume. Consequently, free volume is usually viewed as more accurate than T_g for correlating transport properties in polymers [22].

It is generally accepted that mass transport in a dense polymer membrane is described by a combination of solution and diffusion of permeants. For a membrane that is not swollen, nor plasticized, the amount of permeant that can dissolve in the polymer matrix is dependent on the available sorption sites and typical dual sorption behaviour is often observed. The number of Langmuir sorption sites is strongly related to the free volume distribution of the polymer. Permeant diffusion also depends on the free volume distribution as it diffuses through the polymer by a kind of “hopping” mechanism where the permeant moves around in a free volume element until enough energy has been obtained to “hop” to a neighbouring free volume element. The energy barriers depend on the rigidity of the polymer matrix, the size of the molecule and how the free volume elements are connected, among others. The required energy increases rapidly as the size of the permeant increases as a consequence of lower diffusion coefficient [24].

It is known that glassy polymer membranes can separate gases by molecular sieving. Since the transport of the permeant takes place through the free volume in the polymer a correlation between free volume fraction and transport properties have also been proposed [24]:

$$P = A \cdot \exp(-B / \upsilon_f) \tag{2.3}$$

where P is the permeability (Barrer), A and B are empirical constants which may vary from gas to gas and from one polymer to another, and υ_f is the fractional free volume. This type of correlation has shown to fit quite well with experimental values for structurally related polymers, as illustrated in Figure 2.7. For very different families of polymers, the correlation is more scattered, but follows the same permeability dependence on free volume [22].

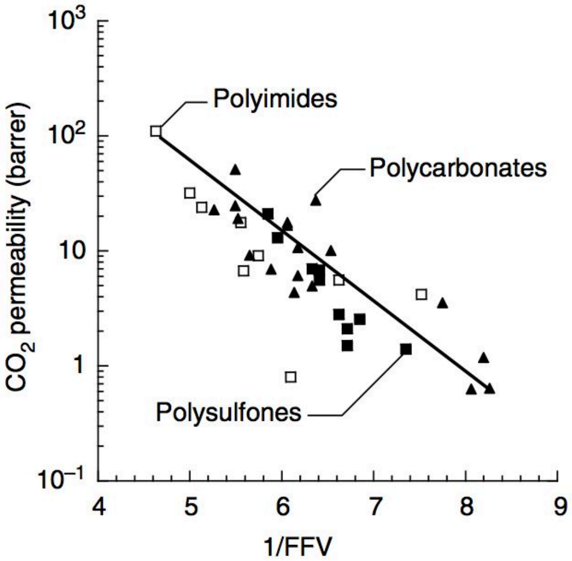

Figure 2.7 Correlation between CO_2 permeability and fractional free volume in glassy aromatic polysulfone, polyimides and polycarbonates. FFV denotes fractional free volume, υ_f [22]

2.4.3 Swelling

Swelling is a very important factor in transport through non-porous membranes. Swelling is a result of interaction between the permeating specie and the polymer. The degree of swelling is defined as the weight fraction of the permeating component inside the membrane relative to the weight fraction of dry polymer. By increasing from a low degree of swelling to a high degree of swelling the diffusion coefficient for a low molecular weight component can typically increase with up to 10 orders of magnitude [12]. Membranes that contain ionic groups tend to absorb water, and charge repulsion might cause the membrane to swell excessively. Highly crosslinked membranes might limit swelling. However, highly crosslinked membranes makes polymer brittle and hard to handle [13]. Swelling can cause increased permeance and reduced selectivity, but selectivity can also be increased by crosslinking [22].

2.4.4 Plasticization

One of the main problems with polymer membranes for gas separation is gas and vapour induced plasticization. Plasticization results in a less rigid membrane with higher polymer chain mobility. Almost all membranes undergo swelling and plasticization under high CO_2, H_2S, SO_2 and organic vapour partial pressure, and the result is often lower membrane separation performance. The mobility of the polymer is highest at the end of the chains. Plasticization may therefore occur more easily at the chain ends than at a section of the chain inside the polymer macromolecule. Reducing the number of chain ends in a polymer might lead to a higher plasticization resistance. Crosslinking can reduce the number of chain ends, and is therefor a common way to reduce plasticization, but there is a trade-off between crosslinking density and gas permeance [24]. As the amount of sorbed permeates increases, the polymer chains are forced apart to accommodate permeant molecules. Plasticization increases the polymer chain spacing and chain mobility. Diffusion coefficients and permeance will then increase. Higher concentration of permeants in the feed stream will cause increased plasticization. Dual sorption theory and mobility models predict decreased permeability in glassy polymers with increased feed pressure, but plasticization might cause the permeability to increase [22]. In some cases plasticization might cause an increase in both selectivity and permeance. A plasticized "reverse selective membrane" (selectively permeates the largest molecule) will have reduced membranes size-sieving ability, but CO_2 sorption will increase with higher free volume at elevated pressure [22].

Polyimides and cellulose acetate are typically used for natural gas sweetening. These membranes are exposed to CO_2-induced plasticization, and the selectivity is less than the ideal selectivity of around 30, retrieved from pure gas measurements. To prevent the membrane from plasticization, expensive pre-treatment is necessary. Perfluorinated Cytop membrane have shown to be a promising alternative for natural gas sweetening at harsh conditions even though the selectivity is lower than for polyimides and cellulose acetate as this membrane does not undergo plasticization and keeps a high level of permeance [22].

2.4.5 Crosslinking

A crosslinked polymer is a polymer in which the polymer chains are connected in a network between connecting sites. It is formed by reactions between sites or groups on existing macromolecules or by interaction between existing macromolecules. The term "crosslinking" can be used to describe a random network of polymer segments. In random crosslinked polymer the solubility in organic solvents gradually decreases with increased crosslinking density, and this might be necessary in some cases to prevent the polymer from dissolving. High crosslinking density can result in a decline in gas permeance, while selectivity might increase [13, 24].

Generally, the aim of crosslinking is to enhance selectivity and prevent swelling and plasticization. Several crosslinking techniques have been reported for polyimides. Monoesterification and transesterification reactions of carboxylic acid, imide ring-opening reactions, grafting by epoxy reactions, UV-induced crosslinking and Diels-Aldrich-type cyclization reactions have been reported. Excess crosslinking might lead to a reduction in both permeance and selectivity [24].

2.5 Gas transport mechanisms through polymer membranes

When molecules that are to be separated do not differ much in size, as for many gas separation cases, a porous membrane may not be effective. For these cases dense membranes are often used. They are not completely dense as there are molecular sized pores (free volume) that allow transport [12]. Solution-diffusion mechanism is often applied to dense membranes, while facilitated transport mechanism is applied for FSC membranes.

2.5.1 Solution-Diffusion mechanism

The pore diameter is in the range of the thermal motion of the polymer chains when the pore diameter is less than 5 Å. Permeation is then a diffusive process controlled by the motion of the polymer chains [22]. The solution-diffusion model applies to pervaporation, reverse osmosis and gas permeation in dense polymer membranes [13].

The starting point of the description of diffusion in membranes is the proposition that the driving forces of pressure, temperature, concentration and electrical potential are interrelated and that the overall driving forces for diffusion is the gradient in chemical potential of the permeant [13]. The flux, J_A ($m^3(STP)/(m^2.h)$), of component A is described as in equation 2.4.

$$J_A = -L_A \frac{\mathrm{d}\mu_A}{\mathrm{d}x} \tag{2.4}$$

where $\mathrm{d}\mu_A / \mathrm{d}x$ (J/mol.m) is the chemical potential gradient of component A, and L_A (m^3(STP).mol/(J.m.h)) is the proportionality coefficient. Restricting the driving forces to concentration and pressure gradients, the chemical potential, μ (J/mol), is written as [13]:

$$\mathrm{d}\mu_A = RT\mathrm{d}\ln(\gamma_A n_A) + \nu_A \mathrm{d}p \tag{2.5}$$

where n_A is the mole fraction (mol/mol), γ_A is the activity coefficient (mol/mol), p is the pressure (Pa), and ν_A is the partial molar volume (m^3/mol). Subscript *A* refers to component A. R is the universal gas constant (J/mol.K) and T is the temperature (K).

Several assumptions are made in any permeation model. The first assumption is usually that the gases on either side of the membrane are in equilibrium with the membrane material at the interface. This gives a continuous gradient in chemical potential, and implies that absorption and desorption of gas molecules are much higher than the rate of diffusion through the membrane. This is the case in most membrane processes, but fails when it comes to facilitated transport membranes, where interfacial absorption can be slow [13]. The second assumption concerns the pressure and concentration gradients in the membrane. The solution-diffusion model assumes that when pressure is applied across the membrane, the pressure within the membrane is constant and equal to the feed gas pressure ($p_A = p_{A,0}$). This implies that solution-diffusion membranes transmit pressure in the same way as liquids. A consequence of this is that pressure across the membrane is represented as a concentration gradient over the membrane, and that concentration gradient is the only contribution to the chemical potential gradient. The chemical potential across the membrane is expressed as a smooth gradient in solvent activity ($\gamma_i n_i$) [13], as illustrated in Figure 2.8.

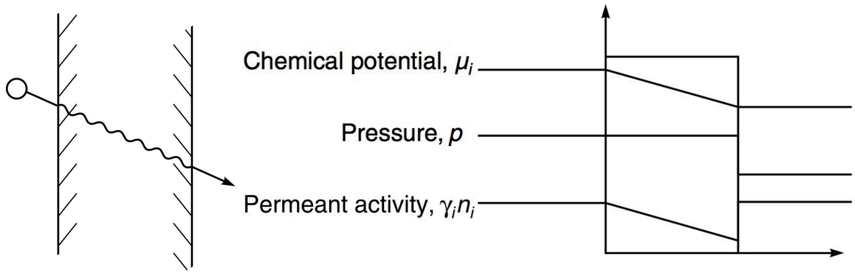
Chemical potential, μ_i
Pressure, p
Permeant activity, $\gamma_i n_i$

Figure 2.8 The driving force gradients for permeation through a membrane according to the solution-diffusion mechanism [22]

Constant pressure removes the latter term in equation 2.5. The gradient provides a flow expressed by combining equation 2.4 and 2.5 [22]. Without a pressure gradient, this gives:

$$J_A = \left(\frac{-RTC_A L_A}{\gamma_A n_A} \right) \left[\frac{\mathrm{d}(\gamma_A n_A)}{\mathrm{d}x} \right] \tag{2.6}$$

In equation 2.6, the gradient of component A is given as a gradient in mole fraction. It is more practical to write the flux equation in terms of concentration (m^3(STP)/m^3) defined as:

$$C_A = m_A \rho v_{A,STP} n_A \tag{2.7}$$

where m_A is the molecular weight (g/mol), ρ is the molar density (mol/m^3), $v_{A,STP}$ is the partial molar volume at STP (m^3(STP)/g) and n_A is the mole fraction (mol/mol). Subscript A refers to component A. By substituting mole fraction gradient with concentration gradient equation 2.6 becomes [22]:

$$J_A = \left(\frac{-RTL_A}{\gamma_A} \right) \cdot \left[\frac{\mathrm{d}(\gamma_A C_A)}{\mathrm{d}x} \right] \tag{2.8}$$

Assuming that γ_A is constant gives:

$$J_A = -RTL_A \cdot \frac{\mathrm{d}C_A}{\mathrm{d}x} \tag{2.9}$$

Equation 2.9 now has the same form as Fick's first law where the term RTL_A can be replaced by the diffusion coefficient D_A (m^2/h) as in equation 2.10. Diffusion can be described as statistical molecular transport that results from random molecular motion. The direction of diffusion is given by the concentration gradient direction. Diffusivity is a kinetic parameter and depends on the geometry of the penetrating molecules. The diffusion coefficient is also dependent on the concentration of interactive systems that can make large molecules have a large diffusion coefficient. It is assumed that the gas diffusion coefficient is constant [12]. Gas diffusivity increases with decreased gas molecular size, increased polymer free volume, increased polymer chain flexibility, and decreasing with polymer-permeant interactions [25].

$$J_A = -D_A \frac{\mathrm{d}C_A}{\mathrm{d}x} \tag{2.10}$$

Integrating over the membrane thickness gives:

$$J_A = \frac{D_A(C_{A,0} - C_{A,\ell})}{\ell} \tag{2.11}$$

where $C_{A,0}$ is the concentration of component A on the feed side, $C_{A,\ell}$ is the concentration of component A on the permeate side and ℓ is the membrane thickness (m). The sorption of ideal systems, where the solubility of the gas in the membrane is independent of concentration, can be described by Henry´s law (linear sorption isotherm). Solubility is a thermodynamic parameter that gives a measure of how much of the permeant that is sorbed by the membrane at equilibrium. The solubility of gases in polymers is generally low (<0.2 vol%) [12]. In general, solubility increases with increasing condensability of the penetrant (i.e. higher critical temperature) and more favourable interactions with the polymer [25]. By defining a gas phase sorption coefficient S_A (m^3(STP)/(m^3.bar)) the concentration of component A at the feed interphase of the membrane can be written as:

$$C_{A,0} = S_A \cdot p_{A,0} \tag{2.12}$$

where $p_{A,0}$ is the partial pressure (bar) of component A on the feed side. Equation 2.12 implicates that the concentration of gas in polymer is proportional to the applied pressure. This is often the case for gases in elastomers. In glassy membranes the sorption isotherm is non linear, and might be described by the dual sorption theory. In the dual sorption theory it is assumed that two sorption mechanisms occurs at the same time, one according to Henry´s law and one according to Langmuir sorption. The concentration of gas in polymer can then be described as the sum of both sorption models. It is difficult to understand how two sorption mechanisms can occur at the same time, but the dual sorption model often gives a good description of experimental data [12]. In the exact same way, the concentration of component A at the membrane/permeate side interface can be written as

$$C_{A,\ell} = S_A \cdot p_{A,\ell} \tag{2.13}$$

Combining equation 2.11, 2.12 and 2.13 gives:

$$J_A = \frac{D_A S_A(p_{A,0} - p_{A,\ell})}{\ell} \tag{2.14}$$

The product D_AS_A is often shortened to a permeability coefficient, P_A (m^3(STP).m/(m^2.h.bar)) [12]:

$$P_A = D_A \times S_A \tag{2.15}$$

By introducing permeability, the flux equation can be written as:

$$J_A = \frac{P_A}{\ell}(p_{A,0} - p_{A,\ell}) \tag{2.16}$$

where $p_{A,0}$ and $p_{A,\ell}$ (bar) is the partial pressure of component A on the feed side and the permeate side, respectively, and ℓ is the thickness of the membrane. The flow rate across a membrane is proportional to the difference in partial pressure and inversely proportional to the membrane thickness. Equation 2.16 is widely used to accurately predict the properties of gas permeation membranes, and different versions of this equation are used for calculating the flux of a component through many types of membranes. The derivation of equation 2.16 clarifies the assumptions behind the equation for gas transport by the solution-diffusion mechanism. First, there is only a concentration gradient inside the membrane. The pressure is assumed constant and equal to the feed pressure. Second, the absorption of a component is proportional to its partial pressure, but independent of the total gas pressure [13]. It is an implicit assumption that the permeability coefficient is constant, and independent of partial pressure of component A. This is invalid for swollen and plasticized membranes. In these cases, the fundamental processes are still occurring, but concentration dependent diffusion and sorption effects must be taken into account [22].

Temperature has a large effect on the transport rate, and the solubility of non-interactive gases in polymers gives an Arrhenius equation for the temperature effect as shown in equation 2.17 [12].

$$S = S_0 \exp(-\Delta H_s / RT) \qquad (2.17)$$

S is the solubility (m^3(STP)/m^3), ΔH_s (J/mol) is the heat of solution, R is the universal gas constant (J/mol.K), T is the temperature (K) and S_0 (m^3(STP)/m^3) is a temperature independent constant. The heat of solution is the sum of the heat of mixing and heat of condensation. It can be both exothermic and endothermic. For CH_4 the heat of solution is a small positive value, so solubility increases slowly with increased temperature [12]. A similar temperature effect can be observed for the diffusion of gases in polymers as shown in equation 2.18 [12].

$$D = D_0 \exp(-E_d / RT) \qquad (2.18)$$

E_d (J/mol) is the diffusion activation energy that is dependent on the gas molecule geometry, R is the universal gas constant, T is the temperature and D_0 (m^2/h) is a temperature independent constant. A combination of equation 2.15, 2.17 and 2.18 gives the permeability coefficient that has a temperature dependency that can be represented by an Arrhenius type of equation as shown in equation 2.19 [12].

$$P = P_0 \exp(-E_p / RT) \qquad (2.19)$$

$E_p = \Delta H_s + E_d$ (J/mol) is the permeation activation energy that depends on chemical and physical structure of the polymer and interactions between the gas and the polymer. P_0 (m^3(STP).m/(m^2.h.bar)) is a temperature independent constant. For small non-interactive gas molecules the temperature effect on the permeability coefficient is mostly determent by diffusion, since solubility does not vary much with temperature [12].

The selectivity describes the membrane ability to separate two gases. The selectivity is a separation factor that can be described as in equation 2.20 [12].

$$\alpha_{A/B} = \frac{y_A / y_B}{x_A / x_B} \tag{2.20}$$

y_A and y_B (-) is the mole fraction A and B in the permeate, while x_A and x_B (-) is the mole fraction of component A and B on the feed side of the membrane. The selectivity is grater than unity, since no separation is achieved if $\alpha_{A/B}=1$. The ideal selectivity is given by the ratio of the permeability coefficients [12]:

$$\alpha_{A/B \text{ ideal}} = \frac{P_A}{P_B} \tag{2.21}$$

By combining equation 2.15 and 2.21 the selectivity can be written:

$$\alpha_{A/B \text{ ideal}} = \frac{D_A}{D_B} \times \frac{S_A}{S_B} \tag{2.22}$$

where D_A/D_B is the diffusivity selectivity and S_A/S_B is the solubility selectivity. The diffusivity selectivity of the membrane material is generally governed by the relative mobility of the permeants. The solubility selectivity is generally governed by the chemistry of the membrane material [13]. The separation of gases is mainly achieved by diffusivity selectivity, since it is more sensitive to polymer structure and changes in a broader range than solubility selectivity [10]. The magnitude of diffusivity selectivity highly depends on whether the membrane material is above or below T_g. In glassy polymers, the diffusivity term is usually dominant. In rubbery polymers, the solubility term is usually dominant [13].

2.5.2 Facilitated transport mechanism

Introducing a carrier in the membrane that forms a complex with a specific gas component can enhance the flux of one of the gas components through the membrane. Because of the selectivity of the carriers, carrier facilitated membranes often achieve spectacular separation between closely related species [13]. Facilitated transport membranes offer an attractive method of achieving high selectivities while maintaining high gas permeance. A specific gas component will be transported through the membrane by the facilitated transport mechanism and by permeant physical dissolution and diffusion [26, 27]. The mechanism for facilitated transport membranes is frequently discussed, as will be seen in this chapter.

There are two types of carriers, a schematic drawing of the two cases is given in Figure 2.9: Mobile carriers (liquid membranes) that can diffuse freely across the membrane, and fixed carriers where the carriers are immobilized in the membrane matrix and cannot move. Mobile carriers reacts with the targeted gas component on the feed side of the membrane, moves across the membrane, and release the component on the permeate side. The diffusivity in the mobile carrier case is higher than in the fixed carrier case, since it involves fewer steps. A membrane system might be an intermediate of the two extremes, e.g. for a gel or a swollen polymer.

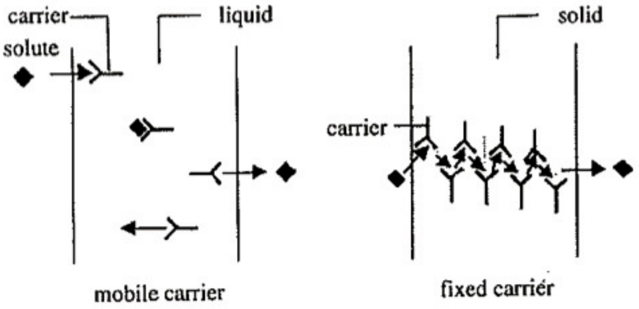

Figure 2.9 Schematic drawing of mobile carrier membrane (left) and fixed carrier membrane (right) [12]

Figure 2.9 (left) shows the mechanism of facilitated transport mechanism with mobile carriers. The steps involved in transport of component A can be distinguished as the following [12]:

1. Solute dissolves in the membrane.
2. Complexation reaction between solute and the carrier at the feed side/membrane interphase forming a solute-carrier complex.
3. The complex diffuses across the membrane.
4. A decomplexation reaction takes place at the membrane/permeate side interphase.
5. The solute is released to the permeate stream.
6. The carrier diffuses back.

Facilitated transport is characterized by either a reversible chemical reaction or formation of a complex and a diffusion process. One approach to model the process is to assume that the rate of reaction is fast compared to the rate of diffusion. The assumption is easy to verify. Diffusion is rate determining if the flux is inversely proportional to the membrane thickness. If sorption/desorption is rate determining the flux would be constant and independent of membrane thickness. To assume a fast reaction rate relative to diffusion rate is a good assumption in many cases [13]. In carrier-mediated membranes, enhanced transport of permeant component A is observed in the presence of a carrier C. Component A and C form a complex AC, as shown in equation 2.23, that will diffuse through the membrane [12].

$$A + C \Leftrightarrow AC \tag{2.23}$$

Component A will diffuse through the membrane partly by free diffusion of pure component A, and partly by solute-carrier diffusion as the complex AC. The total flux will be the sum of the two as given in equation 2.24 [12]. Hence an increased transport of component A can be observed.

$$J_A = \frac{D_A}{\ell}\left(C_{A,0} - C_{A,\ell}\right) + \frac{D_{AC}}{\ell}\left(C_{AC,0} - C_{AC,\ell}\right) \tag{2.24}$$

J_A (m^3(STP)/(m^2.h)) is the total flux of component A. The first term is the diffusion of A according to Fick's first law, as given in equation 2.11. In some cases the first term can be ignored, due to much faster transport of component A as a solute-carrier-complex than as free passive diffusion of pure A [13]. The latter term represents the facilitated diffusion where D_{AC} is the diffusion coefficient of the solute-carrier-complex. ℓ (m) is the membrane thickness. $C_{AC,0}$ (m^3(STP)/m^3) and $C_{AC,\ell}$ (m^3(STP)/m^3) is the concentration of AC at the membrane interface on feed and permeate side, respectively. $C_{AC,0}$ will be much greater than $C_{A,0}$ when the permeation rate of the complex is much higher than of the uncomplexed permeant. A schematic drawing of the diffusion of component A is given in Figure 2.10.

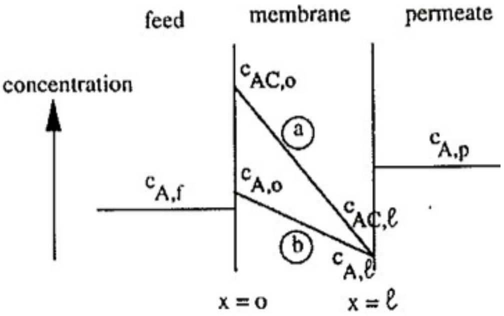

Figure 2.10 Schematic drawing of diffusion of component A via Fick's first law (curve b) and facilitated diffusion (curve a) [12]

When facilitated carriers were first introduced, the carriers were held in a liquid phase, immobilized in the pores of a polymer film. This configuration made the membrane suffer from degradation and instability problems [28-30]. One approach to overcome these limitations was the use of ion-exchange membranes as supports. LeBlanc et al. [31] reported that degradation of carriers was minimized when facilitated carriers were kept within the membrane matrix using electrostatic forces. Liquid loss no longer meant loss of the complexing agent. Singly protonated ethylenediamine cations were used as carriers for CO_2 as shown in equation 2.25.

$$CO_2+2^+H_3N\text{-}C_2H_4\text{-}NH_2 \Leftrightarrow {}^+H_3N\text{-}C_2H_4\text{-}NHCOO^- + {}^+H_3N\text{-}C_2H_4\text{-}NH_3^+ \qquad (2.25)$$

Another method to fix the carriers was reported by Matsuyama et al. [32-34]. High CO_2/CH_4 selectivity was found by utilizing membranes prepared by the plasma-graft polymerization technique. They were multilayer composite membranes consisting of a top plasma polymer layer made of diisopropylamine monomer and a substrate consisting of a silicone skin layer and a porous polyimide support. The membranes showed high permeance due to the thin selective layer, and a moderate CO_2/CH_4 selectivity [32]. Results from testing a membrane of 2-(N,N-dimethyl)aminoethyl methacrylate (DAMA) on a microporous polyethylene support showed high CO_2/N_2 selectivities (130) and high CO_2 permeance when the membrane was swollen with water. It was suggested that the dry membrane was a FSC membrane, and weak acid-base interactions between CO_2 and amine groups secured the facilitated transport of CO_2. The wet membrane, on the other hand, contained tri-substituted amine, DAMA, that could not form carbamate since there was no hydrogen atom to be displaced by CO_2. It was assumed that water-swollen membrane transported CO_2 in the form of HCO_3^- (see Figure 2.11) as would be the case for a supported liquid membrane. The water-containing membrane is not a FSC membrane in the strict sense, but should be called a fixed-reaction-site membrane, or catalyst membrane [33]. It was stated as possible that fixed-reaction-site membranes could achieve selectivities and CO_2 fluxes close to those of mobile carrier membranes. Matsuyama et al. discovered that CO_2 permeance of a membrane in wet state is at least one order of magnitude larger than that of the membrane in dry state, and CO_2/N_2 selectivity of the wet membrane is about twice of the dry membrane [33].

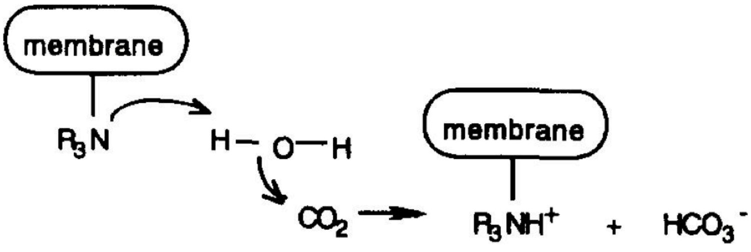

Figure 2.11 Facilitated transport mechanism proposed by Matsuyama et al. [33]

Yoshikawa et al. [35] investigated facilitated transport of CO_2 through a poly(4-vinylpyridine-co-acrylonitrile) membrane, with pyridine acting as a fixed carrier. Acid-base interaction between CO_2 and the fixed carrier was confirmed and they also assumed that the carrier acted as a week base catalyst for the CO_2 hydration reaction and that CO_2 is transported as HCO_3^-. Cussler et al. [29] developed a model to describe transport across FSC membranes. It was assumed that the reacting permeate can only be transported by the complexing agent if two complexing agents are close enough to exchange the reacting permeate between the two. The mechanism is described like a solute Tarzan, illustrated in Figure 2.12, swinging from one carrier vine to the next. The mechanism is also called the “hopping” mechanism. Noble et al. derived a generalized microscopic mechanism for the facilitated transport of a neutral solute through a FSC membrane. The model suggested that facilitated transport was possible even when the fixed sites are too far apart for direct hopping. Mass transfer between sites was thought to occur by simple solute diffusion [28, 36].

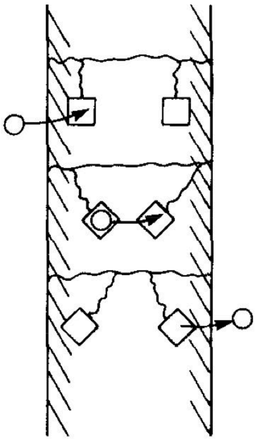

Figure 2.12 Facilitated transport mechanism in a fixed-site-carrier membrane [29]

Cai et al. [37] reported a polyallylamine/polyvinylalcohol blend membrane on a polysulfone support where CH_4 transport behaviour was consistently with solution-diffusion mechanism, while CO_2 was believed to be transported by the facilitated transport mechanism for primary amine group containing compounds, as shown in equation 2.26 and 2.27, as previous researchers have proved [38].

$$\mathrm{RNH_2 + CO_2 \rightleftharpoons RNHCOO^- + H^+} \quad (2.26)$$

$$RNH_2 + H^+ \rightleftharpoons RNH_3^+ \tag{2.27}$$

CO_2 permeance was reported as remarkably high at low pressure, since CO_2 permeance due to solution-diffusion mechanism is very low, so a majority of the transport is contributed by CO_2-carrier-complex permeation. CO_2 permeance dropped rapidly with increased pressure due to less contribution from CO_2-carrier-complex permeation and more contribution from solution-diffusion mechanism. The facilitated transport mechanism of CO_2 was also investigated by Kim et al. [11]. The theory of CO_2 not directly interacts with the fixed amine groups, but carrier-transported in the form of HCO_3^- was adapted. It was assumed that CO_2 is selectively transported as a bicarbonate anion through the water-swollen FSC membrane. It was proposed that permeation by this mechanism could achieve high selectivity and permeance of CO_2 [11]. A schematic diagram of the proposed mechanism is given in Figure 2.13.

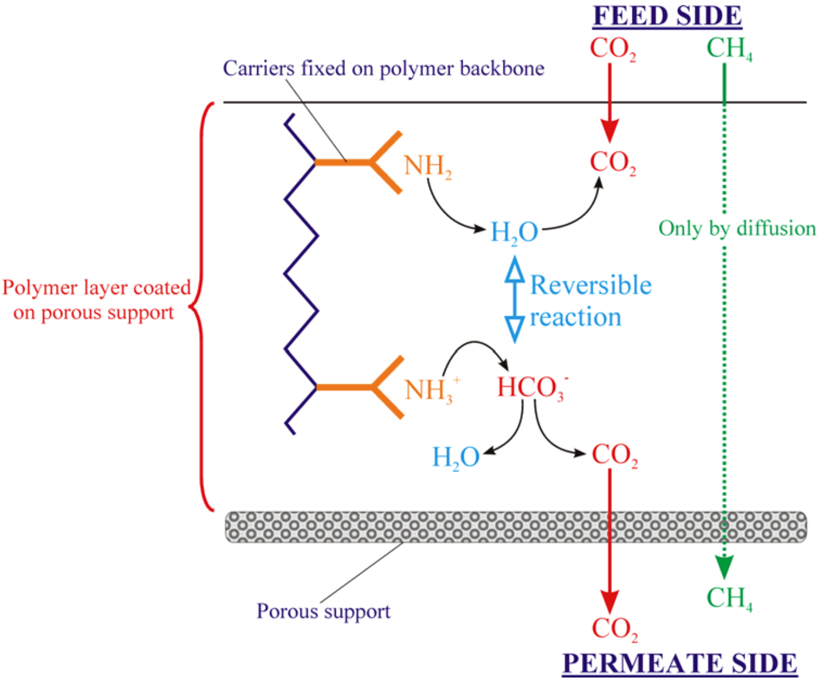

Figure 2.13 A proposed mechanism of facilitated transport in a fixed-site–carrier membrane [11]

CO_2 transport through PVAm/PVA blend membrane follow three steps: 1) dissolution and reaction of CO_2 with water and amino groups to form HCO_3^- at the feed side, 2) diffusion of HCO_3^- through the membrane, 3) decomposition of HCO_3^-, and desorption of CO_2 on the permeate side of the membrane [39]. The week basic amino group will initiate the reaction, but will not be consumed during the reversible reaction. The final reaction with amino groups taking the role as a catalyst, can be described as in equation 2.28 [10].

$$H_2O + CO_2 \rightleftharpoons H^+ + HCO_3^- \tag{2.28}$$

CO_2 does not interact directly with the amino "carriers", but diffuses through the membrane as HCO_3^- in a water-swollen membrane. The mobility in the PVAm/PVA blend membrane is comparable to that of mobile carrier membranes, and a high CO_2 permeance is expected. By simultaneously achieving high CO_2/CH_4 selectivity, the PVAm/PVA FSC membrane is expected to be a well-suited membrane for biogas upgrading.

2.5.3 Gas transport through composite membranes

Composite membranes for gas separation are often asymmetric membranes with a dense top layer. Different transport mechanism can be distinguished depending on the membrane structure. Solution-diffusion mechanism and possibly facilitated transport mechanism occurs in the dense top layer, which is usually the rate-determining step. Knudsen flow and viscous flow occurs in the narrow and wide pores of the support, respectively. Viscous flow occurs when the pore sizes are larger than 10 μm. The gas molecules collide more often with each other than with the pore wall, and no separation is obtained between the gas components. Knudsen flow occurs when the pore sizes are smaller than 10 μm. The mean free paths of the diffusing molecules are in the same range as the pore size, and collisions between gas molecules becomes less frequent than collisions with the pore wall. Knudsen diffusion can have a significant effect in composite membranes where the support layer have pores in the range of 20 nm to 0.2 μm. The gas flux is inversely proportional to the square root of the molecular weight, i.e. the molecules are separated based on differences in molecular weight, $\alpha_{A/B} = \sqrt{m_B / m_A}$ [12]. Surface diffusion is possible at along the pore wall of the support layer. If the gas molecules are condensable, the pores can be filled with these molecules. Extremely high selectivities can be obtained if the more condensable component fills the pores by capillary condensation and blocking the permeation of the non-condensable gases [22].

2.6 Preparation of polymer membranes

There are several techniques for membrane preparation. The chosen preparation technique depends on the desired membrane structure for a specific separation problem. The most important techniques are sintering, stretching, track-etching, phase inversion, sol-gel process, vapour deposition and solution coating [12]. According to equation 2.16 dense polymer membranes will show increased flux by reducing the effective thickness of the membrane. This can be achieved by making a composite membrane where the top layer is a thin selective layer and the sub layer is a porous support.

Flat membranes can be prepared by dissolving a polymer and casting the solution on a support. The casting thickness is controlled by a knife to be between 50 μm and 500 μm. The polymer solution on a support is then put in a bath with non-solvent. The polymer is precipitated according to the exchange of solvent and non-solvent. Important parameters are polymer concentration, evaporation time, humidity, temperature and possible additives to make the desired membrane [12].

Dense membranes of composite polymers are often used for gas separation. To lower the resistance in the selective layer and gain a high mechanical strength, a thin selective layer supported by an asymmetric membrane has been a breakthrough in membrane technology. The asymmetric membrane, e.g. polysulfone, is made by phase inversion. There are several techniques to cast a selective top layer on a support. Some involves solution casting, e.g. dip coating, while others involve polymerization reactions, e.g. interfacial polymerization. Dip coating is a simple and common way to prepare dense membranes with selective top layer for gas separation. Hollow fiber or flat sheet asymmetric membranes with pore sizes in the range of ultrafiltration are immersed in a dilute polymer solution. The polymer then sticks to the top of the support. When removing the membrane from the polymer solution, it is put in an oven to evaporate the solvent and physically crosslink the polymer. The polymer then becomes fixed to the support and the membrane is more resistant to degradation. A selective layer of 1 μm is achievable [12].

2.7 Membrane separation principles

A membrane module separates a feed stream into a retentate stream and a permeate steam by a selective membrane. For gas separation, the driving force for trans membrane transport is a concentration gradient from the feed to the permeate stream. A compressor is often installed on the feed side and vacuum or sweep gas flow is often applied on the permeate side to increase the driving forces, and the pressure drop over a membrane is large. A schematic drawing of a membrane separation process is given in Figure 2.14. There are optimized system designs for different separation problems.

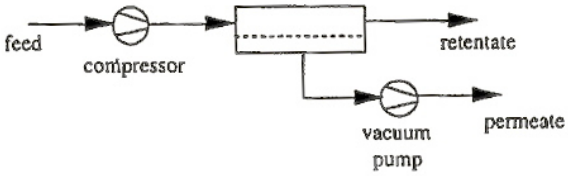

Figure 2.14 Schematic drawing of a membrane separation process [12]

2.7.1 Membrane modules

There are several types of membrane modules. Flat sheet membrane modules have a small membrane area to volume ratio and high pressure drops, so they are manly used in experiments to measure permeability and selectivity of the membrane. Flat sheet membrane modules are easy to fabricate and use, and the membrane area is specified. Flat sheet membranes can be put on top of each other in layers, separated by spacers, in so-called plate-and-frame membrane modules [40]. A complete mixing model can be applied to flat sheet membrane modules when the permeate flow is small relative to the feed flow.

Hollow-fiber membrane modules have the advantage of high surface to volume ratio that make the membrane modules suitable for industrial scale applications. These modules consist of long hollow fibers (3-5 m) with small diameter (inner diameter from 100-500 μm, and outside diameter 200-1000 μm). The hollow fibers are assembled in a shell-and-tube configuration. The feed can enter either from the shell side (outside-in) or from inside the fibers (inside-out). The outside-in configuration will cause less pressure drop. The hollow fibers are closed in one end so that the permeate gas flows countercurrent to the feed and exits the module with permeate from the other hollow fibers [40]. A mathematical model for gas separation by countercurrent and cocurrent hollow fiber membrane modules can by found in [41]. The model applies to binary systems, e.g. separating CO_2 from CH_4.

2.7.2 Complete mixing model

Simple equations can be used to calculate the membrane area needed for a given gas separation problem. Constant permeability coefficients and temperature are frequent assumptions. The simplest equations are derived by assuming complete mixing in the feed and permeate. Other models are based on cross-flow conditions (plug flow at the feed side and complete mixing at the permeate side). In the complete mixing model it is assumed that the concentrations at the feed side are constant at each point in the membrane module, and equal to the retentate concentrations. This gives that the mole fraction of component A at the feed side ($x_{f,A}$) is equal to the mole fraction of component A at the retentate side ($x_{r,A}$), equal to the mole fraction of component A at any point on the high pressure side of the membrane (x_A). The concentration in the permeate stream are also assumed to be constant at any point [12] (see Figure 2.15).

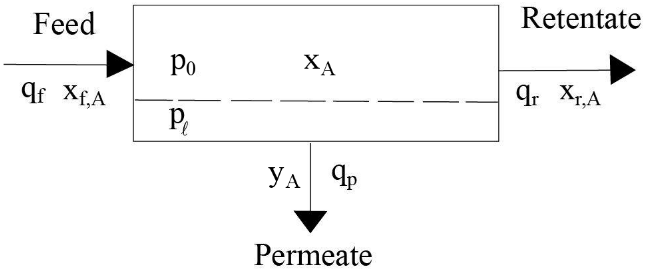

Figure 2.15 Membrane gas separation with perfect mixing at feed and permeate side

The permeate flux can be calculated from equation 2.29 [12]:

$$J_A = \frac{q_{p,A}}{A} \tag{2.29}$$

Where; J_A is the flux of component A (m^3(STP)/(m^2.h)) through the membrane, $q_{p,A}$ is the permeate flow rate of component A (m^3(STP)/h) and A is the membrane area (m^2). By combining equation 2.16 and 2.29 we get an equation describing the flux of gas component A through a membrane assuming perfect mixing.

$$J_A = \frac{P_A}{\ell}\Delta p_A = \frac{P_A}{\ell}(p_0 x_A - p_\ell y_A) \tag{2.30}$$

where P_A is the permeability coefficient of component A (m^3(STP).m/(m^2.h.bar)), ℓ is the membrane thickness (m), p_0 is the pressure (bar) on the feed side (high-pressure side), p_ℓ is the pressure on the permeate side (low-pressure side), and x_A and y_A is are the constant mole fractions (mol/mol) of component A in the feed and permeate side, respectively. The permeate flow is given by equation 2.31.

$$q_{p,A} = q_p y_A = J_A \cdot A = \frac{A \cdot P_A}{\ell}(p_0 x_A - p_\ell y_A) \tag{2.31}$$

The permeance, Q_A (m^3(STP)/(m^2.h.bar)), is defined as the permeability divided by the membrane thickness, as given by equation 2.32.

$$Q_A = \frac{P_A}{\ell} \qquad (2.32)$$

Gas permeability of a membrane is highly dependent on the membrane thickness, and it is therefor difficult to compare membranes with different thicknesses. By using permeance to describe the gas flux it is possible to compare membranes of various thicknesses. Permeance can be calculated from equation 2.33 when the flux, pressure, gas composition and membrane area are known.

$$Q_A = \frac{q_p y_A}{A(p_0 x_A - p_\ell y_A)} \qquad (2.33)$$

Permselectivity can be defined as the ratio of permeance between to components, A and B, as given in equation 2.34.

$$\alpha_{A/B} = \frac{Q_A}{Q_B} \qquad (2.34)$$

2.8 Important applications for gas separation membranes

Membranes are a relative new separation technology, and its importance for the industry is increasing. Membranes are used for a wide variety of applications e.g. food and beverage processing, for medical purposes, desalination of seawater and gas separation. Lately there has been an increased focus on inorganic membranes for fuel cells, membrane reactors and other high-temperature separations [9]. The sale of membrane modules for gas separation is growing rapidly [2], and material selection, membrane formation together with effective modules and system configuration are critical issues to overcome to secure a successful membrane for gas separation [1]. The most important applications of gas separation by membranes are [1, 2]:

- *Nitrogen enriched air.* Membranes are preferred over cryogenic systems and pressure swing absorption (PSA) if the N_2 purity is less than 99.95 % and production volume is low.
- *Natural gas sweetening.* Membranes are preferred over amine absorption if the feed gas flow rate is low and contains a high CO_2 concentration.
- *Hydrogen separation.* Membranes have an economic advantage if the feed gas is delivered at high pressure, and low pressure could be tolerated for the permeate gas.
- *Oxygen enrichment.* Facilitated transport membranes are thought to be the only technology that can achieve high purity oxygen, but the technology has not been proven viable. PSA is the most preferable option.
- *VOC recovery.* The technology of volatile organic compounds separation in air pollution control applications is in development.
- Biogas upgrading [43], CO_2 capture from flue gases [44], SO_2 removal from smelter gas streams, H_2S and water removal from natural gas, NH_3 removal from recycle streams in ammonia synthesis, and olefin/paraffin separation are noted as potential applications for membrane gas separation.

3 Facilitated transport membranes

This chapter describes preparation, characterization and potential applications for facilitated transport membranes. It has been pointed out that further work is needed to produce membranes that are stable at harsh conditions and has a long lifetime. Inexpensive fabrication techniques to make defect free membranes should be available. To make membranes with very thin selective layers will be even more important in the future to secure high fluxes and low cost [9].

Lloyd M. Robeson published an empirical upper bound relationship for gas separation in 1991. There is a trade off between permeability and selectivity of a membrane, and for almost all cases the selectivity decreases when the permeability of the high permeable component increases. The log-log-diagram represents an upper bound of achievement valid for multiple gas pairs e.g. CO_2/CH_4. The Robeson's upper bound (1991) and the revisited Robeson's upper bound (2008) is shown in Figure 3.1 [42]. MMMs and PIMs have been reported with CO_2/CH_4 selectivity and CO_2 permeability in between the 1991 and the 2008 Robeson's upper bond, while FSC membranes and TR polymers have been reported above the 2008 Robeson's upper bond [10, 15].

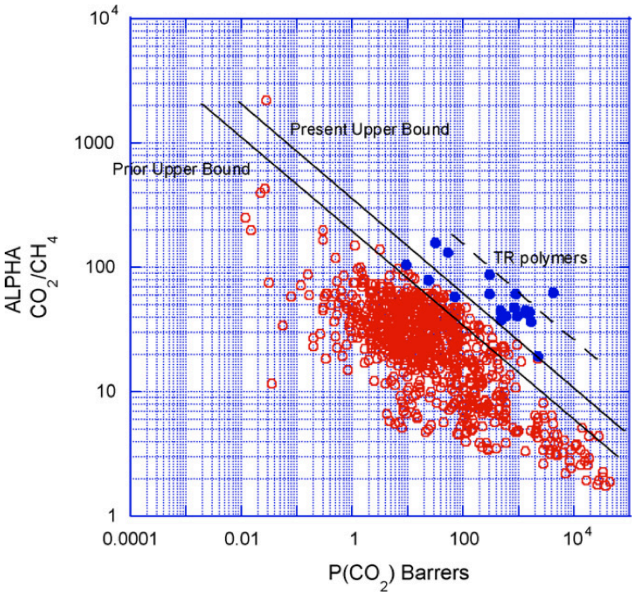

Figure 3.1 The Robeson's upper bound for CO_2/CH_4 separation [42]

3.1 Preparation of FSC membranes

3.1.1 Material selection

Kim et al. [11] prepared a composite PVAm membrane on a polysulfone (PSf) support for CO_2 capture. Crosslinking with NH_4F secured a dense coating layer and kept the amino groups active for CO_2 facilitated transport, resulting in very high CO_2/CH_4 selectivity. Higher molecular weight of PVAm resulted in a remarkable increase in selectivity. Deng et al. [43] prepared a PVAm/PVA blend membrane on a PSf support in 2009. PVA offered a robust mechanical entanglement with PVAm. The selectivity was reported at 45 with a CO_2 permeance of 0.30 m^3 (STP)/(m^2.bar.h) at 2 bar. PVAm with a molecular weight of 25,000 g/mol was used in the experiments. The facilitated transport of CO_2 by PVAm was reported as the assumed transport mechanism, since selectivity and permeance was remarkably higher for a “PVAm/PVA on PSf” compared to a “PVA on PSf” membrane.

A porous support is used to add mechanical strength to a thin selective layer, and obtain a high gas permeance. Pore size and pore size distribution are important factors in selecting a suitable support. Very few studies are available in the literature that deals with the effects of the support membrane on the performance of a composite membrane [10, 27]. Polysulfone is often chosen as support, because the structure of CO_2 is similar to that of sulfone groups, and the sulfone groups apparently favour the solubility of CO_2 [44]. The choice of support was proved to be very important, and polysulfone have been reported with satisfying CO_2/CH_4-selectivity [11].

3.1.2 Material functionalization

Carbon nanotubes (CNTs) have been added to PVAm/PVA blend membranes to increase swelling capacity and mechanical strength and reduce the compaction at elevated pressure. Chen et al. [45] added CNTs to a PVA membrane and reported increased Young’s modulus, tensile strength and toughness. By dissolving raw CNTs in acid before mixing with a PVA solution by ultrasound, CNTs were well dispersed in the polymer matrix. Aggregates of CNTs and poor bonding with the polymer matrix was also observed, because CNTs tend to self-associate in micro-scale aggregates. Disaggregation and uniform dispersion of CNTs are critical issues that must be solved to produce high property materials, but it is challenging, because the high surface area of the CNTs increases the attractive forces between the aggregates. Mechanical dispersion of CNTs with ultrasound is a common way of separating CNTs from each other, but ultrasound treatment can also fragment the CNTs, decreasing their aspect ratio [46]. Surfactants can also be used to secure a stable colloidal dispersion [47]. Experiments have shown that adding small amounts of CNTs (1 wt%) in a PVAm/PVA FSC blend membrane can result in increased swelling capacity and significantly increased CO_2 permeance above 10 bar. CO_2/CH_4 selectivity can remain similar to PVAm/PVA membrane without CNTs. The mechanical reinforcement was believed to be the reason for increased membrane separation performance. Higher mechanical strength can reduce compaction at high pressure, and the nano spacer function could benefit the swelling process [10].

3.1.3 Casting

Polymer membranes can be prepared by dissolving polymers by ultrasound [48], and casting the solution on a glass plate [49-51]. Deng et al. [10] developed a casting technique to mimic the dip coating procedure for flat sheet membranes. An aqueous solution of dissolved polymer by ultrasound was filtered and casted on a PSf ultrafiltration support membrane mounted on a glass plate. A calculated amount of solution was poured on the support and a glass stick scraper was used to form an even distribution, a procedure approved effective by [27]. The thickness of the selective layer was determined by the concentration of polymer in the casting solution and the amount of casting solution. The glass plate was fixed in an upright position to reduce thickness variations and secure a defect free coating. More advanced techniques have been developed to obtain more accurate selective layer thickness. A defect free top layer can be secured by moving a trolley with the membrane fixed to it under blades with a clearance to the trolley adjusted to meet a desired membrane thickness [48]. An adjustable micrometer film applicator can also be used to control coating layer thickness [20].

3.1.4 Post treatment

Crosslinking is a common post treatment procedure of membrane preparation. The term "crosslinking" is usually referring to covalent bonding between groups in a polymer segment. Heat treatment is also referred to as "crosslinking", "thermal crosslinking", "thermal treatment", "physical crosslinking" or "heat crosslinking". The exact mechanism is not known and all terms are used to describe the effects of heat treatment on separation performance. Often, the aim of crosslinking is to enhance selectivity and prevent swelling and plasticization by connecting polymer chains in a network. Koros et al. [49] reported that CO_2/CH_4 separation performance of polyimide membranes could be improved by crosslinking treatment. Stabilized polymer structure reduced unwanted effects of CO_2 induced swelling and plasticization. With increased degree of chemical crosslinking, enhanced CO_2/CH_4 selectivity was found due to reduced swelling and chain mobility. CO_2 permeance was not significantly reduced because lower chain mobility was compensated by increased free volume based on crosslinking. Crosslinking can be done by numerous techniques. Zou et al. reported that formaldehyde can be effectively used for crosslinking of polyallylamine and polyvinylalcohol [26], and glutaraldehyde and NH_4F have been reported as a good crosslinking agent for PVAm/PSf membranes [11, 52].

Heat treatment has been reported to improve separation performance of polymer membranes. Matsuyama et al. [53] found that CO_2/N_2 selectivity of a polyethylenimine (PEI)/PVA blend membrane increased remarkably with increased heat treatment temperature. It was expected that the entanglement of the polymeric carrier with PVA chains and the small pore size of PVA lead to the retainment of carrier in the membrane. Others have also effectively carried out thermal treatment [3, 9, 27, 54]. In 1993, Bos et al. [54] managed to suppress the increase in CH_4 permeance in a polyimide membrane by heat treatment. An increased glass transition temperature was observed, and explained by less flexible polymer chains in the crosslinked polymer. A crosslinked polymer did not dissolve in water, but the crosslinking mechanism was not reported. Deng et al. [10] heat-treated PVAm/PVA blend membranes on PSf support at 90-120 °C, 1-4 h in a convective oven. It was believed that PVA chain bridging prevented PVAm from leaking into the pores of the support. The result was less CO_2 permeance loss at elevated pressure. Heat treatment gave higher swelling-degree and prevented an over-swollen membrane at high relative humidity of the feed gas. It was reported that a stronger polymer network could retain water. The relative crystallinity in the blend membrane decreased because of rearrangement of the crystal regions by heat-treatment [39].

3.2 Characterization of FSC membranes

3.2.1 Scanning electron microscopy

Scanning electron microscopy (SEM) can be used to characterize the structure and morphology of membranes. Both membrane surface and cross-section can be investigated and the thickness of the selective layer can be evaluated using SEM. Clear pictures can be obtained by coating the poor conductive polymer sample with gold [10]. Figure 3.2 shows a SEM image of the cross-section of a PVAm/PVA blend membrane with indication of the selective layer.

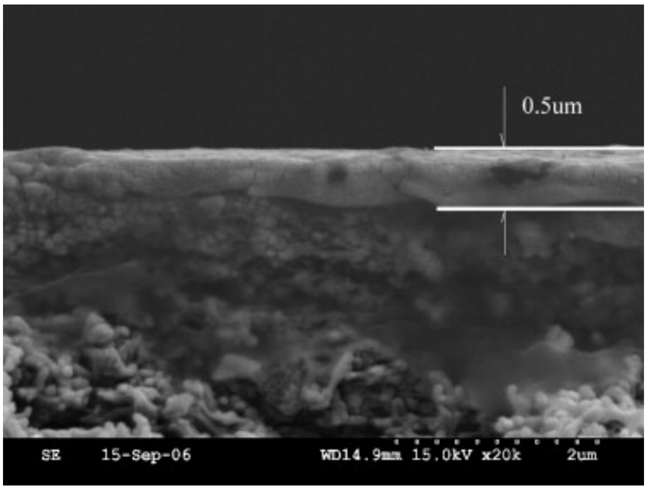

Figure 3.2 SEM image of PVAm/PVA blend membrane cross-section [39]

3.2.2 Gas permeation tests

Gas permeation tests are important techniques to evaluate the separation performance of a membrane. In a gas permeation rig, the influence of many operating conditions such as pressure, relative humidity of gases, temperature, gas flow rates and gas composition can be investigated [55]. Often, a gas mixture is fed to a membrane cell in a permeation setup and the permeate stream is analysed with a gas chromatograph. Gas transport rate and selectivity is calculated based on the gas composition in the permeate stream. It is difficult to measure the membrane thickness if the membrane is water-swollen to various degrees, and permeance is often used in these cases. Permeance of gas component A (Q_A, m^3(STP)/(m^2.h.bar)) is defined as pressure-normalized flux (J_A, m^3(STP)/(m^2.h)) of gas component A through a membrane divided by the partial pressure differences of component A (Δp_A, bar) in the feed and permeate stream, calculated from equation 3.1 [12]:

$$Q_A = \frac{J_A}{\Delta p_A} = \frac{q_{p,A}}{A \times \Delta p_A} \tag{3.1}$$

where $q_{p,A}$ is the permeation flow rate (m^3(STP)/h) and A is the effective membrane area (m^2). The CO_2/CH_4 selectivity is calculated as the ratio of CO_2 permeance over CH_4 permeance as indicated in equation 2.33. Other characterization techniques include *differential scanning calorimetry* (DSC) to study phase transitions, *thermal gravimetric analysis* (TGA) to study thermal decomposition, *X-ray photoelectron spectroscopy* (XPS) to investigate surface composition, etc. [12].

The competing effect, CO_2 permeance with mixed gas is much lower than results obtained by pure gas [27]. The effect has been explained by the competition between CH_4 and CO_2 for sorption sites and diffusion pathways in the polymer [56]. CO_2 dissolved in the polymer matrix can on the other hand loose up the rigid polymer structure and increase the free volume. This can increase the diffusivity of CH_4 and decrease the effect of lower solubility caused by competition with CO_2. Lower CO_2 permeance, and higher CH_4 permeance leads to an overall lower CO_2/CH_4

permselectivity of mixed gases compared to pure gases. Deng et al. [57] investigated the separation of CO_2 from gas mixtures of both CH_4 and N_2. CO_2 permeance of up to 0.83 m^3 (STP)/(m^2.bar.h) was reported for the CO_2/N_2 gas mixture, while only 0.55 m^3 (STP)/(m^2.bar.h) was reached for the CO_2/CH_4 gas mixture. The results suggested that the influence from CH_4 seems stronger than that from N_2. It was explained by CH_4 being more soluble in the water-swollen PVAm/PVA membrane than N_2, and that the larger size of CH_4 may hinder the diffusion of CO_2 and the facilitated transport of HCO_3^- more than N_2 does.

Swelling and plasticization, Swelling of a polymer membrane for gas separation is usually involved with increased permeance and decreased selectivity. In CO_2/CH_4 membrane separation it is known that CO_2 acts as a plasticizer. The plasticization phenomena is not *one* specific physical effect, but the changes of physical properties of polymers that leads to lower separation performance is usually referred to as the plasticization phenomena.

Hydrophilic polymers can be hydrated with water to form water-swollen hydrogel membranes. Recently, the use of hydrogel membranes for gas separation has been investigated [3]. Dry hydrophilic polymer membranes normally have a very low permeance, but the permeance can be increased substantially when the membranes are water-swollen. This is especially the case for acid gases, like CO_2, because of the high solubility in water. The facilitated transport of CO_2 as HCO_3^- through a PVAm/PVA FSC membrane is dependent on water to occur. The swelling behaviour shows crucial influence on the separation performance of the membrane. Little information is available about the effect of relative humidity on swelling behaviour or gas permeation properties, but it has been reported that relative humidity have a large influence on the CO_2/CH_4 separation performance of a PVAm/PVA membrane, and that CO_2 permeance increases exponentially with increased relative humidity [57].

3.3 Potential applications of FSC membranes

3.3.1 Biogas upgrading

Methane produced by anaerobic decomposition of organic matter is a valuable energy carrier. By upgrading biogas to the quality of natural gas or vehicle fuel it may be injected into an existing natural gas grid or used as fuel in cars, buses and trucks. An overview of the biogas production and upgrading is given in Figure 3.3.

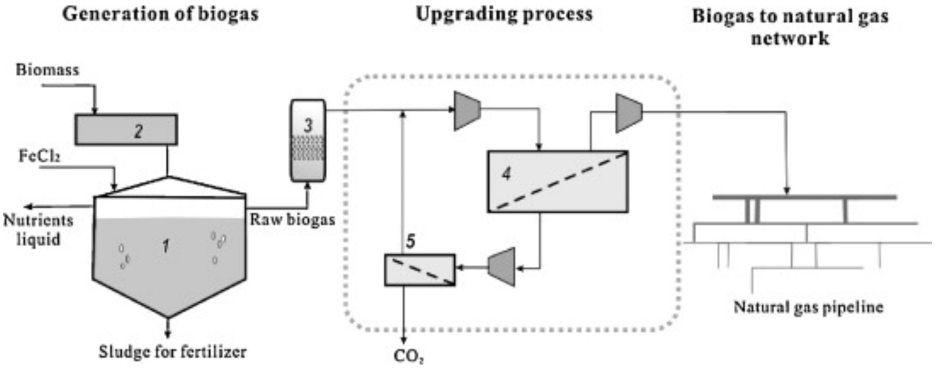

Figure 3.3 Process overview of a biogas production and upgrading system providing gas to a natural gas network. 1: Bioreactor; 2: thickener; 3: filter; 4: 1st stage membrane module; 5: 2nd stage membrane module [58]

A considerable number of biogas plants around the world have shown that biogas production can result in additional available energy with reduced emissions of carbon dioxide and the production of valuable fertilizer. The most common biogas utilization method is Combined Heat and Power (CHP), but it's only a preferred choice if consumers near the plant can use the produced heat. If this is not the case, upgrading biogas to natural gas quality gives better energy utilization. The upgraded biogas can be injected into an already existing natural gas network, or it can be used as vehicle fuel in the form of compressed natural gas (CNG) [7]. The allowable CO_2 concentration in natural gas in US pipelines is 2 vol% or less [13]. Concentration of CO_2 in fuel grade CNG must be less than 0.7 vol% CO_2 [7]. Figure 3.4 show the interior of a membrane upgrading plant.

Figure 3.4 Interior of a membrane upgrading plant [7]

Total membrane area, energy consumption and methane loss are the most crucial factors to be minimized in optimization of a membrane process [7, 58, 59]. Modelling results have shown that it is possible to upgrade biogas to 98 vol% CH_4 with a two-stage cascade with recycle at an energy consumption of 0.3 kWh/m^3. The result was based on a 1000 m^3 (STP)/h biogas upgrading plant with a state-of-the-art membrane. Some methane loss is expected from a membrane biogas upgrading plant. The methane can be used for heating purposes in the anaerobic digester of the plant to secure high energy efficiency [7]. A number of different process designs exist, and a standard two-stage design with recycle, as shown in Figure 3.5, is often used. Here, the biogas is upgraded in two steps. Methane that permeates through membrane module A is lost, but the methane in the permeate stream of membrane module B is recycled.

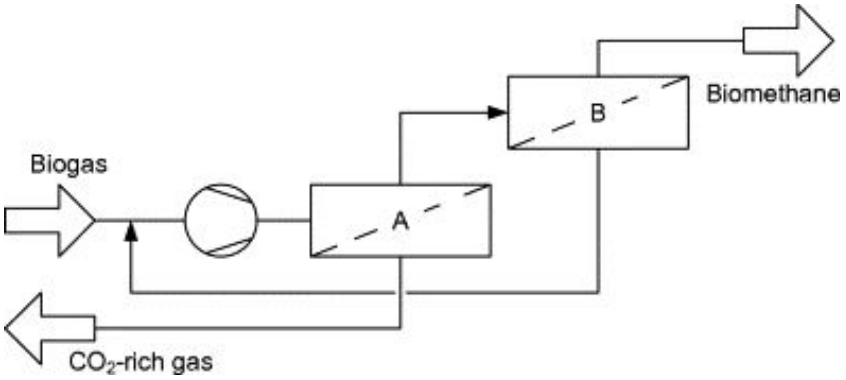

Figure 3.5 Two-stage low-pressure feed cascade with recycle [7]

A single-stage membrane separation system has the advantage of low capital investment, possibly no power required, and a low membrane area. The methane loss is expected to be high. With a two-stage cascade confirmation the investment cost can be increased by a factor of 5 compared to a single separation stage due to higher energy costs and increased membrane area. Methane loss can be significantly reduced by a two-stage cascade confirmation, and will be the chosen process design if methane in the permeate stream is considered as valuable. A three-stage configuration is a combination of the two previous process designs. The retentate stream of the first membrane stage is used as feed gas to the first stage of the cascade. At optimized process conditions, a three-stage configuration will give low separation cost, but it is related to high investment cost and a more complex process [59].

Deng et al. [58] completed a techno-economic evaluation of biogas upgrading process using a PVAm/PVA FSC membrane in 2010. High feed gas pressure resulted in high CH_4 recovery with a single stage design and lowered the membrane area considerably, even though the CO_2 permeance decreased at high pressure. A 2-stage symmetric cascade with recycle, equal to Figure 3.6, was found to be the optimal process design with a feed gas pressure of 20 and 10 bar in the 1st and 2nd membrane module, respectively. Traces of other species as TOC and ammonia must be given considerable attention as they might reduce the membranes separation performance significantly. Either the membrane must be resistant enough to withstand the presence of these gases, or pre-treatment of the biogas is necessary [7].

3.3.2 CO_2 removal from natural gas

CO_2 can cause corrosion in pipelines, and the removal of CO_2 will decrease the transported gas volume and increases the calorific value of natural gas. Amine absorption is considered a state of the art technology for natural gas sweetening, but membranes have also shown a great potential in this area. A technical and economical analysis for CO_2 removal from natural gas using amine absorption and a PVAm/PVA FSC membrane have shown that higher CH_4 purity was obtained with amine absorption compared to a membrane process, but amine absorption requires higher capital costs and running costs, and is potentially harmful to the environment [60]. Figure 3.6 shows the chosen process configuration in a review of polymer membranes in CO_2 removal from natural gas [61]. The first membrane module delivers gas at pipeline specifications in the retentate, while the permeate is recompressed and enters the second membrane module. Permeate from the second stage is vented to air, and the retentate is returned to the primary stage. Methane loss of 1.5 % and compression duty of 0.04 kWh/m^3(STP) has been achieved with this process design at a feed gas flow rate at approximately 12,000 m^3(STP)/h.

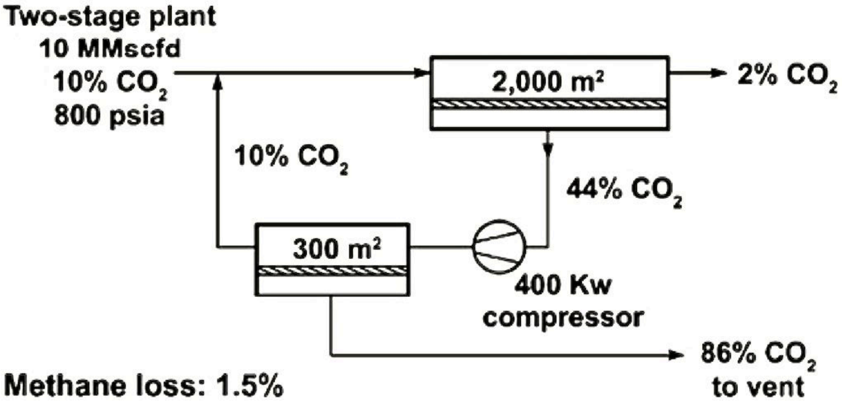

Figure 3.6 Process configuration for CO_2 removal from natural gas [61]

3.3.3 Pre-combustion H_2/CO_2 separation

The advantage of separating CO_2 from a gas stream before combustion is higher CO_2 partial pressure, and therefore, higher driving forces compared to post-combustion. Grainger et al. [62] evaluated the possibility of removing CO_2 from a CO-shifted syngas stream in an integrated gasification combined cycle (IGCC) power plant using a PVAm FSC membrane. After the CO-shift reaction, the FSC membrane separated the feed stream into a H_2-rich stream and a CO_2-rich stream. CO_2 was compressed and stored, while H_2 entered a gas turbine combustion chamber. It was concluded that FSC membranes could be used for H_2/CO_2 separation in IGCC power plants, but improvement of CO_2 permeance at high pressure was noted as important to reduce membrane area and loss of H_2.

3.3.4 CO_2 capture from flue gas

In a fossil fuel power plant, coal, fuel oil or natural gas is combusted to produce thermal and electrical energy. Combustion of hydrocarbons produces CO_2 that can be removed and stored. Hussain et al. [63] investigated the possibility of using a PVAm FSC membrane to separate and capture CO_2 from flue gas mixtures. The results showed that a FSC membrane process was more energy efficient than amine absorption, even for low CO_2 concentrations. It was possible to achieve more than 90 % CO_2 recovery, with CO_2 purity above 90 %. Sandru et al. [55] developed composite hollow fiber membranes for CO_2 capture by coating polyphenylene oxide (PPO) and PSf with PVAm. It was found that vacuum operating mode was preferred over sweep gas mode, because sweep gas permeated into the feed gas and gave additional resistance to CO_2 permeance.

4 Experimental

A good membrane for CO_2 separation shows a high CO_2 permeance and selectivity and high mechanical strength at a low cost. All experiments executed in this work contained PVAm/PVA polymer blends with CNTs, casted on a PSf microporous support.

4.1 Materials

4.1.1 Polyvinylalcohol

Polyvinylalcohol (PVA) is an atactic polymer, but because hydrogen bonds gives intermolecular interactions it shows semi-crystalline character [12]. The glass transition temperature (T_g) is 85 °C and PVA shows low permeability when it is dry. The molecular weight of the repeating unit is 44.00 g/mol. PVA is hydrophilic [13]. In these experiments 90+% hydrolysed PVA powder with a molecular weight of 72,000 g/mol provided by Sigma Aldrich was used. A schematic structure of PVA is shown in Figure 4.1.

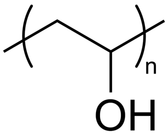

Figure 4.1 Schematic structure of the repeating unit in polyvinylalcohol (PVA) [10]

PVA is completely soluble in water, and is often used as thickener for suspensions and emulsions and in textile and papermaking. PVA can be produced by polymerization and alcoholysis of vinyl acetate [64, 65].

4.1.2 Polyvinylamine

Polyvinylamine (PVAm) has a carbon main chain with amine groups ($-NH_2$) directly connected to the carbon atoms in the main chain. PVAm is a linear polymer with a repeating unit molecular weight of 43 g/mol, and is a polymeric analogue of primary amine. A schematic structure of PVAm is shown Figure 4.2.

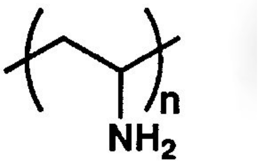

Figure 4.2 Schematic structure of the repeating unit of polyvinylamine (PVAm) [66]

PVAm free base has a T_g (dry) of 45 °C and is amorphous. It is not stable in air because it reacts with CO_2. In these experiments a commercially available polyvinylamine hydrochloride (PVAm·HCl) with a molecular weight of 340,000 from BASF was used. PVAm·HCl is soluble in water, formamide, ethylene glycol and some alcohol/water mixtures. It is not soluble in regular solvents like acetone and alcohols. PVAm·HCl is stable in high salt environments, in strongly acidic environments and at high temperatures. PVAm·HCl is highly crystalline and has a decomposition temperature in the range of 220-250 °C, and a T_g has not been found below this temperature [66]. PVAm can be prepared by converting polyacrylamide by the Hoffmann reaction, or as seen recently produced in industrial scales by radical polymerization of N-vinylformamid (NVF) and N-vinyl-acetamide (NVA) followed by hydrolysis to produce PVAm·HCl. PVAm is expected to be used in industrial applications like pigment retention aids in fine paper, filtration aids, sludge dewatering agents and emulsion breakers [67].

4.1.3 Carbon nanotubes

Carbon nanotubes (CNTs) were used to enhance the mechanical properties of the FSC membranes, and give a nano spacer effect that might improve the swelling capacity and then also the CO_2 separation efficiency at high pressures. The high mechanical properties (high tensile strength and elastic modulus) of CNTs make them well suited for reinforcing polymer membranes. Multiwall carbon nanotubes (VGCF-X^{TM}) were supplied by SHOWA DENKO K. K. The average length of the CNTs was 3 μm, and the average diameter was 10-15 nm. The aspect ratio is then 200-300. The CNTs had a bulk density of 0.08 g/cm^3 and a surface area of 270 m^2/g, and were synthesized by chemical vapour deposition [68].

4.1.4 Polysulfone

Polysulfone (PSf) is a rigid, tough and stable thermoplastic polymer with a T_g of 185 °C. PSf can sustain high pressure and elevated temperature. It is resistant to mineral acids, alkali, electrolytes and oxidizing agents, but not to low polar organic solvents and aromatic hydrocarbons. In these experiments, a PSf ultrafiltration flat sheet membrane with a molecular weight cut off value (MWCO) of 50,000, bought from Alfa Laval, was used as support for preparation of FSC membranes. A schematic structure of PSf is given in Figure 4.3.

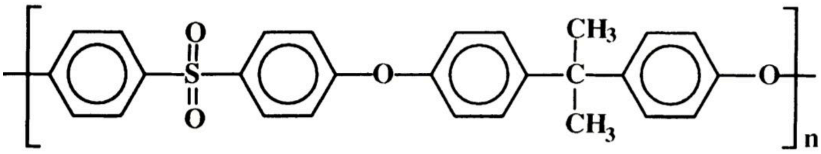

Figure 4.3 Chemical structure of Polysulfone [50]

4.1.5 Gases

Mixed gas containing 35 % CO_2, the rest being CH_4 and N_2 5.0 (>99.999 %) was provided by Yara Praxair in 50 L flasks at 100 bar.

4.2 Membrane preparation

Different casting solutions were prepared in these experiments. All casting solutions were aqueous solutions containing PVAm, PVA and CNTs.

4.2.1 Preparation of aqueous solutions of PVAm, PVA and CNTs

PVAm aqueous solutions were prepared by mixing a calculated amount of purified PVAm with distilled water. The PVAm aqueous solutions were placed on a rotating machine overnight to dissolve the polymer completely. Calculated amounts of solutes and solvents were obtained by weight measurements.

PVA aqueous solutions were prepared by dispersing a calculated amount of PVA in distilled water. To dissolve PVA in water the solutions were heated to 90 °C for 1 hour and then placed on a rotating machine overnight. 1, 3 and 5 wt% solutions of PVAm and PVA were prepared.

Solutions of CNTs were prepared by dispersing a calculated amount of CNTs in distilled water to make a 0.1 wt% solution. The CNTs were dissolved in water by an ultrasonic mixer (Sonics® Vibra Cell™ Ultrasonic processor) for 2 minutes with 5 seconds pulse and 60 % amplitude and thereafter for 20 minutes with 10 seconds pulse and 40 % amplitude. The CNT aqueous solutions were then placed on a rotating machine overnight. Casting solutions of 3 wt% and 5 wt% polymer were prepared by adding a calculated amount of pure, dry CNTs directly to the PVAm/PVA aqueous solutions.

4.2.2 Mixing of the aqueous solutions to prepare casting solutions

1. A calculated amount of CNT aqueous solution, or dry CNTs, and a calculated amount of PVAm aqueous solution were added to a glass bottle and mixed by an ultrasonic mixer for 2 minutes with 5 seconds pulse and 60 % amplitude. The solution was then sonicated in 30 minutes with 10 seconds pulse and 20 % amplitude.
2. A calculated amount of PVA aqueous solution was added to the CNTs/PVAm solution of the same concentration and sonicated in 2 minutes with 5 seconds pulse and 20 % amplitude. The weight ratio of PVAm/PVA was 80/20.
3. The CNT/PVAm/PVA aqueous solution was filtered using a syringe with a 5 μm filter (Acrodisc®) to remove contaminants, polymer particles and CNT aggregates that were not dissolved.

4.2.3 Membrane casting and post-treatment

The solutions were casted on PSf ultrafiltration support membranes. The procedure is developed to mimic dip coating and make a selective layer in the range of 0.2-1 μm.

1. A 100 x 120 mm PSf membrane was taped to a 100 x 150 mm glass plate.
2. The PSf support was washed with 50 °C tap water for 10 minutes to remove the hydrophilic protecting layer, and washed with distilled water afterwards.
3. The solution was dripped on the PSf support using a pipette and scraped with a glass stick to make an even distribution. The membrane was placed in an upright position to make the extra solution flow off. The procedure was repeated with the membrane placed up side down to reduce thickness variations and secure a defect free selective layer.
4. The membrane was dried by placing it in a convection oven at 45 °C overnight.
5. Heat treatment was conducted by placing the membrane in a convection oven at 90-120 °C for 0.5-3 hours.

4.3 Membrane characterization

4.3.1 Gas permeation test

The membrane module used in the gas permeation tests consisted of a circular stainless steel cell consisting of a top half and bottom half. The two parts were demountable and connected with bolts and sealed with rubber O-rings. The top half and bottom half served as feed gas chamber and permeate chamber, respectively. The feed gas and sweep gas inlets were designed to enhance gas mixing to reduce possible concentration polarisation on both feed and permeate side. The membrane was placed in-between the top half and bottom half of the steel cell. A porous metal disk was placed in the bottom half to support the membrane. The porous metal disk was placed upon a support ring that also functioned as a mix enhances. An illustration of the assembly of the cell is given in Figure 4.4.

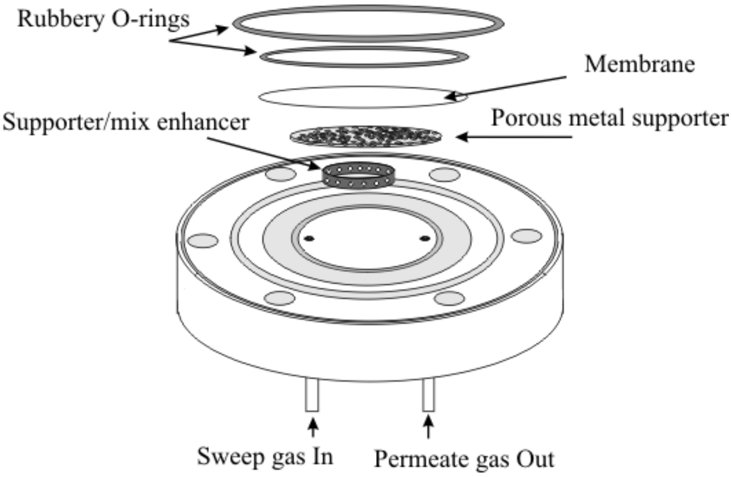

Figure 4.4 Illustration of the assembly of the membrane cell

Membrane selectivity and CO_2 permeance were measured by gas permeation tests in a gas permeation rig at the Department of Chemical Engineering at NTNU. A schematic flow sheet of the permeation rig is shown in Figure 4.5. Feed gas and sweep gas was supplied from gas cylinders and the flow rate could be controlled by float type flow meters while feed pressure was controlled by pressure regulators connected to the gas cylinders. Relative humidity of the feed gas was controlled by adjusting the by-pass stream of the humidifiers, and was measured by online humidity analysers. Data from pressure transmitters and flow controllers were connected with Labview for online measurement and recording. Gas composition at the permeate side was analysed by a gas chromatograph (SRI 8610C).

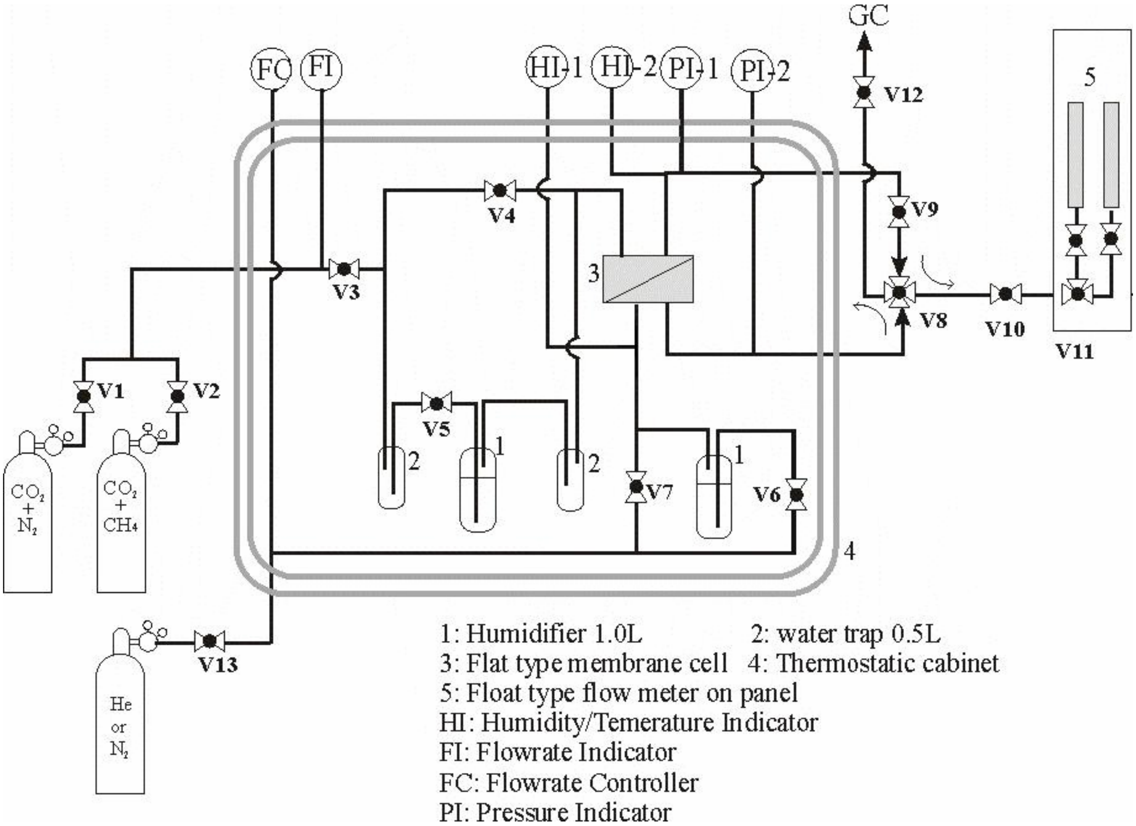
GC
FC
FI
HI-1
HI-2
PI-1
PI-2
V1
V2
V3
V4
V5
V6
V7
V8
V9
V10
V11
V12
V13
1
2
3
4
5
CO₂ + N₂
CO₂ + CH₄
He or N₂
1: Humidifier 1.0L
2: water trap 0.5L
3: Flat type membrane cell
4: Thermostatic cabinet
5: Float type flow meter on panel
HI: Humidity/Temerature Indicator
FI: Flowrate Indicator
FC: Flowrate Controller
PI: Pressure Indicator

Figure 4.5 Experimental set-up for gas permeation tests

Permeance is calculated from equation 4.1 [12]:

$$Q_{CO_2} = \frac{P_{CO_2}}{\ell} = \frac{J_{CO_2}}{\Delta p_{CO_2}} = \frac{q_{p,CO_2}}{A \times \Delta p_{CO_2}} \tag{4.1}$$

where Q_{CO2} (m^3(STP)/(m^2.h.bar)) is the CO_2 permeance, $q_{p,CO2}$ (m^3(STP)/h) is the permeation flow rate, Δp_{CO2} (bar) is the partial pressure difference of CO_2 in feed and permeate and A (m^2) is the membrane area (0.002 m^2).

Permselectivity is calculated as the ratio of CO_2 permeance over CH_4 permeance as indicated in equation 4.2:

$$\alpha_{CO_2/CH_4} = \frac{Q_{CO_2}}{Q_{CH_4}} \tag{4.2}$$

4.3.2 Scanning electron microscopy

A scanning electron microscope (SEM) can form images of a sample by scanning the sample surface with a high-energy beam of electrons. The electrons interact with the atoms in the sample producing secondary and back-scattered electrons that are analysed by a sophisticated microprocessor that creates three-dimensional images. Non-conductive materials must be coated with a thin conductive material, e.g. gold, to prevent accumulation of electrostatic charge in the sample [69].

A Hitachi S-3400N SEM was used to analyse the morphology of the membrane cross-section and surface, and to evaluate the selective layer thickness. The samples for cross section observation were prepared by fracture in liquid nitrogen to obtain a clean-cut cross section. The samples were coated with gold and mounted onto a metal sample holder using conductive carbon tape.

To investigate the effect of dispersing CNTs by ultrasound two samples were prepared for SEM analysis. One sample contained CNTs that were not sonicated. CNTs were dissolved in water and PVA and placed on a rotating machine. In the other sample, CNTs were dispersed in a PVA aqueous solution by ultrasound, following the casting preparation procedure and sonicated for 2 minutes with 5 seconds pulse and 60 % amplitude and thereafter for 30 minutes with 10 seconds pulse and 40 % amplitude. None of the solutions were filtered. The solutions were then cast on a support, mounted to a sample holder and coated with gold.

4.4 Orthogonal experimental design and conjoint analysis

Statistical experimental design methods are commonly used in the process industry. A full factorial design, including all possible combinations of the factors investigated, is often too large to be implemented. Orthogonal experimental design (OED) is a multi-factor experimental design method that selects representative points from the full factorial experiment and can thus represent the overall situation. The advantages of OED are that the number of trails is relatively small, and that it is highly efficient. The full experiment can be evaluated through a fractional experiment, and many factors can be studied and optimized at the same time [70]. The variables that have been chosen for the experiment is commonly referred to as factors, and the designer must carefully decide the levels of the factors [69]. When the factors and levels are set, the orthogonal array can be generated by Statistical Product and Service Solutions (SPSS) software. SPSS was used in this experiment to employ the conjoint analysis to evaluate the experimental results. The importance score of each factor is given as utilities (part-worth). The range of utility values provides information about how important the factor is to the overall performance. Simulations can be carried out based on the results from the conjoint analysis. It is then possible to predict which combination of factor levels that will give the highest performance without carrying out the actual experiment.

5 Results and discussion

5.1 Optimization of membrane preparation conditions

5.1.1 Orthogonal experimental design and results

In order to optimize the membrane preparation conditions and reduce the number of experiments while keeping sufficient information, a statistical method with orthogonal experimental design (OED) was applied. The influence of preparation variables on the separation performance (selectivity and permeance) was studied. The membrane preparation conditions examined were: polymer concentration in the casting solution, CNT content in polymer, heat treatment temperature and heat treatment duration. Table 5.1 gives the OED's factors and levels.

Table 5.1 The factors and levels of the orthogonal experimental design for optimization of membrane preparation conditions

Level	Polymer concentration (wt%)	CNT content in polymer (wt%)	Heat treatment temperature (°C)	Heat treatment duration (h)
1	1	1	90	0.5
2	3	2	105	1
3	5	3	120	3

The OED was generated by Statistical Product and Service Solutions (SPSS) and shown in Table 5.2 together with the membrane performance that was measured. A total of 13 membranes were prepared at different conditions, where no. 10 to 13 were used for model validation. No. 14 and 15 were simulation cases.

Table 5.2 Experimental design and permeation test results for optimization of membrane preparation conditions

No.	Polymer concentration (wt%)	CNT content in polymer (wt%)	Heat treatment temperature (°C)	Heat treatment duration (h)	Selectivity (-)	CO_2 permeance (m^3(STP)/ (m^2.h.bar))
1	3	1	105	1	30	0.06
2	5	1	120	3	19	0.02
3	3	2	90	3	28	0.05
4	1	1	90	0.5	20	0.12
5	5	3	90	1	25	0.05
6	1	2	120	1	20	0.08
7	5	2	105	0.5	29	0.05
8	3	3	120	0.5	30	0.05
9	1	3	105	3	27	0.09
10(a)	1	3	90	1	26	0.11
11(a)	3	3	90	1	31	0.07
12(a)	1	1	105	0.5	31	0.11
13(a)	5	2	120	3	21	0.02
14(b)	1	2	105	3	-	-
15(b)	5	3	120	0.5	-	-

a: Holdout, b: simulation

5.1.2 Analysis of OED

The operating conditions were equal for all the membranes tested. A mixed gas of 35 % CO_2, rest being CH_4, with a feed gas flow rate at 5.3 ml/s and sweep gas (N_2) flow rate at 0.09 ml/s. The feed gas pressure was 5 bar, and the temperature was 25 °C. Relative humidity was kept at 70 %. The normalized membrane performances for all membranes are given in Figure 5.1. Both selectivity and permeance were used to estimate membrane performance.

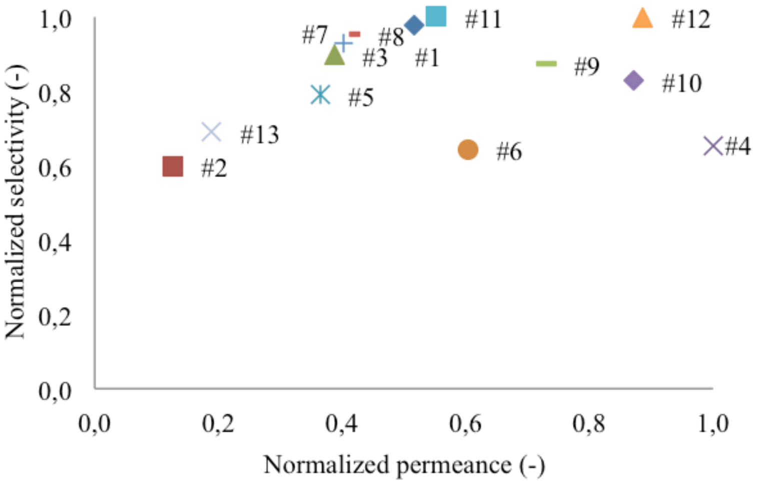

Figure 5.1 Normalized mixed gas permeation test results for the OED experiments for optimization of membrane preparation conditions

Rough trends of how the preparation conditions affect the membrane separation performance can be seen in Figure 5.2. Level 1,2 and 3 refers to the levels given in Table 5.1. Based on the rough trends, polymer concentration and heat treatment duration was modelled as linear factors, while CNT content in polymer and heat treatment temperature were modelled as discrete factors.

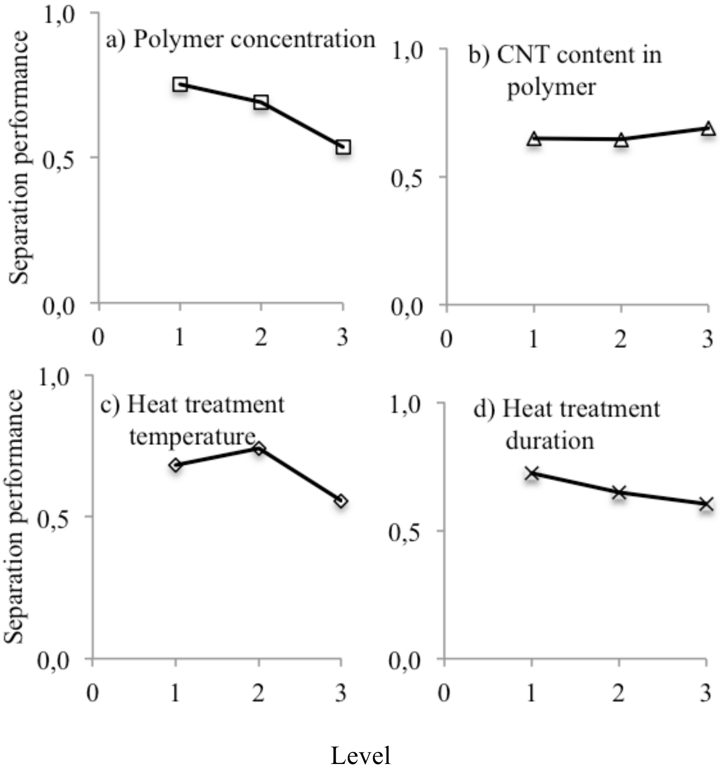

Figure 5.2 Effects of membrane preparation conditions, a) Polymer concentration b) CNT content in polymer c) Heat treatment temperature d) Heat treatment duration, on the membrane separation performance (averaged and normalized CO_2/CH_4 selectivity and CO_2 permeance)

The membranes were then ranked from best to worst in 11 series taking different fractions of selectivity and permeance into account. The experimental results were then used to construct a model to rank the membranes from best to worst. The model relationship coefficient was estimated by Pearson's R and Kendall's tau values (0.935 and 0.761, respectively), which indicates a good relationship between estimated preferences and experimental results. The Kendall's tau value for the holdouts displays 1.000, which gives a perfect match between predicted and actual rankings for the holdouts. This was confirmed by a quick analysis of the preparation conditions and the experimental results.

The importance of each membrane preparation parameter was given by the model as utilities (part-worth) for each factor level and then averaged into importance scores for each factor. Higher utility value indicates better performance. The results are given in Table 5.3 and the relative importance score can be sorted as follows:

Polymer concentration > Heat treatment temperature > Heat treatment duration > CNT content in polymer

The results indicated that polymer concentration, and thereby membrane thickness, will greatly affect the membrane performance. All membranes with a very thin selective layer (low polymer concentration in coating solution) gave high CO_2 permeance due to less resistance in the membrane. Membranes with a thick selective layer (high polymer concentration in coating solution) gave the lowest CO_2 permeance, probably due to higher resistance in the membrane. The membranes with a selective layer thickness in-between the two extremes show medium CO_2 permeance values.

Table 5.3 Utilities and averaged importance scores for different factors in optimization of membrane preparation conditions

Factor	Level	Utility	Average importance score (%)
Polymer concentration (wt %)	1	-0.833	35.3
	3	-2.500	
	5	-4.167	
CNT content in polymer (wt %)	1	0.152	15.0
	2	-0.606	
	3	0.455	
Heat treatment temperature (°C)	90	-0.545	32.3
	105	1.727	
	120	-1.182	
Heat treatment duration (h)	0.5	-0.320	17.4
	1	-0.641	
	3	-1.922	

Membrane no. 12 show both high permeance and selectivity, which indicates that even though the selective layer is very thin, it is possible to obtain a high CO_2/CH_4 separation performance if the other membrane preparation conditions are selected properly.

The second most important factor is heat treatment temperature, and the utilities in Table 5.3 indicates that 105 °C is the optimal temperature. Membrane no. 12 and no. 9 was heat treated at 105 °C and show both high CO_2 permeance and permselectivity. Membranes that are heat treated at 120 °C show overall less CO_2 permeance than membranes heat treated at lower temperature, as also reported by others [10]. The selectivity of these membranes also seems to decrease. The exception is membrane no. 8, that holds a fairly high selectivity, but this might be explained by the short heat treatment duration. Membrane no. 2 and no. 13 were prepared with a thick selective layer and heat treated at high temperature over a long time. They show the lowest CO_2/CH_4 separation performance of all the membranes.

Heat treatment duration is the third most important factor, and the utilities show that less heat treatment duration gives better experimental results. The amount of CNT dispersed in the polymer matrix is the least important parameter in optimization of membrane preparation conditions. The amount of CNTs has little effect, and based on the utilities there is not a clear relationship between the amount of CNTs and the membrane performance.

Table 5.4 gives a simple comparison between a random membrane preparation condition and the optimal membrane preparation condition (1 wt% of polymer in casting solution, 3 wt% CNT in polymer, heat treated at 105 °C for 0.5 h).

Table 5.4 An example of different membrane preparation conditions

Case	Polymer concentration (wt%)	CNT content in polymer (wt%)	Heat treatment temperature (°C)	Heat treatment duration (h)	Total utility
1	3 (-2.500)	1 (0.152)	90 (-0.545)	3 (-1.922)	-4.818
2*	1 (-0.833)	3 (0.455)	105 (1.727)	0.5 (-0.320)	1.029

* Optimal membrane preparation condition

Four membranes were prepared at the given optimal preparation conditions. Normalized CO_2/CH_4 selectivity and CO_2 permeance for these membranes is plotted in Figure 5.3 together with the membrane that showed the best CO_2/CH_4 separation performance, membrane no. 12. None of the membranes prepared at optimal preparation conditions showed higher than average CO_2/CH_4 separation performance. The difference between membrane no. 12 and membranes no. 16A-D is the CNT content in the polymer. Since membrane no. 12 showed the best CO_2/CH_4 separation performance it used further for optimization of the operating conditions, even though it was not prepared at the optimized preparation conditions of the model.

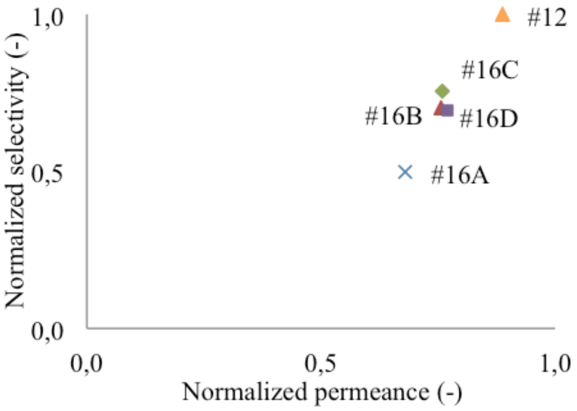

Figure 5.3 Separation performance of four membranes prepared at optimal preparation conditions (16A, 16B, 16C, 16D) compared with the best membrane tested (12)

Membranes 16A-D were prepared by the same procedure, but the experimental results are not equal. 16A show lower membrane separation performance than the others that gave similar results, but there are also variations among them. This shows that there are notable sources of uncertainty in the membrane preparation procedure and the permeation experiments.

Simulation cases are the real power of conjoint analysis as it gives the opportunity of predicting the most preferred case between cases that wore not ranked before. The results from the conjoint analysis can be used to predict membrane properties without executing experiments. Two simulation cases (no. 14 and no. 15) were included in the experimental design, and the results are given in Table 5.5. All three models of Maximum utility, Bradley-Terry-Luce (BTL) and Logit indicated no. 14 would be preferred. The prediction results based on conjoint analysis could be used as a guide for further optimization of membrane preparation condition. The simulation results were not validated by experimental results, but based on the preparation conditions in Table 5.2, it is reasonable to assume that no. 14 will show higher CO_2/CH_4 separation performance.

Table 5.5 Simulation results by conjoint analysis for optimization of membrane preparation conditions

No.	Score (-)	Maximum utility (%)	BTL (%)	Logit (%)
14	6.872	100.0	68.5	89.4
15	3.247	0.0	31.5	10.6

5.1.3 Effect of selective layer thickness

The selective layer thickness has a large influence on the membrane separation performance. The effect of the selective layer thickness can be illustrated with the equation for total flux of CO_2 through the membrane. The first term on the right hand side of equation 2.24 represents the Fickian diffusion while the latter term represents carrier-mediated diffusion. Equation 2.24 shows that a membrane with a thin selective layer will obtain a high gas flux, and therefor also a high gas permeance that is included in determining the membrane separation performance. Concentration of CO_2 at the feed side/membrane interphase, $C_{A,0}$, is proportional to the feed pressure. The concentration of CO_2-carrier-complex at the feed side/membrane interphase, $C_{AC,0}$, is determined by the CO_2-carrier reaction and limited by saturation of carriers [39]. Saturation of carriers probably occurs somewhere in the pressure range investigated in these experiments and $C_{AC,0}$ will then stabilize at a constant value. A membrane with a thin selective layer might be more sensitive to pressure variations than a membrane with a thick selective layer. At low pressure, when $C_{AC,0} >> C_{A,0}$, the thinner membrane could benefit more from the competition between facilitated transport and solution-diffusion mechanism and the separation performance increases. At high pressure, when $C_{A,0} >> C_{AC,0}$, Fickian diffusion might be rate-limiting. A thinner membrane could suffer more from the loss of relative facilitated transport to Fickian diffusion, and consequently a more rapid loss of CO_2/CH_4 selectivity than a membrane with a thicker selective layer. Isolated experiments to investigate the effect of selective layer thickness, while keeping all other membrane preparation factors constant is necessary to make conclusion on the effect of selective layer thickness.

A very thin membrane is more vulnerable to defects. Defects in the selective layer can lead to reduced CO_2/CH_4 selectivity. A thin membrane could be less resistant to pressure effects as reduced water-swelling and increased packing density. The effect is probably most significant at pressures above the interval investigated in this work.

5.1.4 Effect of heat treatment conditions

Figure 5.4 and Figure 5.5 indicates that a dry PVAm/PVA membrane has a very low CO_2 permeance, and that permeance is substantially increased when the membrane is water-swollen. CO_2 has a high solubility in water, and water is needed to transport CO_2 through the membrane by the facilitated transport mechanism. Water swelling is therefor an important factor to maximize CO_2 permeance and selectivity. Heat treatment can be an efficient way to obtain the optimum swelling degree. Crosslinking degree is important for CO_2/CH_4 separation performance, as indicated by medium importance scores for heat treatment from the OED. Over-swelling can result in loss of membrane mechanical strength and sieving effect, as well as weaken the facilitated transport mechanism. The exact mechanism of heat treatment is not known.

The effect of heat treatment temperature on CO_2/CH_4 separation performance goes through a maximum at 105 °C. Heating above this temperature results in lower separation performance. It has been reported elsewhere that optimum swelling degree of a PVAm/PVA membrane is obtained at 105 °C. Heat treatment above 105 °C results in a too strong crosslinking, and therefore lower swelling capacity [39]. Too intensive crosslinking results in restrictions in chain mobility that will decrease gas diffusivity [10]. Figure 5.2 d) suggests that less heat treatment duration will give better CO_2/CH_4 separation performance. However, there are strong interactions between the heat treatment temperature and duration. The optimum heat treatment duration is therefore dependent on the heat treatment temperature.

Figure 5.4 and Figure 5.5 also show that CO_2/CH_4 selectivity at 2 bar increases with increased relative humidity. At 10 bar, selectivity goes through a maximum, and decreases with increased relative humidity at high level of relative humidity. The plasticization phenomena can be a possible explanation for the loss in selectivity. At elevated pressure and high CO_2 concentrations in the feed gas, CO_2 is known to swell and plasticize the membrane. High degree of swelling looses up the polymer matrix, allows more CH_4 to permeate and the result is low selectivity. A combination of water swelling and CO_2 induced swelling can explain the loss in selectivity at elevated pressure and high level of relative humidity. Heat treatment will be more important under these conditions, as heat treatment possibly can prevent over-swelling.

5.1.5 Effect of CNTs

The effect of CNTs is not easy to analyze based on the results from the conjoint analysis. Addition of CNTs has shown to enhance water-swelling capacity of a PVAm/PVA blend FSC membrane. An increased resistance to compaction at high pressure have also been reported [10]. It seems that 5 bar is not high enough to gain a notable effect of CNTs. It is also possible that CNTs will penetrate the selective layer when the selective layer is very thin, as will be discussed further in chapter 5.3.

Figure 5.4 shows the effect of CNT in a PVAm/PVA blend membrane at 2 bar at different levels of relative humidity. One membrane was prepared without CNTs, and one membrane was prepared containing 1 wt% CNTs in polymer. All other preparation and operating conditions were held equal for the two membranes. CNTs do not seem to have any effect on CO_2/CH_4 selectivity under these operating conditions. Both membranes show an increase in selectivity from 10 to 18 by increasing the level of relative humidity from 50 % to 90%.

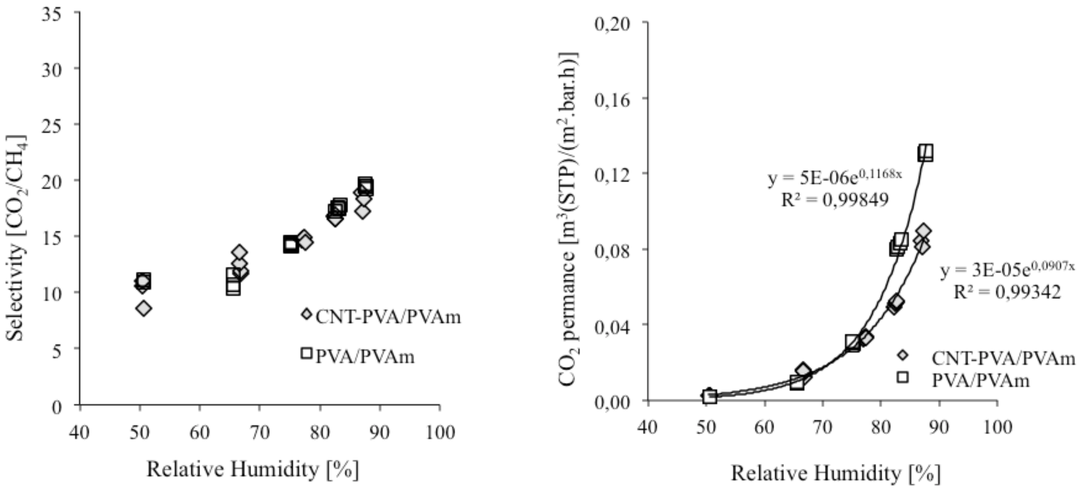

Figure 5.4 The effect of CNT in the PVAm/PVA blend membrane on CO_2/CH_4-selectivity and CO_2 permeance at 2 bar, 25 °C, feed gas (35% CO_2) flow rate at 8.2 ml/s, sweep gas flow rate at 0.07 ml/s and various levels of relative humidity

CNTs seem to have a negative effect on CO_2 permeance at 2 bar. Both membranes with and without CNTs show a clear exponential increase in CO_2 permeance with increased level of relative humidity, but the membrane not containing CNTs obtains higher CO_2 permeance. At 88 RH% the membrane not containing CNTs obtained a CO_2 permeance of 0.13 m^3(STP)/(m^2.bar.h), while just 0.09 m^3(STP)/(m^2.bar.h) was obtained by the membrane containing 1 wt% CNTs. Experimental variations might explain the difference in CO_2 permeance, but a high content of CNTs in the selective layer could also add resistance to gas transport though the membrane, and thereby reduce CO_2 permeance.

Figure 5.5 show the effect of CNTs on selectivity and permeance at 10 bar and various levels of relative humidity. All other factors were held constant. CNTs do not seem to have a significant impact on CO_2/CH_4 selectivity, nor CO_2 permeance. This confirms the results from the conjoint analysis. A slightly higher selectivity and slightly lower CO_2 permeance is obtained for the membrane containing CNTs. A selectivity of 35 was obtained for the CNT reinforced PVAm/PVA membrane, and a selectivity of 33 was obtained for the membrane without CNTs. A CO_2 permeance of 0.06 m^3(STP)/(m^2.bar.h) was obtained by the CNT-PVAm/PVA membrane, while 0.07 m^3(STP)/(m^2.bar.h) was obtained by the PVAm/PVA membrane. The small differences can be a result of experimental uncertainties, rather than the effect of CNTs.

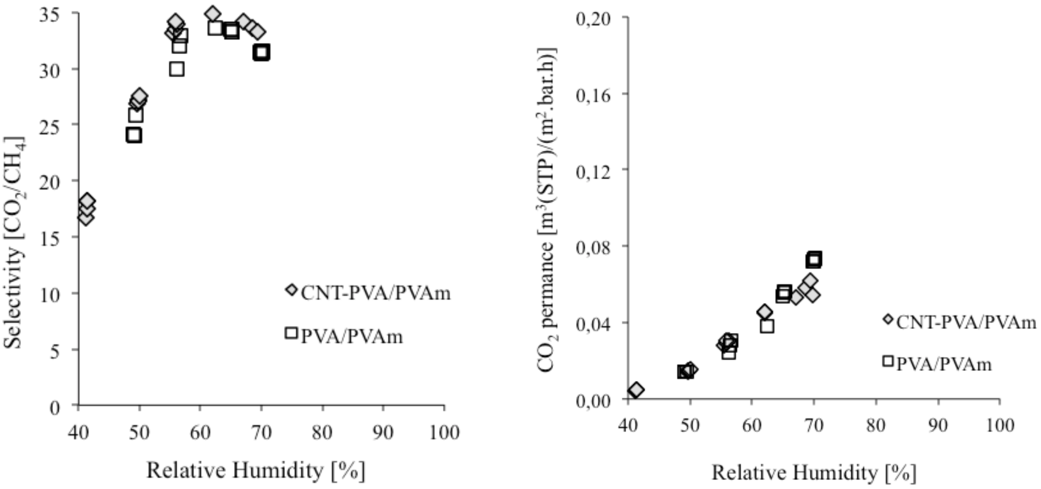

Figure 5.5 The effect of CNT in the PVAm/PVA blend membrane on CO_2/CH_4-selectivity and CO_2 permeance at 10 bar, 25 °C, feed gas flow rate at 8.2 ml/s, sweep gas flow rate at 0.07 ml/s and various levels of relative humidity

Aggregates of polymer and CNTs were separated from the casting solution though a 5 µm filter. The thickness of the selective layer is less than 5 µm. CNTs might cause defects in the selective layer when the selective layer is very thin.

CNTs have previously been found to have a positive effect on selectivity below 10 bar [71]. Further investigation on the effect of CNTs and optimization of preparation conditions is needed to understand the effect of CNTs and utilize its potential to increase the CO_2/CH_4 separation performance of a PVAm/PVA blend membrane.

5.2 Optimization of operating conditions

5.2.1 Orthogonal experimental design and results

An OED was applied to analyse the influence of four process variables on the membrane separation performance. Feed gas pressure, feed gas flow rate, sweep gas flow rate and relative humidity of the feed gas was investigated. Table 5.6 gives the OED's factors and levels.

Table 5.6 The factors and levels of the orthogonal experimental design for optimization of operating conditions

Level	Relative humidity (%)	Pressure (bar)	Sweep gas flow rate (cm^3/s)	Feed gas flow rate (cm^3/s)
1	60	2	0.07	4.1
2	70	5	0.18	8.2
3	80	10	0.29	12.3

The OED was generated by SPSS and showed in Table 5.7 together with the experimental results. 13 operating conditions were tested. No. 10 to 13 served as model validation. No 14 and 15 were simulation cases.

Table 5.7 Experimental design and permeation test results for optimization of operating conditions

No.	Relative humidity (%)	Feed gas pressure (bar)	Sweep gas flow rate (cm^3/s)	Feed gas flow rate (cm^3/s)	Selectivity (-)	CO_2 permeance (m^3(STP)/ (m^2.h.bar))
1	60	5	0.18	8.2	32	0.07
2	70	2	0.29	8.2	34	0.08
3	70	10	0.18	4.1	26	0.09
4	70	5	0.07	12.3	22	0.09
5	80	10	0.07	8.2	23	0.14
6	80	2	0.18	12.3	31	0.16
7	60	2	0.07	4.1	9	0.01
8	60	10	0.29	12.3	30	0.07
9	80	5	0.29	4.1	26	0.13
10(a)	60	2	0.29	4.1	37	0.04
11(a)	60	5	0.29	4.1	30	0.06
12(a)	70	2	0.29	4.1	33	0.08
13(a)	60	2	0.07	12.3	12	0.02
14(b)	80	5	0.07	12.3	-	-
15(b)	60	10	0.29	4.1	-	-

a: Holdout, b: simulation

5.2.2 Analysis of the OED

Normalized CO_2/CH_4 selectivity and CO_2 permeance of the experimental results are given in Figure 5.6. All tests were carried out using membrane no. 12 from optimization of the preparation conditions. Membrane no. 12 was prepared from a casting solution containing 1 wt% polymer with 1 wt% CNTs. The membrane was heat treated for 0.5 hours at 105 °C.

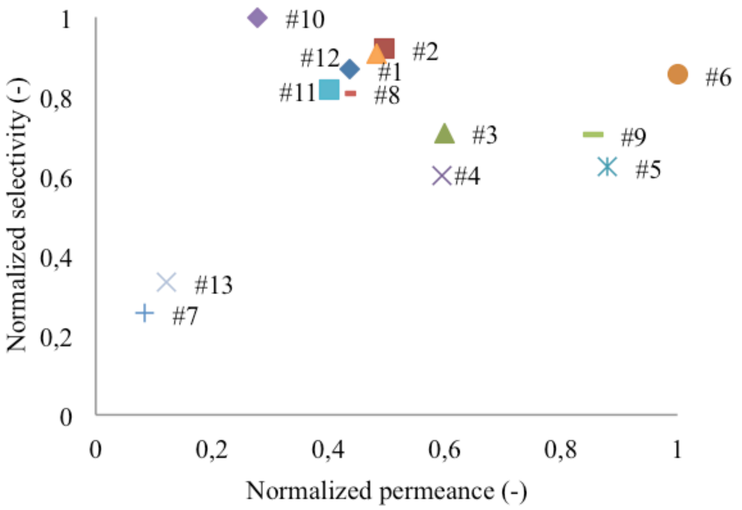

Figure 5.6 Normalized mixed gas permeation test results for the OED experiments for optimization of process operating conditions

Rough trends of the effect of the different operating conditions on the membrane separation performance (average of normalized CO_2/CH_4 selectivity and CO_2 permeance) is given in Figure 5.7, where level 1,2 and 3 represent the levels given in Table 5.6. Based on the rough trends, relative humidity and feed gas flow rate were modelled as linear factors in the conjoint analysis, while pressure and sweep gas flow rate were modelled as discrete factors.

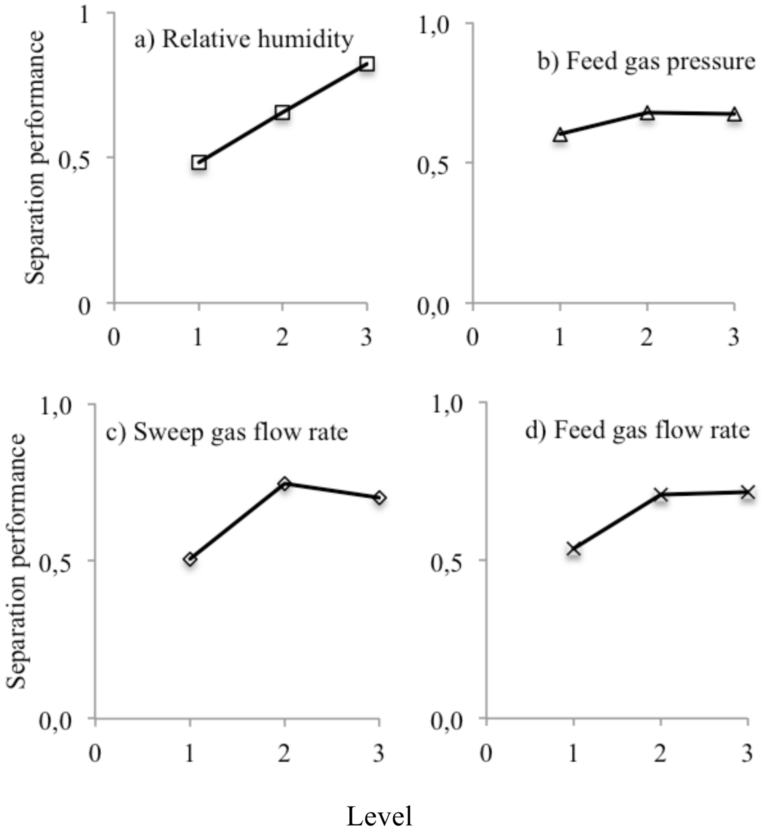

Figure 5.7 Effects of operating conditions, a) Relative humidity b) Feed gas pressure c) Sweep gas flow rate d) Feed gas flow rate, on the membrane separation performance (average normalized CO_2/CH_4 selectivity and CO_2 permeance)

The operating conditions were then ranked from best to worst in 11 series taking different fractions of permeance and selectivity into account. The experimental results were then used to construct a model to rank the operating conditions from best to worst. A Pearson's R value of 0.971 and a Kendall's tau value of 0.889 indicates a good relationship between the estimated preferred operating conditions and the experimental results. Kendall's tau value for the holdouts was 1.000, which gives a perfect match between predicted and actual rankings of the holdout cases. The utilities and importance scores are given in Table 5.8. Higher utility value indicated better performance. The relative importance scores can be sorted as follows:

Relative humidity > Sweep gas flow rate > Feed gas pressure > Feed gas flow rate

This shows that the relative humidity of the feed gas is the most important factor and will greatly affect the membrane separation performance. All operating conditions with high relative humidity show high CO_2 permeance. Test runs with low relative humidity show low CO_2 permeance. At high relative humidity, CO_2/CH_4 selectivity decreases with increased relative humidity but the overall membrane separation performance (a combination of permeance and selectivity) increases with increased relative humidity. Medium level of relative humidity gives membrane separation performance in between the low and high levels.

Table 5.8 Utilities and averaged importance scores for different factors for optimization of operating conditions

Factor	Level	Utility	Average importance score (%)
Relative humidity (%)	60	12.273	46.6
	70	14.318	
	80	16.364	
Feed gas pressure (bar)	2	0.364	11.2
	5	-0.91	
	10	-0.273	
Sweep gas flow rate (cm^3/s)	0.07	-1.667	33.2
	0.18	1.152	
	0.29	0.515	
Feed gas flow rate (cm^3/s)	4.1	0.409	9.0
	8.2	0.818	
	12.3	1.227	

The second most important factor is the sweep gas flow rate. The optimum level was found to be 0.18 cm^3/s. A low sweep gas flow rate combined with low pressure resulted in a low membrane separation performance. At medium and high pressure it was possible to apply a low sweep gas flow rate, and still retain a good separation performance. High level of sweep gas flow rate gave medium separation performance. The large significance score of sweep gas flow rate in the conjoint analysis is partly caused by the very low CO_2/CH_4 separation performance that is observed with the combination of low pressure and low sweep gas flow rate. Pressure and feed gas flow rate are the least important factors in the interval investigated. A high CO_2/CH_4 selectivity and CO_2 permeance was obtained by keeping a low feed gas pressure and high feed gas flow rate. Table 5.9 gives a comparison of a randomly selected operating condition (case 1) together with the optimized operating condition (case 2).

Table 5.9 An example of different operating conditions

Case	Relative humidity (%)	Feed gas pressure (bar)	Sweep gas flow rate (cm^3/s)	Feed gas flow rate (cm^3/s)	Total utility
1	70 (14.318)	2 (0.364)	0.29 (0.515)	12.3 (1.227)	16.424
2*	80 (16.364)	2 (0.364)	0.18 (1.152)	12.3 (1.227)	19.107

* Optimized operating condition

The optimized operating conditions are equal to the operating conditions in the OED test no. 6. Under optimized conditions a CO_2/CH_4 selectivity of 31 with a CO_2 permeance of 0.16 $m^3(STP)/(m^2.h.bar)$ was obtained. Table 5.10 show a comparison of CO_2/CH_4 separation performance in the current work and other FSC and polymer membranes.

Table 5.10 Comparison of membrane separation performance in current work and other polymer membranes and fixed-site-carrier membranes

Membrane	CO_2/CH_4 selectivity (-)	CO_2 permeance ($m^3(STP)/(m^2.h.bar)$)	System	Δp (bar)	Ref.
Polyvinylamine on polysulfone support	700-1100	0.008-0.01	Pure CH_4 and CO_2	2-4	[11]
Polyvinylamine on polysulfone support	206	0.01	Pure CH_4 and CO_2	1.3	[52]
Polyvinylamine on polysulfone support	53	0.01	50/50 vol% CO_2/CH_4	1.3	[52]
Polyimide blend of P84 and Matrimide	44	0.08	50/50 vol% CO_2/CH_4	8	[72]
polyvinylpyrrolidone on a polysulfone support (a)	48	0.46	50/50 vol% CO_2/CH_4	0.03	[44]
salt hydrates, e.g. $((CH_3)_4N)F \times 4H_2O$, immobilized in a support (a)	270	0.19	25/50/25 vol% $CO_2/H_2/CH_4$	4	[73]
Polyvinylalchohol/Polyvinylamine blend membrane on polysulfone support	45	0.30	10/90 vol% CO_2/CH_4	2	[43]
Plasma polymerized membrane from diisopropylamine	17	1.23	3.5/96.5 vol% CO_2/CH_4	0.001	[32]
Polysulfone (Monsanto)	30	0.06	40/60 vol% CO_2/CH_4	10	[8]
Cellulose-Acetate (Grace)	16	0.13	40/60 vol% CO_2/CH_4	10	[8]
polyallylamine/poly(vinyl alchohol) blend membrane on a polysulfone (a)	58	0.07	10/90 vol% CO_2/CH_4	1	[37]
CNT reinforced polyvinylamine/polyvinylalchohol blend membrane on polysulfone support	31	0.16	35/65 vol% CO_2/CH_4	2	This work

a: Both CO_2 permeance and selectivity dropped drastically with increased pressure.

The membrane developed in this work show medium CO_2 permeance and low selectivity compared to other membranes in literature. A membrane module based on CO_2/CH_4 separation performance in this range will require a large membrane area, but could perhaps be economically competitive as it is prepared from low-cost, commercially available polymer. Higher separation performance is expected for this membrane at even higher levels of relative humidity investigated in these experiments. According to literature, the separation performance reported here is also less than required to be preferred over amine absorption, but membranes are often applied in cases of low volumetric flow and high concentrations of CO_2 in the feed gas.

Two simulation cases (no. 14 and no. 15) were included in the experimental design, and the prediction of which one of the cases is the most favorable is shown in Table 5.11. All three models of Maximum utility, Bradley-Terry-Luce (BTL) and Logit indicated no. 14 would be preferred. The prediction results based on conjunct analysis could be used as a guide for further optimization of membrane preparation condition. The simulation cases were not verified with experiments, but it is reasonable to predict that case no. 14 will obtain the highest CO_2/CH_4 separation performance.

Table 5.11 Simulation results from conjoint analysis of optimization of operating conditions

No.	Score	Maximum utility (%)	BTL (%)	Logit (%)
14	5.697	77.3	65.8	76.7
15	2.788	22.7	34.2	23.3

5.2.3 Effect of relative humidity

Figure 5.4 and Figure 5.5 also show the effect of relative humidity of the feed gas. By increasing the relative humidity, an increase in selectivity and an exponential increase in CO_2 permeance is observed. The swelling degree of a PVAm/PVA membrane have been reported to increase exponentially with increased relative humidity [57]. Thus, there seems to be a clear relationship between gas permeance and swelling degree of the membrane. Both CO_2 permeance and CH_4 permeance is increased when the membrane is water-swollen, but the transport mechanisms are thought to be different. The increase in CO_2 permeance by the facilitated transport mechanism is indicated to be larger than the increase in CH_4 permeance by the solution-diffusion mechanism. Based on the strong dependence humidity has on the CO_2 transport it has been suggested that CO_2 follows facilitated transport mechanism [11, 73, 74]. In a wet membrane, CO_2 is transformed into a small and easy-to-move ion, HCO_3^-, and the diffusion coefficient is thought to be enhanced due to lower movement resistance in the water-swollen membrane as a result of higher free volume and chain mobility. Increased permeance with higher degree of swelling with water may also be explained by the less resistance for diffusion of gases in water relative to the base polymer. A polymer with a less rigid structure, and higher free volume will obtain increased gas permeance. It is possible that PVAm/PVA blend membrane takes characteristics of rubbery polymer when highly swollen with water. This can explain an increase in CO_2 permeance, and decrease in selectivity at high levels of relative humidity of the feed gas. The free volume of the polymer can be partly filled with water under these conditions, but this was not investigated in this work.

The dissolution of CH_4 in a dry membrane is only caused by the interaction of CH_4 and polymer. Solubility of both CO_2 and CH_4 will increase in a wet membrane. The polarity of the membrane will increase with more CO_2 being dissolved as HCO_3^-; so non-polar CH_4 will not easily dissolve, which can explain an increase in CO_2/CH_4 selectivity. A slight decrease in selectivity is observed for some membranes at high levels of relative humidity. Loosening of polymer structure by over-swelling at high relative humidity might reduce the sieving capacity to CH_4, resulting is a loss of CO_2/CH_4 selectivity, also reported by [43]. Optimal heat treatment conditions are essential to be able to operate at high relative humidity while keeping CO_2/CH_4 separation performance.

5.2.4 Effect of sweep gas flow rate

Sweep gas is applied to reduce the concentration of permeant on the permeate side of the membrane to secure a high concentration gradient over the membrane. High concentration gradient leads to high diffusion. When a low sweep gas flow rate is applied, high CO_2 concentration is present on the permeate side of the membrane. Weak driving forces for diffusion leads to low CO_2 permeance. CH_4 permeance will also be at a low level and less than CO_2 permeance, because CH_4 is only transported by the solution-diffusion mechanism. High selectivity is usually obtained at low sweep gas flow rate. When sweep gas flow rate is increased, the driving forces for transport of both CO_2 and CH_4 will increase. An observed drop in selectivity indicates a higher increase in CH_4 permeance compared to the increase in CO_2 permeance.

According to the results from the conjoint analysis, the optimum sweep gas flow rate is 0.18 cm^3/s. Too low sweep gas flow rate gives low CO_2 permeance and too high sweep gas flow rate gives reduced CO_2/CH_4 selectivity. Back flushing of sweep gas is also possible at high levels of sweep gas flow rate. At low pressure, sweep gas might permeate through the membrane, increasing resistance to CO_2 transport in the other direction as well as pollute the retentate stream. For a biogas plant it is an advantage to apply low sweep gas flow rates, preferably no sweep gas at all, as there are costs involved with separating sweep gas from the product stream and sweep gas consumption, and that high selectivity is obtained at low sweep gas flow rates. Nitrogen was used as sweep gas in these experiments, but the concentrations of nitrogen in upgraded biogas must be below 5 % m/m [7]. Water vapour could also be used as sweep gas, as it is easy to remove from upgraded biogas, and will contribute to the facilitated transport of CO_2.

5.2.5 Effect of pressure and feed gas flow rate

CO_2/CH_4 separation performance is increased when the feed gas pressure is reduced. This can be explained by the membrane being more water-swollen at low pressure. At higher pressure the membrane is not able to swell as much, and the CO_2 permeance decreases. At low pressure, when the carriers are not saturated, facilitated transport mechanism could be the largest source of CO_2 transport across the membrane. At pressures above the saturation level, solution-diffusion mechanism will be dominating. The solubility coefficient is likely to be reduced at elevated pressure. According to the solution-diffusion mechanism, a decrease in solubility coefficient leads to a decrease in permeance. Figure 5.4 and Figure 5.5 shows a CO_2 permeance at 0.13 and 0.07 $m^3(STP)/(m^2.bar.h)$ at 2 and 10 bar, respectively. A decrease in permeability with increased pressure have been reported as a result of compaction of soft hydrogel membranes [3]. It appeared to be most significant in membranes with a large degree of swelling.

In glassy polymers, an expected loss in selectivity as pressure is increased is explained by CO_2 permeance being more affected than CH_4 permeance. A swollen membrane is thought to increase CH_4 permeance more than CO_2 permeance, and therefor also lead to a decrease in selectivity [54]. Due to the carrier saturation, the main characteristic of FSC membranes is represented by the decrease of both CO_2 permeance and selectivity towards CH_4 with increasing CO_2 feed partial pressure [55]. Figure 5.4 and Figure 5.5 shows a selectivity of 18 is observed at 2 bar, and a selectivity of 35 is observed at 10 bar. As CO_2 permeance is reduced by increased feed gas pressure, the results suggest that pressure effect have a larger influence on CH_4 permeance than on CO_2 permeance. Another explanation is that the carriers are not saturated at 2 bar, and that the facilitated transport of CO_2 is enhanced with increased pressure in the interval of investigation. Neither the facilitated transport mechanism, nor the effect of pressure on FSC membranes is fully understood.

The results from the conjoint analysis indicate that pressure is not a very important parameter in optimization of membrane operating parameters. Since CO_2/CH_4 separation performance is a combination of selectivity and permeance, the experimental results show a seemingly pressure independent separation performance. The separation performance benefits from increased CO_2/CH_4 selectivity, but is partly balanced by decreased CO_2 permeance.

Membranes with a very thin selective layer (<1 μm) are likely to be more vulnerable to pressures effects than membranes with a thicker selective layer (>1 μm). CO_2 permeance have been reported to decrease at a higher rate with increased pressure for membranes with a thin selective layer compared to membranes with thicker selective layers [39]. Pressure also influences the humidity of the system. The point of maximum selectivity will occur at a lower level of relative humidity when increasing the pressure, as reported in the specialization project [71]. When pressure is increased, the absolute humidity of the system will also increase if the relative humidity is kept constant. Swelling of the membrane is related to how much water vapour that is absorbed in the polymer, so when the pressure is increased, the point when the membrane is over-swollen and selectivity decreases could possibly occur at a lower level of relative humidity.

The results from the conjoint analysis indicate that the effect of feed gas flow rate in the interval investigated is not of great importance. A higher CO_2 permeance might be observed when applying a high feed gas flow rate, because CO_2 concentration on the feed side of the membrane will be kept near constant and high driving forces for Fickian diffusion and facilitated transport are obtained even though some CO_2 will permeate through the membrane. Feed gas flow rate probably has limited effect on CO_2/CH_4 separation performance.

5.3 Scanning electron microscopy analysis

Scanning electron microscopy (SEM) analysis was executed to measure the selective layer thickness of the membranes and examine the membrane surface. The dispersion of CNTs and the effect of dissolving CNT aggregates was also investigated.

5.3.1 Effect of dissolving carbon nanotubes with ultrasound

CNTs that were supplied by SHOWA DENKO K.K. should have an average length of 3 µm and an average diameter of 10-15 nm. The SEM image in Figure 5.8 a) shows that CNTs are packed together in large aggregates, some larger than 500 µm in diameter. The CNT aggregates were not easily broken or dissolved in PVA aqueous solution. Figure 5.8 b) shows CNTs in PVA after dissolution with ultrasound. The aggregates are clearly fractured, but with a broad size distribution. Some aggregates are still in the size range of 200 µm, but many CNTs and aggregates were found in a size range below 1 µm, which indicates that CNTs can be dispersed in water by ultrasound.

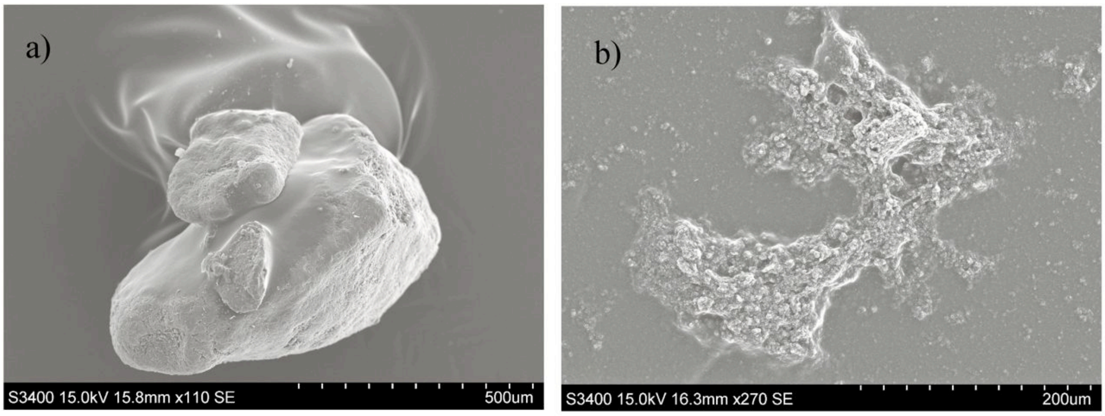

Figure 5.8 SEM image of CNT aggregates in a) CNTs dissolved in water and PVA and b) CNTs dissolved by ultrasound in water and PVA

The thickness of the membrane selective layer in these experiments is in the range of 0.5-10 µm. Some of the CNT aggregates are larger than the thickness of the selective layer, thus it is important to filter the polymer/CNT solution before casting the selective layer on the support. A 5 µm filter was used, which implies that CNT aggregates larger than the thickness of the selective layer can be present in the coating solution. The filter was quickly blocked by CNT aggregates, and the lost CNTs are a source of uncertainty in how much CNT content there is in the membranes. The CNTs are supposed to increase the mechanical strength and free volume of membrane, however, large CNT aggregates can cause defects in the selective layer. Therefore, a suitable thickness of selective layer and good dispersion of CNTs should be well controlled to prepare high performance FCS membranes.

Figure 5.9 shows close-up SEM images of CNT aggregates with and without dispersion by ultrasound. Dispersion in PVA makes a coating layer of polymer on top of the CNT aggregates, maybe also inside the tubes, so the tube shape of CNTs is only partly visible. It is possible that CNTs and polymer can be mixed quite well in a polymer-CNT matrix. This is likely to give higher mechanical strength to the membrane, but possibly not enhance CO_2/CH_4 separation performance at the operating conditions tested in these experiments.

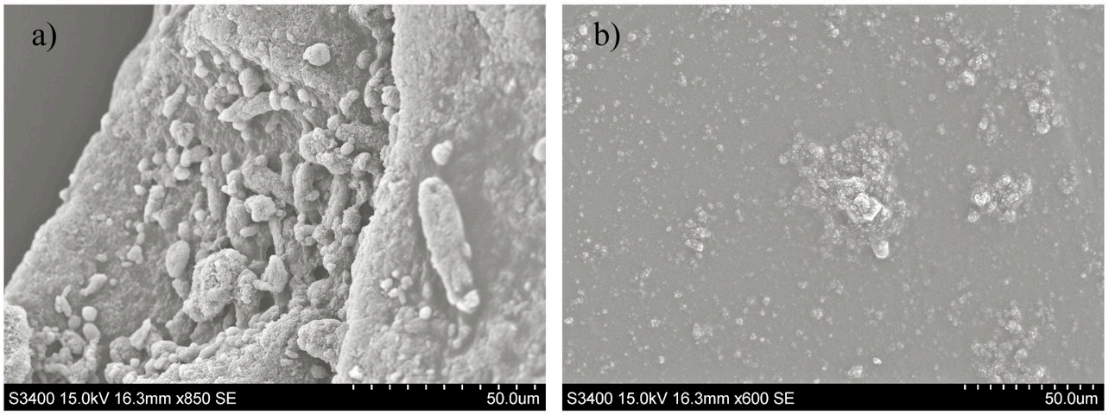

Figure 5.9 SEM image of CNT aggregates in a) CNTs dissolved in water and PVA and b) CNTs dissolved by ultrasound in water and PVA

5.3.2 SEM analysis of membranes

SEM analysis was executed to investigate the cross section and surface of the membranes, as well as to measure selective layer thickness. The thickness of the selective layer is not a constant value, as the membrane is water-swollen under operating conditions. Figure 5.10 shows SEM images of polysulfone (PSf) support membrane without a CO_2 selective PVAm/PVA layer. It can be seen that PSf has a sponge type asymmetric and porous structure, and that the pore size decreases close to the PSf surface.

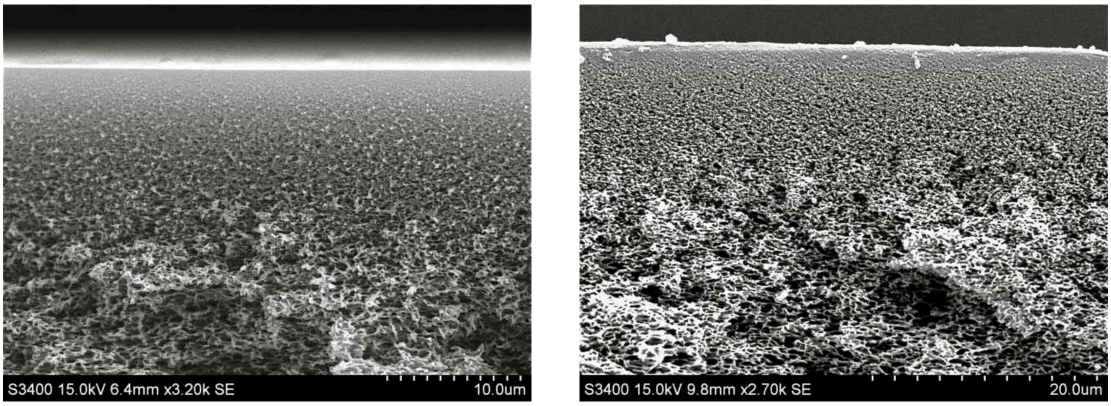

Figure 5.10 SEM pictures of PSf support membrane with asymmetric structure at 2700 and 3200 x magnification

Figure 5.11 shows a SEM image of membrane no. 12. The average selective layer thickness was estimated to be 375 nm. This membrane has a very thin selective layer shows a high CO_2 permeance and CO_2/CH_4 selectivity. A defect free surface is important to obtain high selectivity, and only small amounts of CNTs were found in SEM analysis of this membrane. It is possible that the small amount of CNTs did not affect the separation performance of this membrane. Figure 5.11 a) show no CNTs in the cross section, and Figure 5.11 b) show that the CNT aggregates are small and distributed well on selective layer. CNTs are visible on the membrane surface, and the high selectivity suggests that CNTs are well covered by polymer. The cracks visible on the surface are likely to have originated from sample preparation.

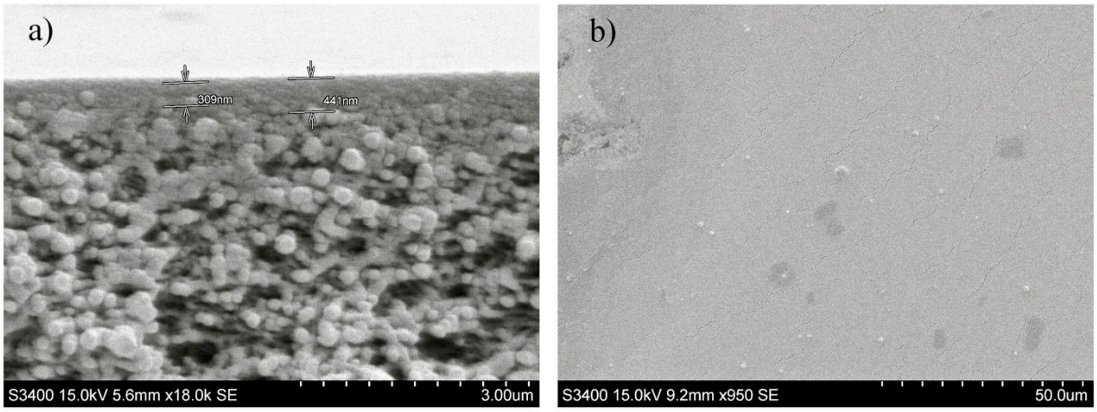
a)
b)
309nm
441nm
S3400 15.0kV 5.6mm x18.0k SE
3.00um
S3400 15.0kV 9.2mm x950 SE
50.0um

Figure 5.11 SEM image a) cross section and b) surface of membrane no. 12: 1 wt% polymer, 1 wt% CNT in polymer, high CO_2/CH_4 separation performance

Figure 5.12 shows SEM images of the cross section and surface of membrane no. 5 that is prepared with the highest level of polymer and CNT content. Membrane no. 5 show below average CO_2/CH_4 selectivity, and very low CO_2 permeance. The thickness of the selective layer varies from 1 μm to 8 μm throughout the membrane cross section. Where the selective layer is very thick, as shown in Figure 5.12 a) much of the selective layer is filled up with CNTs. Figure 5.12 b) shows that CNTs fills much of the surface of the membrane. The large variance in selective layer thickness can be a result of uneven distribution of coating solution, but also from CNTs that might contribute to an increase in selective layer thickness, especially when aggregated.

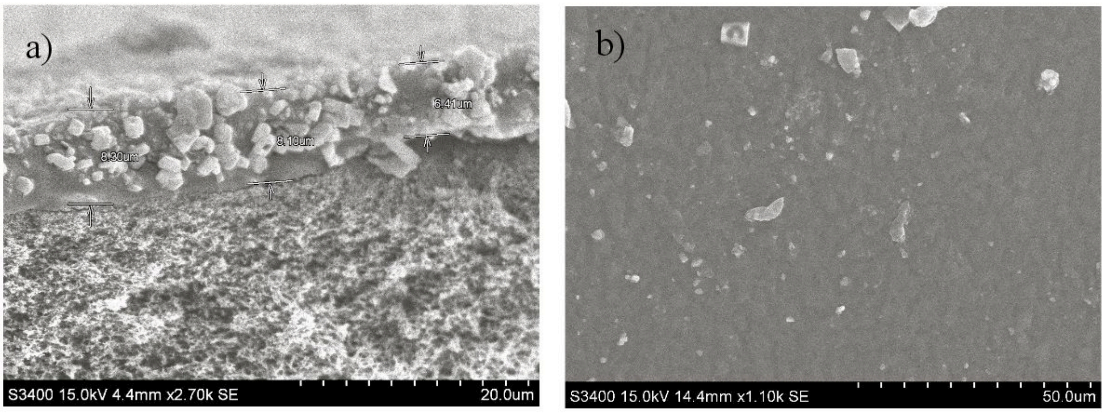
a)
b)
6.41um
8.18um
8.30um
S3400 15.0kV 4.4mm x2.70k SE
20.0um
S3400 15.0kV 14.4mm x1.10k SE
50.0um

Figure 5.12 SEM image of a) cross section and b) surface of membrane no. 5: 5 wt% polymer in coating solution, 3 wt% CNTs in polymer. Low CO_2/CH_4 separation performance

A thick, dense, selective layer often presents low gas permeance due to a higher transport resistance. Therefore, large amount of CNTs added into polymer matrix may increase the resistance of CO_2 transport through membrane instead of improving the permeance by increasing of free volume.

Figure 5.13 shows the correlation between concentration of polymer in the casting solution and the thickness of the selective layer. Thickness variations in the selective layer were found for membranes that were prepared from a casting solution with the same concentration of polymer. This is especially notable at 5 wt% polymer, where the average selective layer thickness varies from 1.31 µm to 4.95 µm. Variations in selective layer thickness can be partly explained by uncertain contents of CNTs in the casting solution. Various degrees of swelling and effects of pressure are other sources of variation.

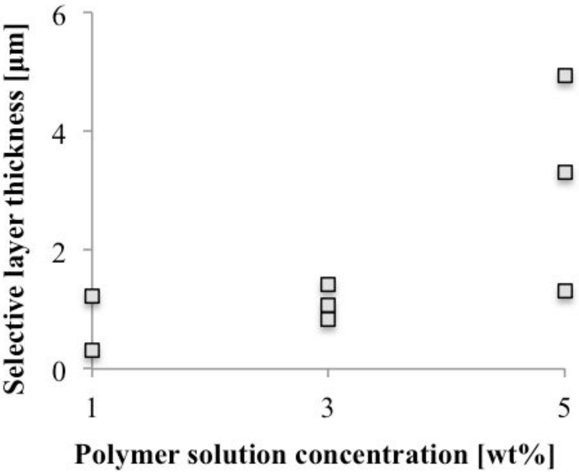

Figure 5.13 Comparison between measured selective layer thickness by SEM analysis with the corresponding concentrations of polymers in the casting solution

6 Process simulation

6.1.1 Process description

Ecopro is a biogas plant in Verdal municipality, Nord-Trøndelag County, and data from Ecopro were used as simulation basis in this work. 30,000 tonnes a year of food waste and sludge are collected and processed. Ecopro produces approximately 300 Nm^3/h of biogas with the composition noted is Table 6.1 and valuable fertilizer. The biogas is turned into 30 GWh/year of energy by a combined heat and power system that generates 42 % electricity and 58 % heat.

Table 6.1 Biogas composition at Ecopro

Component	Volume fraction (-)
CH_4	0.600
CO_2	0.390
O_2	0.002
N_2	0.008
H_2S	$6\cdot10^{-6}$

The biogas from Ecopro contains 8 mg/Nm^3 of H_2S, which has to be reduced to less than a limit of 5 mg/m^3 for natural gas. The CO_2 content should be reduced to less than 0.7 vol% for fuel applications and less than 2 vol% as a natural gas substitute in a gas grid [7]. Figure 6.1 shows a flow sheet of a biogas generating system integrated with a membrane separation unit for biogas upgrading. Organic waste enters a bioreactor where microorganisms decompose the organic waste to biogas, mainly CH_4 and CO_2, and fertilizer. H_2S, particles and water vapour is removed before the membrane modules. Removal of water vapour will not be necessary when a FSC membrane is used. H_2S can be removed with a desulfurization agent, e.g. $FeCl_2$. Most of the H_2S will then be removed as particles. A set of membrane modules separates biogas into a CH_4-rich stream (product) and a CO_2 rich stream (vented, stored or sold for other applications). Upgraded biogas is compressed to meet product specifications, which can be a natural gas substitute or vehicle fuel.

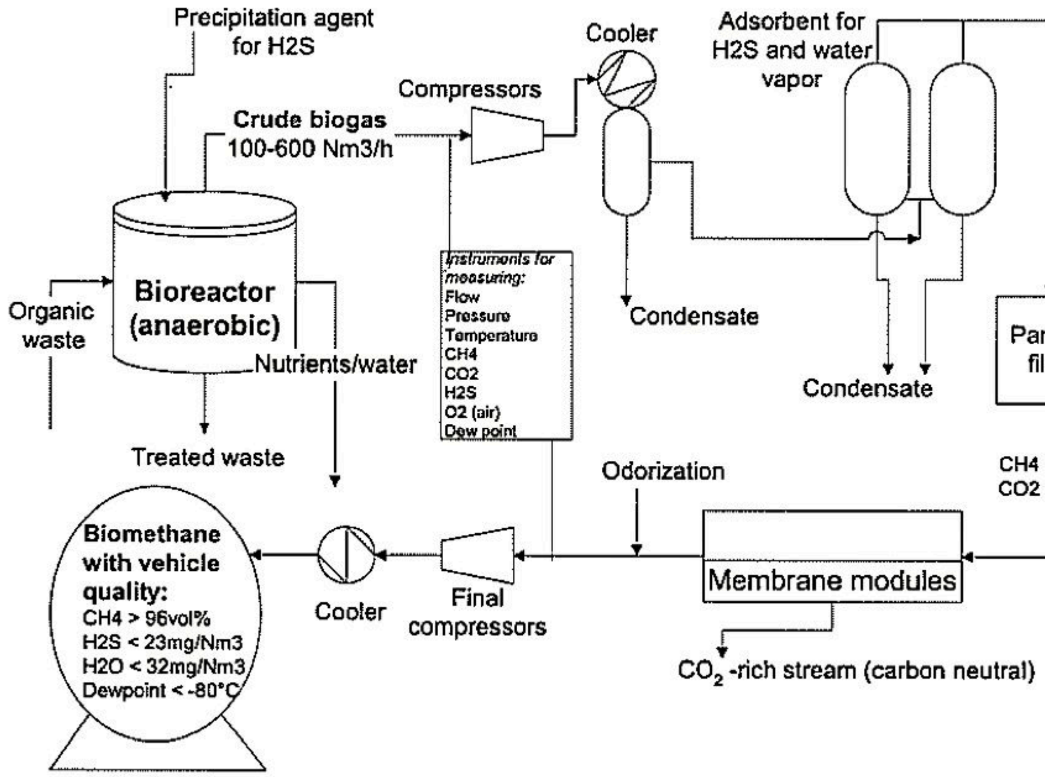
Precipitation agent for H2S
Cooler
Adsorbent for H2S and water vapor
Compressors
Crude biogas 100-600 Nm3/h
Instruments for measuring:
Flow
Pressure
Temperature
CH4
CO2
H2S
O2 (air)
Dew point
Organic waste
Bioreactor (anaerobic)
Nutrients/water
Condensate
Condensate
Particle filter
Treated waste
Odorization
CH4
CO2
Biomethane with vehicle quality:
CH4 > 96vol%
H2S < 23mg/Nm3
H2O < 32mg/Nm3
Dewpoint < -80°C
Cooler
Final compressors
Membrane modules
CO2 -rich stream (carbon neutral)

Figure 6.1 Flow chart of a typical biogas upgrading process [75]

6.1.2 Process design and simulation basis

The process designs are given in Figure 6.2. In process design 1 the feed gas is first compressed to the feed gas pressure level of the membrane module. The retentate is purified CH_4, while CO_2 and some CH_4 permeates through the membrane and exits the membrane module on the permeate side. The permeate is then recompressed and enters the second membrane module. CH_4 is recovered in the retentate stream and recycled to the first membrane module, while CO_2 exits the process in the permeate stream of the second membrane module. Some CH_4 is lost in the permeate stream.

In process design 2 feed gas is compressed and enters the first membrane module. The permeate stream that exits the process contains mostly CO_2, and some CH_4. The retentate gas enters the second membrane module where purified CH_4 exits in the retentate stream. The permeate stream contains some CH_4 and is recycled to the first membrane module.

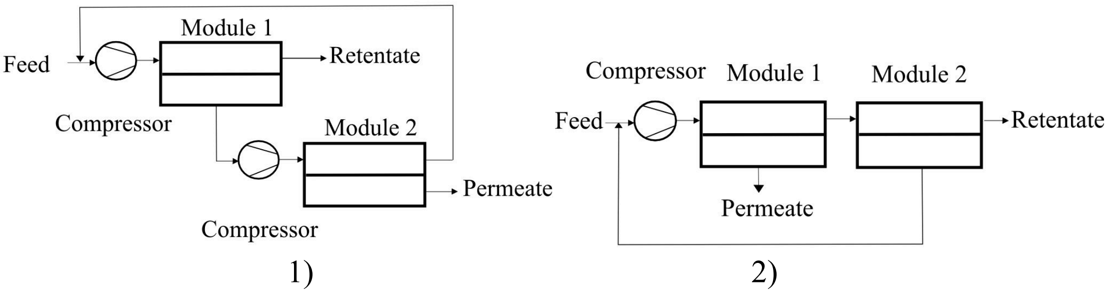

Figure 6.2 Process design 1 and 2 used for simulation

Four simulation cases are given in Table 6.2. The objective of the simulation was to conclude which of the process designs that were preferred for upgrading biogas after economic parameters and investigate the influence of pressure on the simulation results. Chembrane, a simulation membrane module for UniSim, was used to simulate four cases for upgrading of biogas. The feed gas flow rate was set to 300 Nm^3/h, with a feed gas composition of 60 vol% CH_4 and 40 vol% CO_2. This is approximately the real flow rate and composition at the Ecopro plant, given in appendix A. Two different process designs were simulated at 2 and 5 bar feed gas pressure.

Table 6.2 Basis for simulation case A, B, C and D

Case	Process design	Membrane feed gas pressure (bar)
A	1	2
B	2	2
C	1	5
D	2	5

The product of all simulation cases was vehicle fuel grade methane (99.3 vol% methane at 200 bar). Since methane recovery is a very important economic parameter a methane recovery of 98 vol% was set. The membrane area of the two modules used in the simulation cases was adjusted to meet these criteria. A CO_2/CH_4 selectivity of 31 with a CO_2 permeance of 0.16 m^3(STP)/(m^2.h.bar), found by optimization of the operating conditions, was used in the simulation cases.

Assumptions,

1. The initial pressure of biogas was set to 1 atm.
2. Compression ratio was limited to 3.5 due to restrictions in outlet temperature.
3. The compressor efficiency was set to 75 %.
4. Pressure drop in heat exchangers and from the feed side to the retentate side in the membrane modules was set to 0 bar.
5. Both membrane separation modules operates at 25 °C.

6.2 Simulation results and economic cost estimation

6.2.1 Simulation results

Table 6.3 summarizes the results of the four simulation cases. The influence of process design and feed gas pressure on the size and number of process equipment (total membrane area, number of compressors and heat exchangers) and process variables (recycle ratio and compression duty) are given. Capital cost and running cost for biogas upgrading are also given for each simulation case.

Table 6.3 Results of simulation case A, B, C and D

	Case			
Parameters	A	B	C	D
Process design	1	2	1	2
Raw feed biogas flow rate (Nm^3/h)	302	302	302	302
Membrane feed gas pressure (bar)	2	2	5	5
Upgraded biogas flow rate (Nm^3/h)	181	181	181	181
CH_4 purity (vol%)	99.3	99.3	99.3	99.3
CO_2 putiry (vol%)	97.0	97.0	97.0	97.0
CH_4 recovery (vol%)	98.0	98.0	98.0	98.0
Recycle ratio	8.195	10.59	0.86	1.91
Total membrane are (10^3 m^2)	160	167	7.2	7.9
Compression duty (kW)	105	144	78	99
Number of compressors	6	5	7	5
Number of heat exchangers	6	5	7	5
Capital cost (US$ million)	59.715	62.213	4.775	4.622
Running cost (US$/Nm^3 upgraded biogas)	2.696	2.810	0.589	0.603

Pressure is an important process variable. Increasing the feed gas pressure will reduce CO_2 permeance, but the membrane area will be significantly reduced with increased cross-membrane pressure difference according to equation 6.1:

$$q_{p,CO_2} = Q_{CO_2} \cdot A \cdot \Delta p_{CO_2} \tag{6.1}$$

where $q_{p,CO2}$ is the permeation flow rate of CO_2 (m^3(STP)/h), Q_{CO2} is CO_2 permeance (m^3(STP)/(m^2.h.bar)), A is the effective membrane area (m^2) and Δp_{CO2} is the partial pressure differences of CO_2 (bar) in the feed and permeate stream. An increase in feed gas pressure from 2 to 5 bar reduces the total membrane area from $160 \cdot 10^3$ m^2 to

$7.2 \cdot 10^3$ m^2 with process design 1. A lower CO_2 permeance is expected at 5 bar, but higher pressure than 2 bar is preferred due to the dramatic decrease in total membrane area. It could be expected that the total membrane area at low pressure will be less than calculated since the facilitated transport mechanism, which is not included in the simulation model, plays an important role in the trans-membrane transport of CO_2 at low pressure.

The recycle ratios of the low-pressure cases A and B are very high compared to case C and D. The requirement of 99.3 vol% CH_4 in the product steam in the low-pressure cases (A and B) causes a large membrane area. Large amounts of CH_4 will then permeate through the membrane and exit the membrane module in the permeate stream. To secure a methane loss of just 2 vol% a fairy small membrane area is needed in membrane module 2. The result is a large recycle stream. This causes the need for larger equipment size and higher compression duty. Simulation case B has a recycle flow rate/feed gas flow rate-ratio of 10.59 and a total compression duty of 144 kW. Case C has a recycle ratio of 0.86 and a total compression duty of 78 kW, or 0.43 kWh/Nm^3 upgraded biogas. This is higher than results found in literature, probably caused by applying lower permeation data in the membrane modules simulated in this work. A flow sheet of simulation case D is given in Figure 6.3. The mass and energy balance of the flow sheet is given in appendix B.

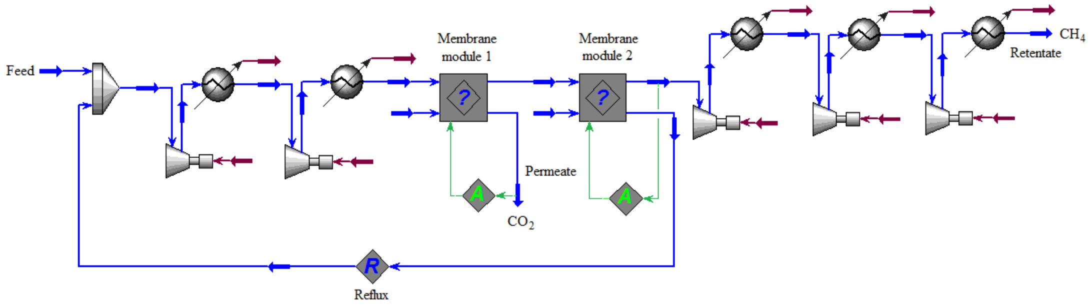

Figure 6.3 Flow sheet of the simulated process of case D in UniSim

Process design 2 needs less compressors and thereby also less heat exchangers than process design 1, because the permeate stream of membrane module 1 does not need to be compressed. Less equipment gives reduced capital cost. On the other hand a larger total membrane area is needed for process design 2, which increases the capital cost.

Pressure drop from the feed side to the retentate side of the membranes, as well as over the heat exchangers was assumed to be zero. There will be a pressure drop in membrane separation process, but it will probably not constitute a significant part of the total energy requirements, nor the number of compressors. Nitrogen was used as sweep gas in the simulation cases, and set to a low flow rate to prevent sweep gas from permeating through the membrane and cause contamination of the product. It is possible that a larger sweep gas flow rate is required in a real biogas separation process, and other gases or vapours (e.g. water vapour) that is easy to separate from the product stream should be considered.

6.2.2 Economic cost estimation

The running costs per Nm^3 upgraded biogas were US$0.589 and US$0.603 for case C and D, respectively. The low running costs of case C originates from the low recycle ratio and thereby low compression duty. Even though the total membrane area is less for case C than case D the capital cost is higher, because two more compressors and heat exchangers are needed in case C than in case D. Case D will have a shorter payback time than case C, and will be the most profitable alternative. The net cash flow of case D is plotted in Figure 6.4.

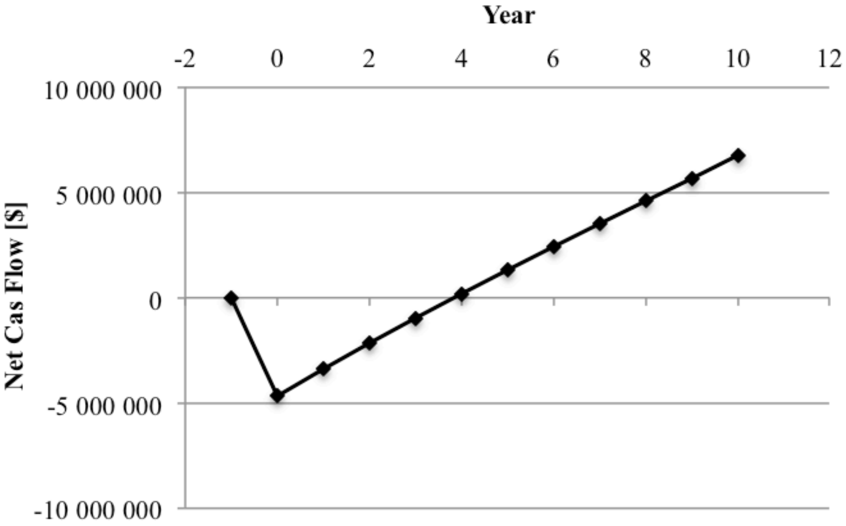

Figure 6.4 Net cash flow diagram of case D

The payback time is calculated by equation 6.2.

$$\text{Pay-back time} = \frac{\text{Total investment}}{\text{Average annual cash flow}} \tag{6.2}$$

With a price of US$1.55/$Nm^3$ upgraded biogas at 200 bar containing 99.3 vol% methane the pay-back time of the investment is about 4.1 years. For case C the pay-back time is 4.2 years. With an internal rate on return on 11,5 % the net present value of the membrane process is US$2.07 million. The low feed gas pressure cases A and B will not be suitable for upgrading of biogas as the running costs are higher than the price of the product. See appendix C for calculations.

It is not easy to conclude which process design is most favourable. The choice of process design does not have a large influence on the capital or running costs, especially when compared to the influence of pressure. Case C has the advantage of low recycle ratio, less total membrane area, and less compression duty. A drawback is a higher total number of compressors and heat exchangers. The reason for having two compressors to compress the gas from 1 to 5 bar was a set maximum outlet temperature of 150 °C of the compressors. If a more temperature resistant material was chosen, or a compressor system designed to compress low pressure gas by a factor higher than 3.5 was used it is possible that only one more compressor is needed in case C than in case D, and that process design 1 would be the more economic competitive alternative. Process design 1 has been found to be the optimal alternative by others [58].

The equations used for calculating equipment cost were based on larger production volumes than what have been studied in this case. Compressors less than 20 kW were cost estimated as if they were 20 kW and heat exchangers less than 10 m^2 were cost estimated as if they were 10 m^2 to be able to use the equations for equipment cost. Thus are the estimated capital costs higher than what real capital cost will be, or the estimations can be used on a scaled up biogas plant. The gas used in this experiment only contains CH_4 and CO_2. Real biogas may contain tracks of many other gases and vapours like hydrogen sulphide, air components, TOC, sometimes ammonia, chlorine, toluene etc. Permeance, selectivity and membrane lifetime can be decreased by the presence of other gases.

Methane loss is an important economic parameter for a biogas upgrading facility. In the simulation cases, the loss of methane was set to 2 vol%. At a biogas plant there is a need of heat (the bioreactor needs 40 °C). An alternative process design could be optimized with integration of methane loss for the purpose of heat production. This might result in another preferred process design as the membrane area and the recycle ratio is greatly reduced by allowing a higher methane loss. Figure 6.5 shows a sensitivity analysis of how the net present value of the biogas upgrading plant after 10 years changes with a +/- 10 % change in the price of upgraded biogas, feed biogas, electricity, cooling water and membrane module. The net present value of the biogas upgrading plant is most sensitive to the change in price of upgraded biogas. The change in cost of membrane module and the value of the raw biogas feedstock are the costs that have the largest impact on the net present value. Variations in the cost of electricity and cooling water do not have a notable effect on the net present value. The price of upgraded biogas must be above US$1.22/$Nm^3$ for the biogas upgrading plant to have a positive net present value after 10 years.

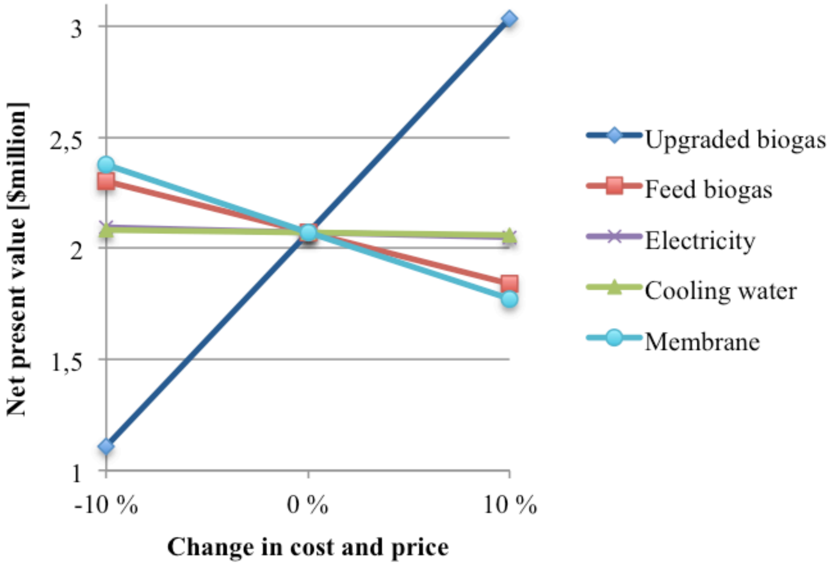

Figure 6.5 Sensitivity analysis of case D that show how net present value changes with a +/- 10% change in price of upgraded biogas and cost of feed biogas, electricity, cooling water and membrane module

7 Uncertainty

7.1 Experimental

The preparation technique used to mimic the dip coating procedure includes manual work without strict standardization. The procedure was not performed in the exact same way each time. The coating step of the membrane preparation technique might result in membranes with different selective layer thicknesses, even if prepared following the same procedure.

Loss of polymer and CNTs by filtering is expected. Some of the polymer and CNTs will be retained in the filter. The actual polymer concentration and CNT content in the polymer might be lower than calculated. During sonication the casting solution becomes hot. Some water will evaporate, and the polymer concentration might be higher than calculated. Some loss of polymer is also expected.

The thickness of the selective layer is not constant, as the membrane is water-swollen to different degrees under operating conditions. Measurement of selective layer thickness in dry state is therefore not the same as during experiments, and thickness variations were observed throughout the cross section of the membrane. This is one of the reasons why gas transport through the membrane is reported as permeance, not permeability.

Measurement of permeation data at low sweep gas flow rates and low pressure gave uncertain results. The permeate flow is low, and the results from the GC contains large fluctuations. CO_2 permeance does not show a clear exponential trend. A combination of low feed gas pressure and low sweep gas flow rate should be avoided to get stable results.

A stopwatch and bubble flow meter was used to calculate sweep gas flow rate and feed gas flow rate. There is a linear relationship between the measured values, and calculated flows. The linear function is generated at low flow rates, and extrapolated to higher operating flow rates. There are sources of uncertainties at both the manual readings, and in the regression. The sweep gas flow rate at 0.29 cm^3/s has a standard deviation of 0.022 cm^3/s, and the sweep gas flow rate of 0.07 cm^3/s has a standard deviation of 0.005 cm^3/s. The linear relationship has a coefficient of determination, R^2, for calculations of the feed gas flow rate was equal to 0.9887.

The experimental set up needs time to stabilize. Relative humidity is the largest source of uncertainty as small adjustments generates large changes in relative humidity of the feed gas. Relative humidity is also the factor that needs the longest time to stabilize. By increasing the relative humidity from low to high values at the same rate twice or more, slightly different permeation data are likely to be obtained each time. CO_2/CH_4 selectivity and CO_2 permeance was reported as an average of 2-3 values at stabilized conditions. The average standard deviation of CO_2 permeance is 0.002 $m^3(STP)/(m^2.h.bar)$ and the average standard deviation of CO_2/CH_4 selectivity is 0.7.

7.2 Simulation and economics

A process simulation will always differ from real process. Simulation was executed to evaluate the process feasibility at an early development stage. More accurate and precise simulations are needed in the following stages of development. The Chembrane membrane module used in UniSim only considers trans-membrane transport of gases by solution diffusion mechanism. The real CO_2 permeance will probably be higher than the simulation results, especially at low pressure, due to the contribution of the facilitated transport mechanism.

The largest source of uncertainty in the operating economic evaluation is the price of upgraded biogas. The price of 99.3 vol% methane as vehicle fuel reported here is a normal price at gas stations, but if Ecopro were first to sell upgraded biogas to a gas station the price would be lower. The price of upgraded biogas can be less than estimated and still be economic competitive, as discussed earlier.

The type of end use of biogas sets the quality demands, and upgrading biogas to 99.3 vol% CH_4 requires a large membrane area. Other applications might demand a lower CH4 concentration in the product stream (e.g. as natural gas substitute or for fuel applications that requires less CH_4 purity).

Cost estimation of the upgraded biogas plant is based on simple calculations, and large levels of uncertainty is therefor involved. The cost of equipment will probably be less then estimated, since the equipment is dimensioned for larger production volumes than needed, based on the simulation results. The total fixed capital is calculated from a simple model, and more accurate calculations are needed to make a good estimate of the investment cost.

8 Conclusion

This master's thesis has focused on testing and optimization of PVAm/PVA blend membrane. A high performance membrane was developed by commercially available polymer. Based on the prepared PVAm/PVA FSC membrane, process simulation and cost estimation was used to investigate the process feasibility of biogas upgrading.

OED was applied to investigate the influence of membrane preparation conditions on its selectivity and CO_2 permeance. The relative importance of the preparation condition parameters were found to be: polymer concentration in casting solution > heat treatment temperature > heat treatment duration > content of CNTs in polymer. The optimized membrane preparation condition in the interval of investigation was: 1 wt% polymer in the casting solution, containing 3 wt% of CNTs, heat-treated at 105 °C for 0.5 h. It was found that a membrane with a very thin selective layer (375 nm) was able to give both high CO_2/CH_4 selectivity and CO_2 permeance.

Reinforcing the PVAm/PVA membrane with CNTs was investigated, but no significant effect was found within the range of investigation. SEM analysis has shown that CNTs gathers in large aggregates, and it was found that an even distribution of well-dispersed CNTs is needed to secure a defect free selective layer.

OED was applied to investigate the influence of operating conditions in a permeation rig. The relative importance of the operating condition parameters was sorted in the following order: relative humidity > sweep gas flow rate > feed gas pressure > feed gas flow rate. The optimized operating conditions in the interval of investigation was found at a feed gas pressure of 2 bar with a relative humidity of 80 %, and a feed gas flow rate and sweep gas flow rate at 12.3 cm^3/s and 0.18 cm^3/s, respectively. A CO_2/CH_4 selectivity of 31 with a CO_2 permeance of 0.16 $m^3(STP)/(m^2.h.bar)$ was obtained at optimized conditions. The separation performance is less than for other membranes reported in literature.

A conceptual design of a biogas upgrading process with a feed gas flow rate at 300 Nm^3/h was conducted. By simulating a two-stage membrane module separation system with recycle it was possible to purify biogas up to 99.3 vol% CH_4 and obtain a CH_4 recovery of 98 %, based on permeation data from the prepared PVAm/PVA membrane. The total membrane area was reduced a lot by increasing the feed gas pressure from 2 to 5 bar. The capital cost of the most promising simulation case was estimated to US\$4.622 million, and the running costs were estimated to be US\$0.603/Nm^3 upgraded biogas. The total membrane area was 7900 m^2. The most important economic parameter for upgrading biogas is the price of upgraded biogas for vehicle fuel, and a price of US\$1.22/Nm^3 is necessary to secure a positive net present value of the project after 10 years.

9 Suggestions for future work

In this work it was found that CO_2 permeance was increasing with decreased membrane thickness, without loss of CO_2/CH_4 selectivity. Even thinner selective layers than tested in these experiments should be investigated as membrane separation performance may increase even more outside the membrane thickness interval reported here.

Optimization of dissolving of CNTs is essential to prepare a defect free membrane with a thin selective layer. CNT aggregates must be dissolved into single tubes so that the selective layer is not penetrated, preventing increased CH_4 permeance and overall resistance to CO_2 transport. Dissolving CNTs with ultrasound has shown to be effective, but optimization of the procedure is needed. Other possibilities for dissolving CNT aggregates, like the use of surfactants, can be investigated. Casting an ultrathin skin layer of PVA on top of the CNT reinforced PVAm/PVA membrane could also be done to eliminate possible pinholes caused by penetration of CNTs through the selective layer. A decrease in CO_2 permeance can be expected due to increased thickness of the selective layer. Other nano particles than CNTs (e.g. SiO_2, TiO_2) could also be added to the polymer as other nano particles might give better results than CNTs.

The effect of heat treatment should be further investigated as the results from the conjoint analysis indicate that less heat treatment duration gives the best membrane performance in the interval investigated. Optimum heat treatment duration is dependent on the temperature. The mechanism of heat treatment should also be investigated to understand the effect of heat treatment and optimize the heat treatment conditions to achieve high separation performance.

Spinning hollow fiber membranes, and preparation of hollow fiber membrane modules will be an important step in further investigation of the PVAm/PVA blend membrane. Many commercial membrane modules are made of hollow fibers, and investigation of up-scaling effect can determine the PVAm/PVA membrane potential for commercialization.

High-pressure applications, like separating CO_2 from natural gas, demand a membrane with higher mechanical strength. Optimal membrane thickness is assumed to increase with higher pressure as well as the effect of CNTs is assumed to be more significant. Further investigation on high-pressure applications for PVAm/PVA membranes are required to reveal the full potential.

Biogas consists of other gases than just CO_2 and CH_4. Test should be run with real biogas to investigate the effect of other gases on the membrane separation performance. H_2S, which is present in biogas and natural gas, is likely to decrease the CO_2 transport through the membrane with around ten percent, because H_2S competes with CO_2 transport. CH_4 transport through the membrane might be enhanced [24].

The economic cost estimation in this work is based on simple equations, and gives only a brief overview of the capital costs and running costs. A more detailed economic evaluation should be conducted to give a more precise impression of the economic feasibility of a biogas upgrading plant. Optimization of operating condition in the simulation case can be optimized to achieve higher separation performance, and reduce capital costs and running costs.

References

1. Koros, W.J. and G.K. Fleming, *Membrane-based gas separation.* Journal of Membrane Science, 1993. **83**(1): p. 1-80.
2. Baker, R.W., *Future Directions of Membrane Gas Separation Technology.* Industrial & Engineering Chemistry Research, 2002. **41**(6): p. 1393-1411.
3. Liu, L., A. Chakma, and X. Feng, *Gas permeation through water-swollen hydrogel membranes.* Journal of Membrane Science, 2008. **310**(1–2): p. 66-75.
4. *International Energy Outlook 2011 - Highlights*. 2012 [cited 2012 January 31]; Available from: http://www.eia.gov/forecasts/ieo/index.cfm.
5. IPCC2007, *Summary for Policymakers*, in *Climate Change 2007: The Physical Science Basis. Contribution of Working Group I to the Fourth Assessment Report of the Intergovernmental Panel on Climate Change.*, S. Solomon, Qin, D., Manning, M., Chen, Z., Marquis, M., Averyt K.B., Tignor, M., Miller H.L., Editor, Cambridge, United Kingdom and New York, USA: Cambridge University Press 2007.
6. IPCC2011, *Summary for Policymakers*, in *IPCC Special Report on Renewable Energy Sources and Climate Change Mitigation*, O. Edenhofer, Pichs-Madruga R., Sokona, Y., Seyboth, K., Matschoss, P., Kadner, S., Zwickel, T., Eickemeier, P., Hansen, G., Schlömer, S., von Stechow, C., Editor, Cambridge, United Kingdom and New York, NY, USA: Cambridge University Press.
7. Makaruk, A., M. Miltner, and M. Harasek, *Membrane biogas upgrading processes for the production of natural gas substitute.* Separation and Purification Technology, 2010. **74**(1): p. 83-92.
8. Röhr, M. and R. Wimmerstedt, *A comparison of two commercial membranes used for biogas upgrading.* Desalination, 1990. **77**(0): p. 331-345.
9. Shekhawat, D., D.R. Luebke, and H.W. Pennline, *A Review of Carbon Dioxide Selective Membranes: A Topical Report*, in *DOE/NETL-2003/1200,* 2003, United States Department of Energy.
10. Deng, L., *Development of Novel PVAm/PVA Blend FSC Membrane for CO_2 Capture*, at *Deparment of Chemical Engineering,* 2009, NTNU: Trondheim.
11. Kim, T.-J., B. Li, and M.-B. Hägg, *Novel fixed-site–carrier polyvinylamine membrane for carbon dioxide capture.* Journal of Polymer Science Part B: Polymer Physics, 2004. **42**(23): p. 4326-4336.
12. Mulder, M., *Basic Principles of Membrane Technology*. 2 ed. 1996, Dodrecht, The Netherlands: Kluwer Academic Publishers.
13. Baker, R.W., *Membrane Technology and Applications*. 2. ed. 2004, New York: McGraw-Hill.
14. Jones, C.W. and W.J. Koros, *Carbon molecular sieve gas separation membranes-I. Preparation and characterization based on polyimide precursors.* Carbon, 1994. **32**(8): p. 1419-1425.
15. Bernardo, P., E. Drioli, and G. Golemme, *Membrane Gas Separation: A Review/State of the Art.* Industrial & Engineering Chemistry Research, 2009. **48**(10): p. 4638-4663.

16. Park, H.B., et al., *Thermally rearranged (TR) polymer membranes for CO2 separation.* Journal of Membrane Science, 2010. **359**(1–2): p. 11-24.

17. Iarikov, D.D. and S. Ted Oyama, *Chapter 5 - Review of CO2/CH4 Separation Membranes*, in *Membrane Science and Technology*, S.T. Oyama and M.S.-W. Susan, Editors. 2011, Elsevier. p. 91-115.

18. Himeno, S., et al., *Synthesis and Permeation Properties of a DDR-Type Zeolite Membrane for Separation of CO2/CH4 Gaseous Mixtures.* Industrial & Engineering Chemistry Research, 2007. **46**(21): p. 6989-6997.

19. Jiang, L.Y., T.-S. Chung, and R. Rajagopalan, *Dual-layer hollow carbon fiber membranes for gas separation consisting of carbon and mixed matrix layers.* Carbon, 2007. **45**(1): p. 166-172.

20. Tsai, C.-Y., et al., *Dual-layer asymmetric microporous silica membranes.* Journal of Membrane Science, 2000. **169**(2): p. 255-268.

21. Lozano, L.J., et al., *Recent advances in supported ionic liquid membrane technology.* Journal of Membrane Science, 2011. **376**(1–2): p. 1-14.

22. Yampolskii, Y., I. Pinnau, and B. Freeman, *Materials Science of Membranes for Gas and Vapor Separation*. 2006, Chichester, England: John Wiley & Sons, Ltd.

23. Kimmerle, K., T. Hofmann, and H. Strathmann, *Analysis of gas permeation through composite membranes.* Journal of Membrane Science, 1991. **61**(0): p. 1-17.

24. Yampolskii, Y. and B. Freeman, *Membrane Gas Separation*. 1 ed. 2010, Chichester, UK: John Wiley & Sons LTd.

25. Lin, H. and B.D. Freeman, *Materials selection guidelines for membranes that remove CO2 from gas mixtures.* Journal of Molecular Structure, 2005. **739**(1–3): p. 57-74.

26. Zou, J. and W.S.W. Ho, *CO2-selective polymeric membranes containing amines in crosslinked poly(vinyl alcohol).* Journal of Membrane Science, 2006. **286**(1–2): p. 310-321.

27. Shen, J., et al., *Facilitated transport of carbon dioxide through poly(2-N,N-dimethyl aminoethyl methacrylate-co-acrylic acid sodium) membrane.* Separation and Purification Technology, 2006. **51**(3): p. 345-351.

28. Noble, R.D., *Analysis of facilitated transport with fixed site carrier membranes.* Journal of Membrane Science, 1990. **50**(2): p. 207-214.

29. Cussler, E.L., R. Aris, and A. Bhown, *On the limits of facilitated diffusion.* Journal of Membrane Science, 1989. **43**(2–3): p. 149-164.

30. Noble, R.D., *Analysis of ion transport with fixed site carrier membranes.* Journal of Membrane Science, 1991. **56**(2): p. 229-234.

31. LeBlanc Jr, O.H., et al., *Facilitated transport in ion-exchange membranes.* Journal of Membrane Science, 1980. **6**(0): p. 339-343.

32. Matsuyama, H., K. Hirai, and M. Teramoto, *Selective permeation of carbon dioxide through plasma polymerized membrane from diisopropylamine.* Journal of Membrane Science, 1994. **92**(3): p. 257-265.

33. Matsuyama, H., M. Teramoto, and H. Sakakura, *Selective permeation of CO2 through poly 2-(N,N-dimethyl)aminoethyl methacrylate membrane prepared*

by plasma-graft polymerization technique. Journal of Membrane Science, 1996. **114**(2): p. 193-200.

34. Matsuyama, H., et al., *Facilitated transport of CO2 through various ion exchange membranes prepared by plasma graft polymerization.* Journal of Membrane Science, 1996. **117**(1–2): p. 251-260.
35. Yoshikawa, M., et al., *Selective permeation of carbon dioxide through synthetic polymer membranes having pyridine moiety as a fixed carrier.* Journal of Applied Polymer Science, 1988. **35**(1): p. 145-154.
36. Noble, R.D., *Generalized microscopic mechanism of facilitated transport in fixed site carrier membranes.* Journal of Membrane Science, 1992. **75**(1–2): p. 121-129.
37. Cai, Y., et al., *Gas transport property of polyallylamine–poly(vinyl alcohol)/polysulfone composite membranes.* Journal of Membrane Science, 2008. **310**(1–2): p. 184-196.
38. Donaldson, T.L. and Y.N. Nguyen, *Carbon Dioxide Reaction Kinetics and Transport in Aqueous Amine Membranes.* Industrial & Engineering Chemistry Fundamentals, 1980. **19**(3): p. 260-266.
39. Deng, L., T.-J. Kim, and M.-B. Hägg, *Facilitated transport of CO2 in novel PVAm/PVA blend membrane.* Journal of Membrane Science, 2009. **340**(1–2): p. 154-163.
40. Geankoplis, C.J., *Transport Processes and Separation Process Principles*. 4 ed. 2003, New Jersey: Pearson Education, Inc.
41. Thundyil, M.J. and W.J. Koros, *Mathematical modeling of gas separation permeators — for radial crossflow, countercurrent, and cocurrent hollow fiber membrane modules.* Journal of Membrane Science, 1997. **125**(2): p. 275-291.
42. Lloyd M, R., *The upper bound revisited.* Journal of Membrane Science, 2008. **320**(1-2): p. 390-400.
43. Deng, L., et al., *PVA/PVAm Blend FSC Membrane for Natural Gas Sweetening*, in *Proceedings of the 1st Annual Gas Processing Symposium*, E.A. Hassan, et al., Editors. 2009, Elsevier: Amsterdam. p. 247-255.
44. Zhang, Y., Z. Wang, and S. Wang, *Novel fixed-carrier membranes for CO2 separation.* Journal of Applied Polymer Science, 2002. **86**(9): p. 2222-2226.
45. Chen, W., et al., *Enhanced mechanical properties and morphological characterizations of poly(vinyl alcohol)–carbon nanotube composite films.* Applied Surface Science, 2005. **252**(5): p. 1404-1409.
46. Lu, K.L., et al., *Mechanical damage of carbon nanotubes by ultrasound.* Carbon, 1996. **34**(6): p. 814-816.
47. Vaisman, L., H.D. Wagner, and G. Marom, *The role of surfactants in dispersion of carbon nanotubes.* Advances in Colloid and Interface Science, 2006. **128–130**(0): p. 37-46.
48. Hashemifard, S.A., A.F. Ismail, and T. Matsuura, *Co-casting technique for fabricating dual-layer flat sheet membranes for gas separation.* Journal of Membrane Science, 2011. **375**(1–2): p. 258-267.

49. Staudt-Bickel, C. and W. J. Koros, *Improvement of CO2/CH4 separation characteristics of polyimides by chemical crosslinking.* Journal of Membrane Science, 1999. **155**(1): p. 145-154.
50. Bos, A., et al., *CO2-induced plasticization phenomena in glassy polymers.* Journal of Membrane Science, 1999. **155**(1): p. 67-78.
51. Wessling, M., et al., *Plasticization of gas separation membranes.* Gas Separation &amp; Purification, 1991. **5**(4): p. 222-228.
52. Dong, C., et al., *Preparation of polyvinylamine/polysulfone composite hollow-fiber membranes and their CO2/CH4 separation performance.* Journal of Applied Polymer Science, 2006. **101**(3): p. 1885-1891.
53. Matsuyama, H., et al., *Facilitated transport of CO2 through polyethylenimine/poly(vinyl alcohol) blend membrane.* Journal of Membrane Science, 1999. **163**(2): p. 221-227.
54. Bos, A., et al., *Plasticization-resistant glassy polyimide membranes for CO2/CO4 separations.* Separation and Purification Technology, 1998. **14**(1–3): p. 27-39.
55. Sandru, M., S.H. Haukebø, and M.-B. Hägg, *Composite hollow fiber membranes for CO2 capture.* Journal of Membrane Science, 2010. **346**(1): p. 172-186.
56. R.M, B., *Diffusivities in glassy polymers for the dual mode sorption model.* Journal of Membrane Science, 1984. **18**(0): p. 25-35.
57. Deng, L. and M.-B. Hägg, *Swelling behavior and gas permeation performance of PVAm/PVA blend FSC membrane.* Journal of Membrane Science, 2010. **363**(1–2): p. 295-301.
58. Deng, L. and M.-B. Hägg, *Techno-economic evaluation of biogas upgrading process using CO2 facilitated transport membrane.* International Journal of Greenhouse Gas Control, 2010. **4**(4): p. 638-646.
59. Bhide, B.D. and S.A. Stern, *Membrane processes for the removal of acid gases from natural gas. I. Process configurations and optimization of operating conditions.* Journal of Membrane Science, 1993. **81**(3): p. 209-237.
60. Peters, L., et al., *CO2 removal from natural gas by employing amine absorption and membrane technology—A technical and economical analysis.* Chemical Engineering Journal, 2011. **172**(2–3): p. 952-960.
61. Scholes, C.A., G.W. Stevens, and S.E. Kentish, *Membrane gas separation applications in natural gas processing.* Fuel, (0).
62. Grainger, D. and M.-B. Hägg, *Techno-economic evaluation of a PVAm CO2-selective membrane in an IGCC power plant with CO2 capture.* Fuel, 2008. **87**(1): p. 14-24.
63. Hussain, A. and M.-B. Hägg, *A feasibility study of CO2 capture from flue gas by a facilitated transport membrane.* Journal of Membrane Science, 2010. **359**(1–2): p. 140-148.
64. http://www.polymerprocessing.com. *poly(vinyl alcohol).* [cited 2011 20.10.]; Available from: http://www.polymerprocessing.com/polymers/PVOH.html.
65. BouLing Chemical Co., L. *polyvinyl alcohol PVA.* [cited 2011 2010]; Available from: http://www.wanwei-pva.com/polyvinyl-alcohol-PVA.htm.

66. Pinschmist, R.K. and D.J. Sag. *Polyvinylamine (Overview)*. [cited 2011 18.10]; Available from: http://www.polymersnetbase.com.
67. Uyama, S. and K. Uyama. *Polyvinylamine (Preparation, Properties and Applications*. [cited 2011 18.10]; Available from: http://www.polymersnetbase.com.
68. SHOWA_DENKO. *Multiwall Carbon Nanotubes Manufactured by SHOWA DENKO K. K.* 2012 [cited 2012 27.04]; Available from: http://www.sdk.co.jp/english/products/137/139.html.
69. He, X., *Development of Hollow Fiber Carbon Membranes for CO2 Separation*, at *Department of Chemical engineering,* 2011, NTNU: Trondheim.
70. Zhu, J., et al., *Optimization method for building envelope design to minimize carbon emissions of building operational energy consumption using orthogonal experimental design (OED).* Habitat International, (0).
71. Berstad, E., *Testing and optimization of CNTs reinforced PVAm/PVA blend membrane and process for biogas upgrading*, 2011, Norwegian University of Science and Technology, NTNU: Trondheim. p. 35.
72. Visser, T., N. Masetto, and M. Wessling, *Materials dependence of mixed gas plasticization behavior in asymmetric membranes.* Journal of Membrane Science, 2007. **306**(1–2): p. 16-28.
73. Quinn, R., J.B. Appleby, and G.P. Pez, *New facilitated transport membranes for the separation of carbon dioxide from hydrogen and methane.* Journal of Membrane Science, 1995. **104**(1–2): p. 139-146.
74. Way, J.D., et al., *Facilitated transport of CO2 in ion exchange membranes.* AIChE Journal, 1987. **33**(3): p. 480-487.
75. Hägg, M.-B. and J.A. Lie, *Upgrading biogas by membranes for vehicle fuel or injection into the European Gas Network*, in *ECI Conferences,*2006: Tomar, Portugal.
76. Sinnott, R.K., *Chemical Engineering Design*. 4 ed. Vol. 6. 2005, Burlington: Elsevier.
77. Hillestad, M., *Lecture notes: Driftskostnader, TKP 4165 - Prosessutforming*, 2010.
78. Sinnott, R. and G. Towler, *Chemical Engineering Design*. 5 ed. 2009, Burlington: Elsevier.
79. Skogestad, S., *Prosessteknikk: Masse- og energibalanser*. 2 ed. 2003, Trondheim, Norway: Tapir akademisk forlag.
80. Solheim, O.E., *E-mail correspondance*, 2010, Cambi.

Appendix A: Gas composition at Ecopro

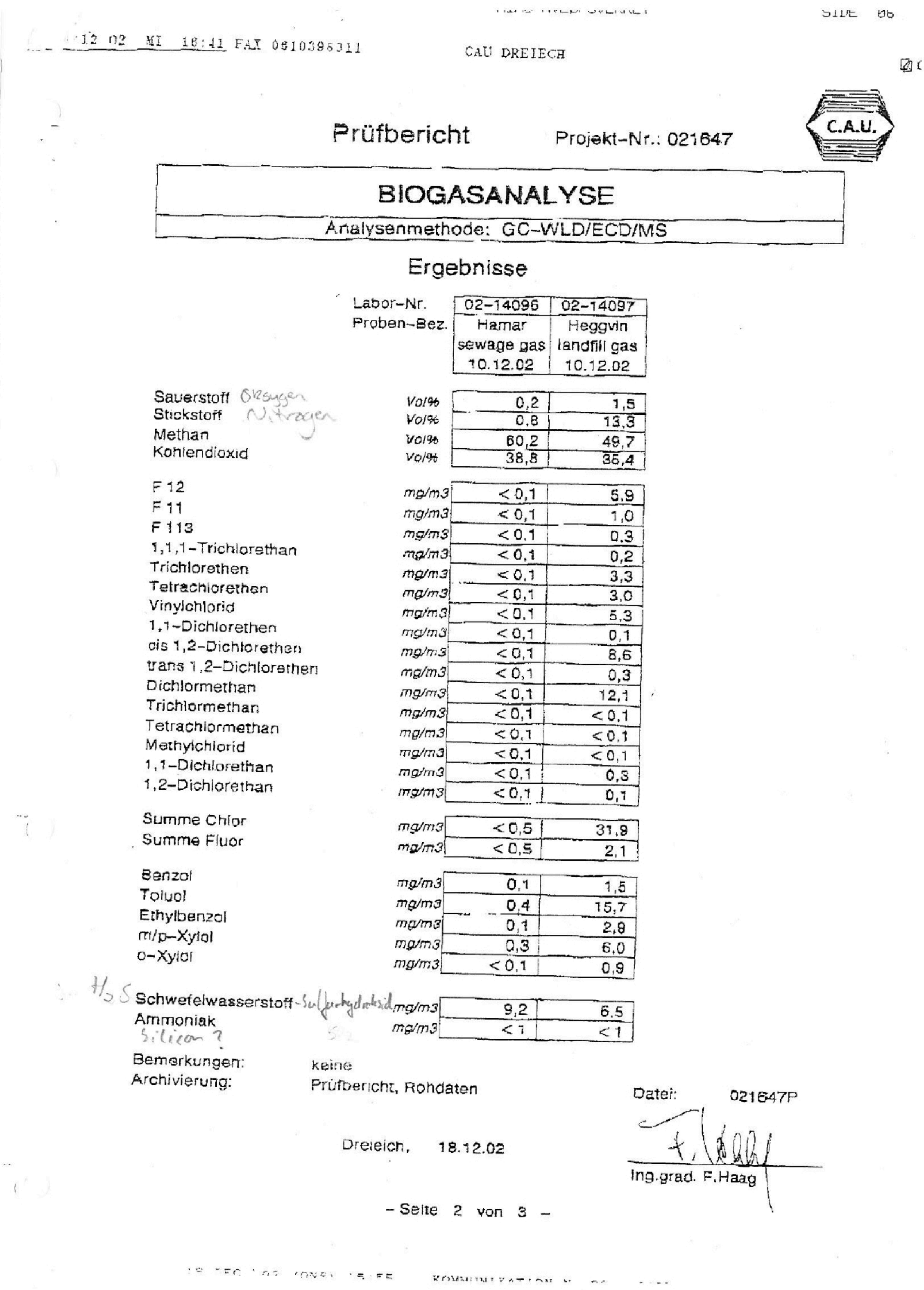

12 02 MI 18:41 FAX 0610396311 CAU DREIECH SIDE 06

C.A.U.

Prüfbericht

Projekt-Nr.: 021647

BIOGASANALYSE

Analysenmethode: GC-WLD/ECD/MS

Ergebnisse

		02-14096	02-14097
Labor-Nr.		02-14096	02-14097
Proben-Bez.		Hamar sewage gas 10.12.02	Heggvin landfill gas 10.12.02
Sauerstoff Oksygen	Vol%	0,2	1,5
Stickstoff Nitrogen	Vol%	0,8	13,3
Methan	Vol%	60,2	49,7
Kohlendioxid	Vol%	38,8	35,4
F 12	mg/m3	< 0,1	5,9
F 11	mg/m3	< 0,1	1,0
F 113	mg/m3	< 0,1	0,3
1,1,1-Trichlorethan	mg/m3	< 0,1	0,2
Trichlorethen	mg/m3	< 0,1	3,3
Tetrachlorethen	mg/m3	< 0,1	3,0
Vinylchlorid	mg/m3	< 0,1	5,3
1,1-Dichlorethen	mg/m3	< 0,1	0,1
cis 1,2-Dichlorethen	mg/m3	< 0,1	8,6
trans 1,2-Dichlorethen	mg/m3	< 0,1	0,3
Dichlormethan	mg/m3	< 0,1	12,1
Trichlormethan	mg/m3	< 0,1	< 0,1
Tetrachlormethan	mg/m3	< 0,1	< 0,1
Methylchlorid	mg/m3	< 0,1	< 0,1
1,1-Dichlorethan	mg/m3	< 0,1	0,3
1,2-Dichlorethan	mg/m3	< 0,1	0,1
Summe Chlor	mg/m3	< 0,5	31,9
Summe Fluor	mg/m3	< 0,5	2,1
Benzol	mg/m3	0,1	1,5
Toluol	mg/m3	0,4	15,7
Ethylbenzol	mg/m3	0,1	2,8
m/p-Xylol	mg/m3	0,3	6,0
o-Xylol	mg/m3	< 0,1	0,9
H_2S Schwefelwasserstoff - Sulfurhydroksid	mg/m3	9,2	6,5
Ammoniak	mg/m3	< 1	< 1
Silicon ?			

Bemerkungen: keine

Archivierung: Prüfbericht, Rohdaten

Datei: 021647P

Dreieich, 18.12.02

F. Haag

Ing.grad. F.Haag

- Seite 2 von 3 -

Appendix B: Mass and energy balance of simulation case D

The total mass balance of simulation case D, illustrated in the flow sheet in Figure 6.3, is given in Table B.1.

Table B.1 Mass balance of simulation case D

Flow rate in (kmol/h)		Flow rate out (kmol/h)	
Feed gas	13.68	CO_2 rich stream	5.47
		CH_4 rich stream	8.21
Sum	13.68	**Sum**	13.68

The energy balance of simulation case D, illustrated in the flow sheet in Figure 6.3, is given in Table B.2.

Table B.2 Energy balance of simulation case D

Heat flow in (MJ/h)		Heat flow out (MJ/h)	
Feed gas	-2738	CO_2 rich stream	-2103
Compressor 1	184	CH_4 rich stream	-658
Compressor 2	48	Heat exchanger 1	181
Compressor 3	39	Heat exchanger 2	50
Compressor 4	37	Heat exchanger 3	42
Compressor 5	34	Heat exchanger 4	42
		Heat exchanger 5	50
Sum	-2396	**SUM**	-2396

Appendix C: Economic calculations

C.1 Cost estimation

Compressors, Centrifugal compressors were used below 50 bar, while reciprocating compressors were used to compress CH_4 to 50 bar and above. Equation C.1 [76] was used to calculate the capital cost of the compressors. The compressors that were below 20 kW were cost estimated as 20 kW since the formula only is valid for compressors above 20 kW.

$$C_b = C \cdot S^n \cdot \frac{I_{2012}}{I_{1998}} \tag{C.1}$$

where C_b (US$) is the total cost, C=1920 for centrifugal compressors and C=2700 for reciprocation compressors, S (kW) is the capacity of the compressor and n=0.8 is an exponential factor. $I_{2012}/I_{1998}=1.49$ [77] is the chemical engineering plant cost index, used to adjust the cost to a 2012 cost level. Compressor efficiency is estimated to be 0.75. The compressor capacities and equipment costs for case A, B, C and D are given in Table C.1, Table C.2, Table C.3 and Table C.4.

Table C.1 Compressor capacities and investments costs for case A

Case A	Capacity (kW)	Cost (US$ thousand)
K-100	20	35
K-101	78	95
K-102	20	35
K-103	20	35
K-104	20	45
K-105	20	45
Total		**290**

Table C.2 Compressor capacities and investments costs for case B

Case B	Capacity (kW)	Cost (US$ thousand)
K-100	142	155
K-102	20	35
K-103	20	35
K-104	20	45
K-105	20	45
Total		**315**

Table C.3 Compressor capacities and investments costs for case C

Case C	Capacity (kW)	Cost (US$ thousand)
K-100	20	35
K-101	20	35
K-102	20	35
K-103	20	45
K-104	20	45
K-105	26	40
K-106	24	40
Total		**275**

Table C.4 Compressor capacities and investments costs for case D

Case D	Capacity (kW)	Cost (US$ thousand)
K-100	20	35
K-101	68	85
K-102	20	35
K-103	20	45
K-104	20	45
Total		**245**

Heat exchangers, U-tube shell and tube heat exchangers were used for cost estimation. Equation C.2 [78] was used to calculate the cost.

$$C_b = (a + b \cdot S^n) \cdot \frac{I_{2012}}{I_{2007}} \tag{C.2}$$

Where a=24000 and b=46 are constants, S (m^2) is the heat exchanger area, n=1.2 is an exponential factor and $I_{2012}/I_{2007}=1.13$ corrects for increase in cost from 2007 to 2012.

The heat exchanger area is calculated from equation C.3 and A.4 [79].

$$Q = U \cdot A \cdot \Delta T_{lm} = m_c \cdot c_{p,c} \cdot \Delta T_c \tag{C.3}$$

Where Q (kW) is the heat transferred across the heat exchanger, U ($kW/m^2.K$) is the heat transfer coefficient, m_c (kg/s) is the cooling water flow, $c_{p,c}$ is the heat capacity of water (4.18 kJ/kg·°C), ΔT_c (K) is the temperature difference of cooling water and ΔT_{lm} (K) is the logarithmic mean temperature was calculated from equation C.4.

$$\Delta T_{lm} = \frac{\Delta T_1 - \Delta T_2}{\ln(\Delta T_1 / \Delta T_2)} \tag{C.4}$$

All heat exchangers were calculated to be less than 10 m^2 because of the low gas flow rates. 10 m^2 were still used to calculate the cost of the heat exchangers due to the minimum area of 10 m^2 that is needed for the formula to be valid. The cost of a heat exchanger is then calculated to be US$30,000.

Membranes, Polymer membranes were estimated to a cost of US$20/m^2 by co-supervisor Dr. Xuezhong He. An estimated lifetime of five years was used for the membrane modules. With a project lifetime of 20 years, a total of four membrane modules are needed, so the total membrane capital cost was calculated as four times the cost of one membrane module. The costs of membranes in the different cases can be found in Table C.5.

Table C.5 Cost estimation of membranes for simulation case A, B, C and D

Case	Area (m^2)	Cost of 4x modules (US$ thousand)
A	160,000	12,800
B	167,000	13,360
C	7,200	576
D	7,900	632

C.2 Project fixed capital cost

Cost estimation of a chemical plant is often based on the cost of the mayor equipment. A factor model [76] was used to estimate the total fixed capital cost, which is shown in Table C.6.

Table C.6 Total fixed capital cost for simulation case A, B, C and D

Item	Factor	Cost (US$ thousand)			
		Case A	Case B	Case C	Case D
Compressors		290	315	275	245
Heat exchangers		180	150	210	150
Membranes		12,800	13,360	576	632
Total purchase cost	C_e	**13,270**	**13,825**	**1,061**	**1,027**
f_{er} Equipment erection	0.3				
f_p Piping	0.8				
f_i Instrumentation and control	0.3				
f_{el} Electrical	0.2				
f_c Civil engineering work	0.3				
f_s Structures and buildings	0.2				
f_l Lagging and paint	0.1				
ISBL cost $C=\sum C_e$	**3.2**	**42,464**	**44,240**	**3,395**	**3,286**
Design and engineering	0.3				
Contingency	0.1				
Total fixed capital cost	**4.5**	**59,715**	**62,213**	**4,775**	**4,622**

C.3 Running costs

Biogas, The biogas from Ecopro is estimated at a price of ¢3.5/kWh. Ecopro produces 2,667,000 Nm^3/year of biogas which contains 6 kWh/Nm^3 of energy [80].

The cost of biogas is calculated by equation C.5.

$$\text{Cost of biogas} = \text{energy containment} \cdot \text{production of biogas} \cdot \text{price} \tag{C.5}$$

This gives a running cost of US$560,000/year.

Electricity, The cost of electricity is estimated to US¢6.14/kWh [77]. The compressors will count for most of the electricity consumption. The cost of electricity in the four cases is given in Table C.7, with an estimated 8000 operating hours per year.

Table C.7 The cost of electricity for simulation case A, B, C and D

Case	**Price of electricity (US¢/kWh)**	**Total compression duty (kW)**	**Cost of electricity (US$/year)**
A	6.14	105	55,000
B	6.14	144	75,000
C	6.14	78	40,000
D	6.14	99	50,000

Cooling water, The price of cooling water is estimated to US¢18/m^3 [77]. The cost of cooling water in the four cases is listed in Table C.8, with an estimated 8000 operating hours per year.

Table C.8 The cost of cooling water for simulation case A, B, C and D

Case	**Price of cooling water (US¢/m^3)**	**Water consumption (m^3/year)**	**Cost of cooling water (US$/year)**
A	18	155,000	30,000
B	18	210,000	40,000
C	18	120,000	25,000
D	18	145,000	30,000

Total running costs, It is estimated that the process operators that currently work at Ecopro will operate the separation process without hiring more staff. The total running costs are shown in Table C.9.

Table C.9 Total running cost for simulation case A, B, C and D

Item		**Cost (US$ thousand)**			
Variable costs		**Case A**	**Case B**	**Case C**	**Case D**
Biogas		560	560	560	560
Electricity		55	75	40	50
Cooling water		30	40	25	30
Total variable costs		**645**	**675**	**625**	**640**
Fixed cost					
Maintenance	5% of ISBL	2,214	2,212	170	165
Land tax	2% of ISBL	850	885	68	66
Insurance	1% of ISBL	425	443	34	33
Total fixed cost		**3,399**	**3,540**	**272**	**264**
Total operating costs without depreciation		**4,044**	**4,215,000**	**897,000**	**904**
Running cost (US\$/Nm^3 upgraded biogas)		**2.696**	**2.810**	**0.598**	**0.603**

C.4 Running income

All four cases give a production of approximately $1,5 \cdot 10^6$ Nm^3 upgraded biogas per year. The price of upgraded biogas for vehicle fuel at 200 bar was set to US\$1.55/Nm^3 in collaboration with supervisor Professor May-Britt Hägg if the biogas was to be sold directly at a gas station to customers. This gives an income of US$2.325 million/year for all cases. The net present value and cash flow is calculated from the work sheet in Table C.10 [77].

Table C.10 Work sheet for calculations of net present value and cash flow

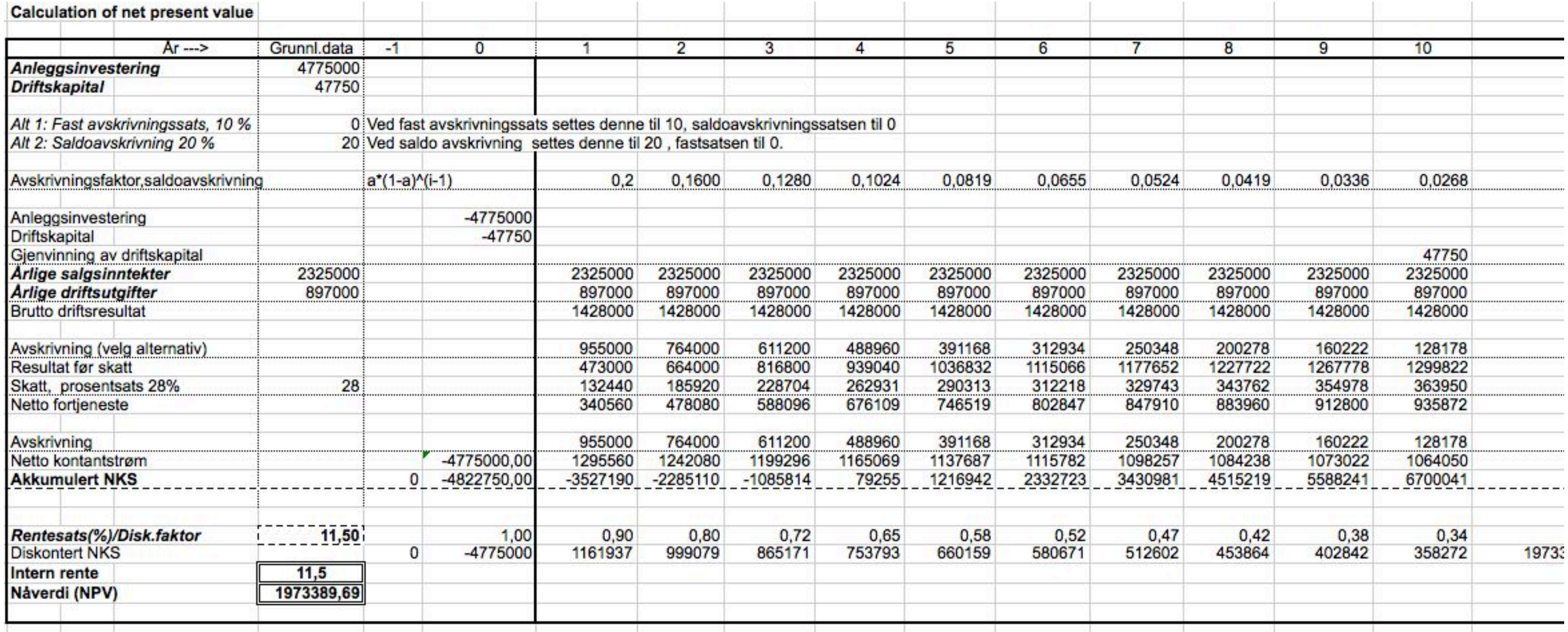

Calculation of net present value

År --->	Grunnl.data	-1	0	1	2	3	4	5	6	7	8	9	10	
Anleggsinvestering	4775000													
Driftskapital	47750													
Alt 1: Fast avskrivningssats, 10 %	0	Ved fast avskrivningssats settes denne til 10, saldoavskrivningssatsen til 0												
Alt 2: Saldoavskrivning 20 %	20	Ved saldo avskrivning settes denne til 20 , fastsatsen til 0.												
Avskrivningsfaktor,saldoavskrivning		a*(1-a)^(i-1)		0,2	0,1600	0,1280	0,1024	0,0819	0,0655	0,0524	0,0419	0,0336	0,0268	
Anleggsinvestering			-4775000											
Driftskapital			-47750											
Gjenvinning av driftskapital													47750	
Årlige salgsinntekter	2325000			2325000	2325000	2325000	2325000	2325000	2325000	2325000	2325000	2325000	2325000	
Årlige driftsutgifter	897000			897000	897000	897000	897000	897000	897000	897000	897000	897000	897000	
Brutto driftsresultat				1428000	1428000	1428000	1428000	1428000	1428000	1428000	1428000	1428000	1428000	
Avskrivning (velg alternativ)				955000	764000	611200	488960	391168	312934	250348	200278	160222	128178	
Resultat før skatt				473000	664000	816800	939040	1036832	1115066	1177652	1227722	1267778	1299822	
Skatt, prosentsats 28%	28			132440	185920	228704	262931	290313	312218	329743	343762	354978	363950	
Netto fortjeneste				340560	478080	588096	676109	746519	802847	847910	883960	912800	935872	
Avskrivning				955000	764000	611200	488960	391168	312934	250348	200278	160222	128178	
Netto kontantstrøm			-4775000,00	1295560	1242080	1199296	1165069	1137687	1115782	1098257	1084238	1073022	1064050	
Akkumulert NKS		0	-4822750,00	-3527190	-2285110	-1085814	79255	1216942	2332723	3430981	4515219	5588241	6700041	
Rentesats(%)/Disk.faktor	**11,50**		1,00	0,90	0,80	0,72	0,65	0,58	0,52	0,47	0,42	0,38	0,34	
Diskontert NKS		0	-4775000	1161937	999079	865171	753793	660159	580671	512602	453864	402842	358272	19733
Intern rente	**11,5**													
Nåverdi (NPV)	**1973389,69**													

Appendix D: Original project description

M-BH-3: Testing and optimization of PVAm/PVA blend membranes for biogas upgrading

This project will focus on the testing and optimizing of polyvinylamine/polyvinylalcohol (PVAm/PVA) blend membrane for biogas upgrading. The objective of this project is to develop a high performance membrane biogas upgrading. Based on the prepared PVAm/PVA fixed-sit-carrier (FSC) membranes, process simulation will also be conducted to evaluate membrane separation performance and process feasibility using HYSYS and economic cost estimation

The scope of this work can be specified as follows:

1. Permeation tests of the blend FSC membranes at different pressures (2bar, 5bar and 10bar). The membranes will be prepared in various conditions with various thicknesses. The tests will be performed in an advanced mixed gas permeation rig with a humidity regulator and an automatic operating monitoring and controlling system.
2. Optimization of the membrane preparation conditions based on the membrane separation performance at elevated pressures. The effects of cross-linking temperature and time, membrane thickness addition of carbon nano tubes (CNTs) will be investigated and the optimized membrane preparation condition determined.
3. Optimization of operating conditions based on membrane separation performance.
4. Characterizations of the blend membranes using SEM.
5. Conceptual design and process simulation for biogas upgrading process.

Co-supervisor Dr. Xuezhong He

Reserved for Eivind Berstad

Appendix E: Risk assessment

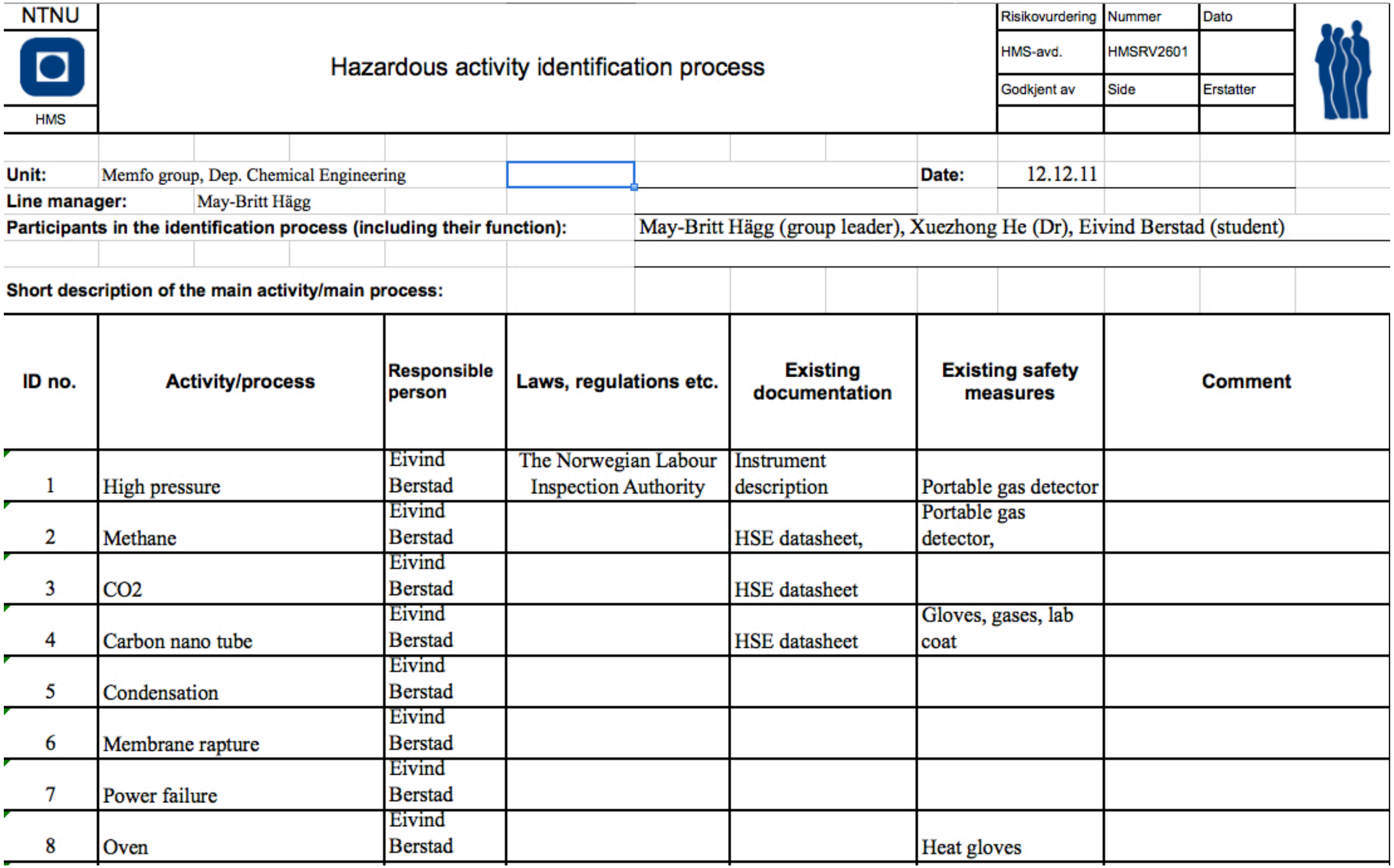

NTNU HMS	Hazardous activity identification process	Risikovurdering	Nummer	Dato
		HMS-avd.	HMSRV2601	
		Godkjent av	Side	Erstatter

Unit: Memfo group, Dep. Chemical Engineering **Date:** 12.12.11

Line manager: May-Britt Hägg

Participants in the identification process (including their function): May-Britt Hägg (group leader), Xuezhong He (Dr), Eivind Berstad (student)

Short description of the main activity/main process:

ID no.	Activity/process	Responsible person	Laws, regulations etc.	Existing documentation	Existing safety measures	Comment
1	High pressure	Eivind Berstad	The Norwegian Labour Inspection Authority	Instrument description	Portable gas detector	
2	Methane	Eivind Berstad		HSE datasheet,	Portable gas detector,	
3	CO2	Eivind Berstad		HSE datasheet		
4	Carbon nano tube	Eivind Berstad		HSE datasheet	Gloves, gases, lab coat	
5	Condensation	Eivind Berstad				
6	Membrane rapture	Eivind Berstad				
7	Power failure	Eivind Berstad				
8	Oven	Eivind Berstad			Heat gloves	

NTNU	Risk assessment	Utarbeidet av	Nummer	Dato
		HMS-avd.	HMSRV2603	04.02.11
HMS /KS		Godkjent av	Side	Erstatter

Unit: Memfo group, Dep. Chemical Engineering **Date:** 12.12.11

Line manager: May-Britt Hägg

Participants in the identification process (including their function): *May-Britt Hägg (group leader), Xuezhong He (Dr), Eivind Berstad (student)*

Signatures:

ID no.	Activity from the identification process form	Potential undesirable incident/strain	Likelihood:	Consequence:				Risk value	Comments/status Suggested measures
			Likelihood (1-5)	Human (A-E)	Environment (A-E)	Economy/ material (A-E)	Reputation (A-E)	Human	
1	High pressure	Leakage	4	A	B	A	A	🟨	Keep gas inside the rig, and vented.
2	Methane	Explotion	1	E	B	D	E	🟨	
3	CO2	Leakage	4	A	A	A	A	🟩	
4	Carbon nano tube	Inhale powder	1	B	B	A	A	🟩	
5	Condensation	Formation of hydrates will affect MFC, GC	3	A	A	A	A	🟩	Drain water before GC
6	Membrane rapture	Malfuntion of valves and pressure build up	3	A	A	A	A	🟩	Check pressure, exchange membrane
7	Power failure	No ventilation, no control	3	A	A	A	A	🟩	Reset manually after power failure
8	Oven	Burn	3	A	A	A	A	🟩	